JPC 429

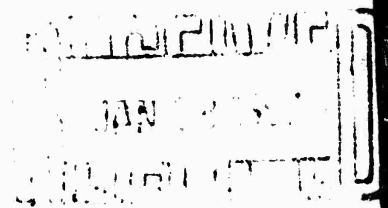# An Experimental Investigation of the Velocity and Temperature Profiles in the Boundary Layer Above an Unstable Evaporating Film of Liquid Under the Influence of a Moving Stream of Hot Gas

Technical Memorandum

by

D. L. Crabtree, Jr.
C. F. Warner

September 1966

JET PROPULSION CENTER
PURDUE UNIVERSITY

SCHOOL OF MECHANICAL ENGINEERING
LAFAYETTE, INDIANA

PURDUE UNIVERSITY

AND

PURDUE RESEARCH FOUNDATION

Lafayette, Indiana

Report No. TM-66-9

AN EXPERIMENTAL INVESTIGATION OF THE VELOCITY
AND TEMPERATURE PROFILES IN THE BOUNDARY LAYER
ABOVE AN UNSTABLE EVAPORATING FILM OF LIQUID
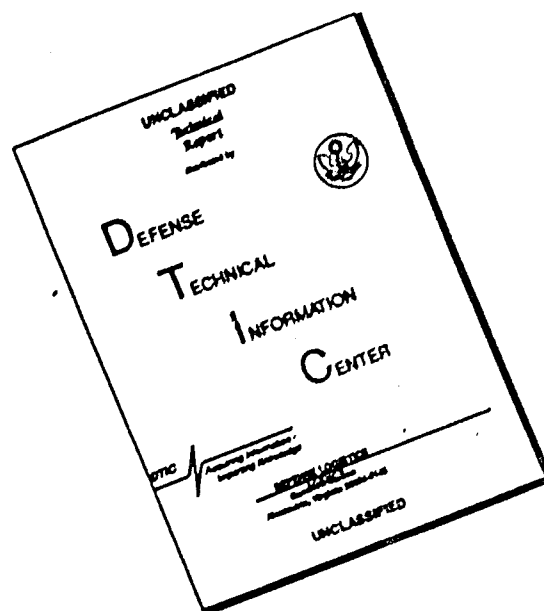UNDER THE INFLUENCE OF A MOVING STREAM OF HOT GAS

Technical Memorandum

by

D. L. Crabtree, Jr.
C. F. Warner

Jet Propulsion Center
Purdue University

September, 1966

DISCLAIMER NOTICE

ACKNOWLEDGMENTS

ERRATA SHEET

Page	Line	Correction
xi	5	Insert "of" after Professor
3	2 under 1.2	Insert to read "conducted are presented in"
6	last line	Insert to read "less than the effects"
36	2	Delete "at the"
36	3 from bottom	Change "eminating" to "emanating"
42	2 from bottom in footnote	Change "stram" to "stream"
43	7	Delete "friction" after "<u>overall</u>"
54	2	Insert "of" after "radius"
62	5 from bottom	Change "Similarity" to "Similarly"
98	2	Change "sillouetted to "silhouetted"
103	5	Change "become" to "became"
111	2 from bottom before 3.3.2	Change "calculatee" to "calculated"
111	6 from bottom	Change "abcissa" to "abscissa"
122	5 from bottom	Change "dimensionles" to "dimensionless"
131	Table 10	Change "0.00085" to "0.000085"

TABLE OF CONTENTS

TABLE OF CONTENTS (Continued)

TABLE OF CONTENTS (Continued)

LIST OF TABLES

LIST OF FIGURES

LIST OF FIGURES (Continued)

LIST OF FIGURES (Continued)

ABSTRACT

Crabtree, Jr., Donald Louis. Ph.D., Purdue University, January
1967. An Experimental Investigation of the Velocity and Temperature
Profiles in the Boundary Layer Above an Unstable Evaporating Film of
Liquid Under the Influence of a Moving Stream of Hot Gas. Major Pro-
fessors: Dr. Cecil F. Warner, Professor Mechanical Engineering, and
Dr. Maurice J. Zucrow, Professor Emeritus of Mechanical Engineering.

This thesis presents the results of measurements of the velocity
and temperature profiles in the boundary layer above an unstable evapor-
ating film of water. Entrained liquid as droplets was present in the
boundary layer. The measurements were made at one liquid flow rate at
the following gas flow conditions:

Total temperature	980R
Total pressure	250 psia
Gas velocity	100 ft/sec
Axial static pressure gradient	less than 0.02 psi/ft

Photographs taken at 3μ sec were obtained of the interfacial structure
of the liquid film. The temperature of the film was also measured. The
experiments were conducted in a tunnel with a rectangular cross section
1½ in. x 4 in. and 22 in. long, onto one side of which was injected the
liquid as a film. Measurements in the boundary layer were carried out
for both wet and dry walls.

The profiles of velocity and temperature in the boundary layer on the wetted wall correlated to power law distributions of 1/7 and 1/6, respectively; the velocity boundary layer on the dry wall correlated to a 1/8.3 power law distribution.

The friction coefficient for the wett.d wall was determined to be 40 percent greater than for the dry wall. The ratio of the friction coefficient to the Stanton number for the wetted wall was 2.4 which is in approximate agreement witn that value predicted by Reynolds analogy.

1. INTRODUCTION

1 1 <u>General</u> <u>Discussion</u>

In the last decade considerable research has been directed toward the investigation of the interaction of a moving gas stream with a thin film of liquid. The research has dealt with numerous aspects of this flow situation, such as film formation, wetting or coverage, surface instability[*], effective roughness, heat and mass transfer coefficients, pressure drop and friction coefficient and liquid entrainment in the gas stream to name a few. Under virtually all circumstances several of the aforementioned items are of interest simultaneously. Such a situation leads to difficulty in isolating specific effects and defining with certainty their physical nature. This situation is born out in the literature which contains numerous contradictions regarding even the most simple cases of a liquid film and a moving gas stream. It is no small wonder then, that in practical applications involving liquid films and moving gas streams

---

[*] In the present work surface instability is used to imply the presence of large wavelength waves traveling over the substructure of the liquid film. Entrainment of liquid from the crests of the waves in the gas stream is a result of the occurrence of such waves.

there exists a degree of arbitrariness and a lack of confidence regarding what is actually occurring.

The particular practical application which motivated the present investigation is liquid film cooling in rocket motors. In liquid film cooling a thin film of liquid is utilized to protect the walls of the combustion chamber and nozzle from the deleterious effects of the very hot combustion gases. The investigation of film cooling in rocket motors has been conducted for many years at the Jet Propulsion Center, Purdue University, as well as numerous government and industrial installations. Yet, at the present time a workable understanding of the details of the interphasial interactions which govern the process of film cooling in rocket motors is not available. The aforementioned situation arises from two sources. First, as has been noted, the simultaneous occurrence of intense heat and mass transfer coupled with the surface characteristics of instability and concomitant surface roughness make difficult the isolation of separate effects. Second, direct measurement of the parameters needed to evaluate the physical situation is impractical in a rocket motor because of the severe internal environmental conditions. The regions of flow of interest in the case of film cooling are the liquid film and the turbulent boundary layers of velocity, temperature and concentration above the evaporating film. To circumvent the difficulties of obtaining the measurements in a rocket motor the present investigation was conducted employing an experimental flow

configuration involving a moderately hot gas stream flowing over a liquid film. Measurements could be obtained for the boundary layers of velocity and temperature in the gas stream above the surface of the liquid film. There were established several simultaneous interactions between the gas and the liquid which were in many ways analagous to liquid film cooling in a rocket motor. It is felt that such an analogy will give an insight to the same mechanisms inherent in liquid film cooling even though the analogy must be structured at widely different operating conditions between the experimental model and the actual case of film cooling in a rocket motor.

The investigation presented herein, being a new experimental problem, was in many ways exploratory. Evaluation of the experimental apparatus and techniques of measurement employed went hand in hand with the determination of the experimental results. The program initiated with the subject research is continuing.

1.2 Objectives of the Investigation

The flow conditions for which the bulk of the present investigation was conducted in Table 1. The liquid was injected onto the test plate which comprised the floor of the tunnel as shown in Figure 1, p. 8. The width of the liquid film was initially that of the tunnel, namely, four inches. The flow rate of liquid and the conditions of the gas stream were such that the liquid film exhibited surface characteristics corresponding to the inception of instability with bulk entrainment of liquid as droplets in the gas stream.

Table 1

Flow Conditions for the Investigation

Gas	Air*
Liquid	Water
Total temperature	980R
Total pressure	250 psia
Velocity	100 ft/sec
Axial static pressure gradient	less than .02 $\frac{psi}{ft}$
Test plate	4 in. x 22 in.
Tunnel cross section	4 in. x 1 1/2 in.

The surface of the liquid film was viewed through glass viewing ports located in the sides of the tunnel. The boundary layer measurements were carried out along the centerline of the test plate at several selected locations downstream from the liquid injector. The temperature distribution in the test plate, below the liquid film, was measured by means of imbedded thermocouples.

The background of previous research and analytical relations required to evaluate and correlate the results of the investigation are presented in Section 2, "Interactions Between a Thin Film of Liquid and a Moving Stream of Hot Gas."

---

* The gas was a mixture of the products of combustion of air and methyl alcohol with additional diluent air. The quantities of combustion products in the working fluid were sufficiently low enough to justify the assumption of air alone

1.3 Closure

The experimental investigation did not produce measurements for
the concentration boundary layer. Further, because of experimental
difficulties, no reliable mass balance of bulk flow of liquid could
be determined between the entance and exit of the test section.
The lack of these results is a disadvantage insofar as the complete
evaluation of data is concerned.

2. INTERACTIONS BETWEEN A THIN FILM OF LIQUID AND A MOVING STREAM OF HOT GAS

2.1 Introduction

The purpose of this section is to present a background for the discussion presented later of the results of the subject investigation. The present section is oriented toward the subject investigation.

A detailed treatment of the flow of a thin liquid film under the influence of a moving gas stream is not in the scope of the present work. The fundamental problem will be briefly outlined but the many details of the treatment of the problem are relegated to the literature. The discussion does present descriptive and working relations necessary to the evaluation and correlation of the results of the investigation.

The scope of the discussion is broadly restricted as follows:

1 The co-current flow of a turbulent hot gas over a flat plate on which is flowing a thin film of liquid.

2. The gaseous boundary layer is turbulent and there is no axial static pressure gradient.

3. The evaporative mass transfer leads to effects in the boundary layer which are an order of magnitude less the effects

of momentum and heat transfer.

4. The liquid film is unstable and some liquid is entrained as droplets in the gas stream.

5. The liquid is inert and non-reactive.

The emphasis on the boundary layer phenomena will be limited to the profiles of velocity and temperature in the boundary layer. The effect of mass transfer on the aforementioned two boundary layers was not detectable as a first order effect as was the heat and momentum transfer to the liquid film. The presence of mass transfer will be noted in the discussion where applicable but will not be treated to the same extent as the exchange mechanisms of heat and momentum.

2.2 Description of the Physical Situation
in the Subject Investigation

Figure 1 presents a schematic diagram of the tunnel containing the test section employed in the investigation[*] Air at a total temperature of 980R, and a total pressure of 250 psia entered a straight duct termed the lead section. The air was thoroughly mixed by several sets of turbulence grids, the last set being located at the entrance to the lead section. In the lead section a turbulent velocity boundary layer began forming immediately after the

---

[*] A detailed description of the experimental apparatus and the experimental procedures employed is presented in Appendices B and C.

Figure 1. Schematic Diagram of the Experimental Tunnel

turbulence grids; the boundary layer was tripped by spanwise rods attached to the walls of the lead section. The flow in the lead section was essentially adiabatic.

Located 18 inches downstream of the entrance to the lead section was the liquid injector. The liquid was injected spanwise as a thin film onto the test plate. From the point of first contact between the gas and the liquid a temperature boundary layer began to grow. The liquid film flowed over the 22-inch length of the test plate. The central 50 percent portion of the test plate was wetted by the film for this length. The flow continued for 10 inches beyond the terminal end of the test plate and exhausted through a nozzle. The axial static pressure gradient in the test section was maintained at $\pm$ 02 psi per foot by an adjustable roof hinged at the fore end of the test section. The essentially zero pressure gradient began 2 inches upstream from the point of injection of the liquid

With the previously described model in mind let us now briefly examine the conditions of the gas and liquid flows and their interactions

The velocity boundary layer in the gas flow developed on all four sides of the lead section. The thickness of the velocity

boundary layer, δ^*, was approximately 0.35 inches at the terminal end of the lead section. The small amount of heat lost from the flowing gas through the walls of the lead section did not cause the growth of an appreciable temperature boundary layer. Hence, at the entrance to the test section the flow was characterized as being isothermal. The turbulence intensity, $\frac{u'}{u_e}$, in the core of the gas stream at the entrance to the test section was approximately 0.02 and decayed to approximately 0.01 at the exit of the test section (see Appendix B).

The liquid was injected tangentially onto the test plate parallel to the direction of the gas flow. The liquid covered the width of the test plate at the point of injection. The mean velocity of the liquid at the point of injection was approximately 0.4 ft/sec. Immediately at the first contact between the liquid film and the gas stream several effects occurred simultaneously to the liquid film. The liquid was accelerated by the force of interfacial shear. The film rapidly decreased in thickness, becoming on the order of one or two thousandths of an inch thick

---

[*] Appendix A presents the nomenclature for the symbols employed herein. Most of the symbols are taken for convenience from Turbulent Boundary Layers in Compressible Gases by S. S. Kutateladze and A. I. Leont'ev, and correspond to those introduced by the translater, D. B. Spalding (31). The less common symbols are defined in the text at the occasion of their first usage. Where a symbol represents a turbulent quantity, such representation is understood to be a time mean quantity.

or so downstream from the injector slot The surface of the film became unstable and liquid entrainment became established several inches downstream from the injector slot. Heat transfer and evaporative mass transfer were present from the injector slct on downstream.

The gas stream underwent a stepwise change in the boundary conditions of both wall temperature and surface roughness after entering the film covered test section. A further change in the boundary conditions was brought about by the introduction of mass transfer and liquid entrainment. A temperature boundary layer was initiated and underwent rapid growth in thickness, Δ, over the first 6 inches of the liquid film, the growth rate then decreased as the flow moved further downstream. The foregoing effects required the readjustment of the shear stress and its distribution in the boundary layer and, consequently, brought about a change in the growth parameters of the gaseous boundary layer

From the preceding discussion it can be seen that the interactions between the liquid film and the gas stream are difficult to evaluate on the basis of cause and effect No clear distinction can be made, for example, between the effect of roughness of the liquid film on the growth of the boundary layer, and then, separately, the effect of heat transfer on the coefficient of friction. The resultant effects of the combined causes of interaction are, however, reflected in the structure of the velocity, temperature and concentration boundary layers. The remainder of this major section

discusses some of the principal effects of certain gas-liquid inter-
actions and their influence on the structure of the boundary layers.

2.3 Characteristics of the Liquid Film

The present section discusses the bulk and surface characteris-
tics of a thin liquid film. Estimates derived from the literature
are given for the numerical values of the characteristic parameters
of the liquid film associated with the subject investigation. Much
of the discussion material and the numerical estimates are based on
sources relating to annular two-phase flow. In all of the sources
used herein the annular two-phase flow comprised a liquid film of
water flowing on the inside of a circular duct through which was
flowing air, usually in co-current flow. In some cases the air was
heated but generally the conditions interior to the duct were
essentially ambient. Published results are available for both
stable and unstable films. Since the flow conditions of the
reference sources were substantially different from those in Table
1, Section 1.2, the estimated values of the film parameters are to
be taken as representative predicted values.

2.3.1 Bulk Characteristics

Consider a liquid injected parallel to the surface of a smooth
flat plate over which is flowing a hot gas. The thickness of the
liquid film at injection is no more than an order of magnitude
greater than the value of the thickness which will be achieved

in equilibrium flow with the gas a short distance downstream from the point of injection. As the liquid and gas flows adjust to each other, the following changes occur within some "adjustment distance" downstream of the point of injection:

1. The liquid is exposed to interfacial shear stress arising from the gas flow, and is accelerated to where the shear stress distribution in the liquid supports the interfacial shear stress caused by the gas flow.

2. The temperature of the liquid rises (in the present case) until an equilibrium temperature is achieved, an equilibrium temperature brought about by the processes of heat and mass transfer and the thermodynamic properties of the liquid

3. The transient characteristics of surface instability associated with the acceleration of the liquid and the adjustment of interfacial shear stress give way to "steady state" instability characteristics.

The distance the flow must travel before each of the various initial adjustments of the liquid film is completed depends, of course, on a combination of factors. The effect of these factors on the various adjustments will not be discussed here. It will suffice to say that the adjustment distances in the present investigation were on the order of 10 to 20 percent the length of the test section. If the liquid was injected uniformly spanwise, the film remains free of dry patches (where the surface of the test plate is

exposed) until near the termination of the film at the end of the test plate. The discussion which follows deals with the steady state film between the end of the adjustment distances and the onset of termination.

The velocity distribution through the liquid film can be derived by the solution of the momentum equation for incompressible flow. Thus (1)[*]

$$u = \frac{\tau_s}{\rho_l} \int_0^y \frac{dy}{\nu_l + \nu_{lt}} \qquad (2\text{-}1)$$

where

τ_s = shear stress

ν_l = molecular kinematic viscosity of the liquid

ν_{lt} = effective eddy kinematic viscosity of the liquid

ρ_l = density of the liquid

For the special case of laminar flow of the film and where $\nu_l \approx$ constant through the film equation 2-1 reduces to

$$u = \frac{\tau_s}{\rho_l \nu_l} \, y \qquad (2\text{-}2)$$

For the case where there is a turbulent contribution to the viscosity term, the assumption generally made is that the universal law of the wall is applicable to the liquid film. Figure 2 presents

---

[*] Numbers in parentheses refer to references listed in the List of References.
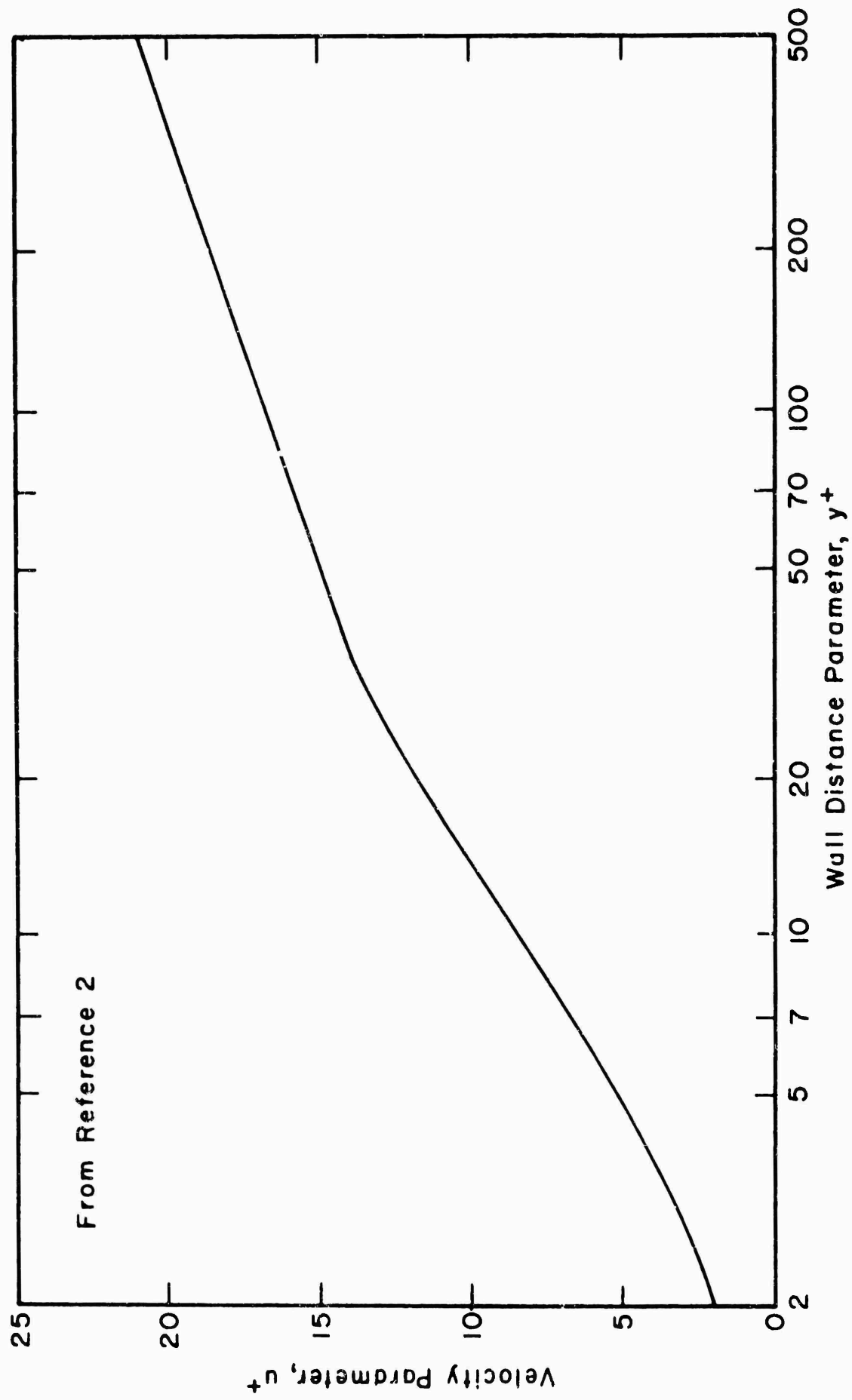
Figure 2. Universal Law of the Wall for an Incompressible Turbulent Boundary Layer on a Smooth Surface

the law of the wall for the incompressible turbulent boundary layer on a smooth surface. The dimensionless parameters u^+ and y^+ are defined for the liquid as

$$u^+ = \frac{u}{(\tau_s/\rho_1)^{\frac{1}{2}}} \tag{2-3}$$

$$y^+ = \frac{y(\tau_s/\rho_1)^{\frac{1}{2}}}{\nu_1} \tag{2-3a}$$

Once the interfacial shear stress is determined, the u-y relationship for the liquid film has a solution obtained from the universal law of the wall. The term $(\tau_s/\rho)^{\frac{1}{2}}$ is termed the friction velocity and has the symbol u_τ, ft/sec.

The mass flow rate of liquid per unit spanwise length, $\dot{m}_1'$, and the flow mean thickness of the liquid film, δ_f, are related through continuity as

$$\dot{m}_1' = \rho_1 \int_0^{\delta_f} u \, dy \tag{2-4}$$

For the case where the film is laminar equations 2-2 and 2-4 can be combined to yield an expression for the flow mean thickness of the liquid film. Thus

$$\delta_f = \left[\frac{2 \, \dot{m}_1' \, \nu_1}{\tau_s} \right]^{\frac{1}{2}} \tag{2-5}$$

Equation 2-4 can be written in a nondimensional form. Thus

$$W^+ = \int_0^{\delta_f^+} u^+ \, dy^+ \qquad (2\text{-}6)$$

where the dimensionless liquid flow rate, W^+, is

$$W^+ = \frac{\dot{m}_1}{\rho_1 \nu_1} \qquad (2\text{-}7)$$

and the dimensionless film thickness, δ_f^+, is

$$\delta_f^+ = \frac{\delta_f (\tau_s/\rho_1)^{\frac{1}{2}}}{\nu_1} \qquad (2\text{-}8)$$

The significance of W^+ relative to the physical characteristics of the flow of the liquid film is discussed in the next section

A method for predicting the temperature of the gas-liquid interface is presented in detail by Gater (1) and Knuth (5). The temperature of the gas-liquid interface, T_s, can be related to the bulk flow parameters by specifying (a) an interfacial energy balance and (b) an analogy between the rates of heat and mass transfer In Gater's derivation the interfacial energy balance was specified such that all of the heat incident onto the surface of the film resulted in the evaporation of the liquid, and the analogy was specified such that the Stanton number for heat transfer was equal to the Stanton number for mass transfer

Figure 3 (reproduced from Reference 1) presents the temperature at the interface, T_s, as a function of the static pressure for air in contact with water for several free stream temperatures. The dashed lines denote the flow conditions of the present investigation. The important point brought out by the figure is that the assumption that the temperature at the interface is equal to the saturation temperature for the liquid at the prevailing static pressure can prove to be in considerable error, especially at lower gas stream temperatures.

2.3.2 Surface Characteristics

<u>Stability and Entrainment.</u> In many discussions of film stability the characteristic interfacial structures of the liquid film are used to describe the "stability regime" in which the film exists, and the regime is then related to some parameter of the liquid flow and/or the gas flow. The following discussion of the characteristic interfacial structures of the liquid films in the present investigation is quoted from Gater (1). The discussion deals with a series of photographs obtained by Gater and the author during the preliminary phases of the present investigation. Figure 4 presents the photographs[*] of liquid films of water displaying

---

[*] See Appendix B for the description of the apparatus employed to obtain the photographs.
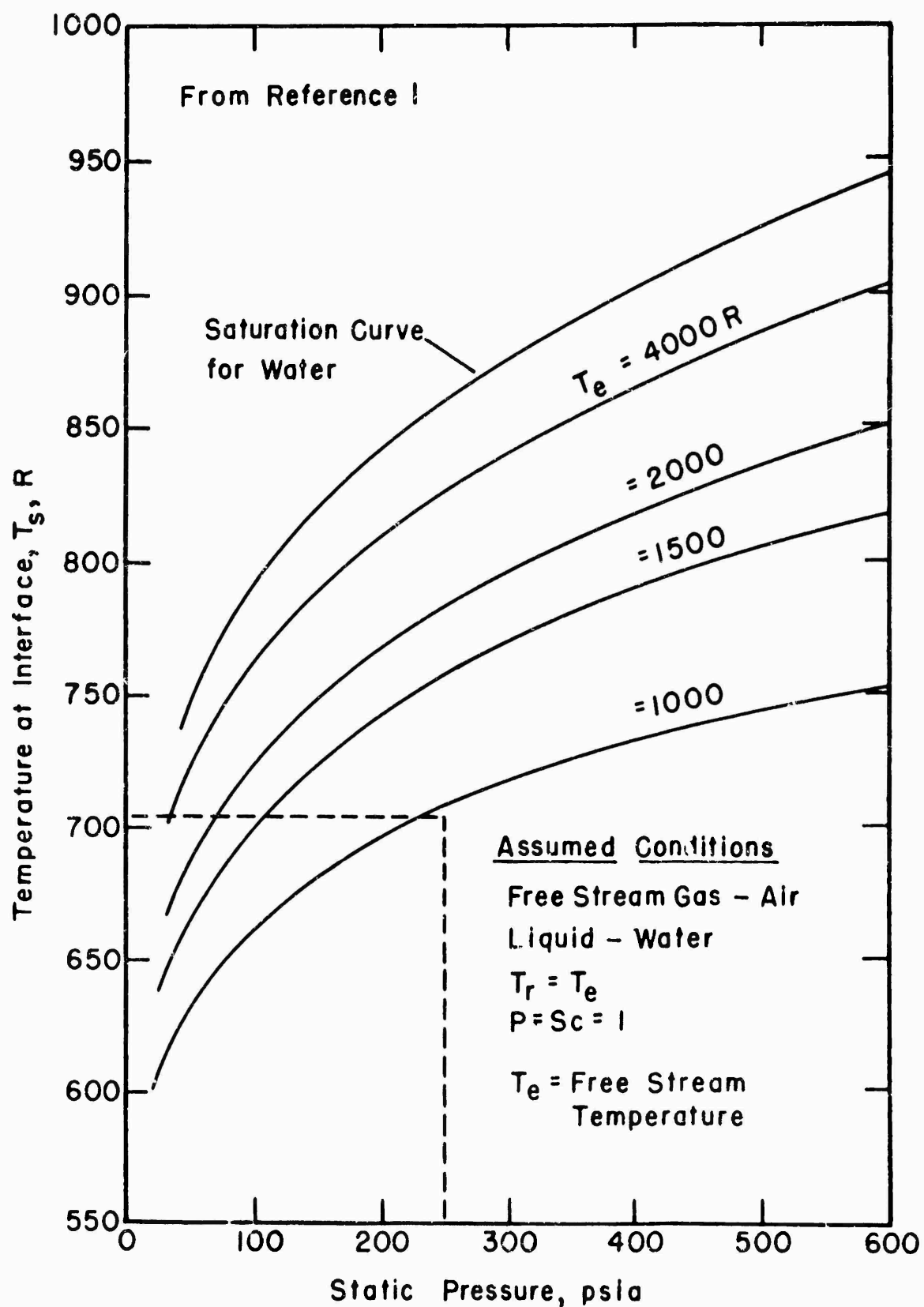
Figure 3. Temperature at the Gas-Liquid Interface as a
as a Function of the Static Pressure

x-scale: $\overset{\text{o}}{\underset{\rule{0pt}{0pt}}{\vrule}}\underset{\rule{0pt}{0pt}}{\quad\quad\quad}\overset{\frac{1}{4}\text{ in}}{\vrule}$

$\leftarrow u_e$

a. smooth (u_e=88 fps , $x-x_0$=9ins , m_0'=0·001 lb/in-sec)

$\leftarrow u_e$

b."pebbled" (u_e=50 fps , $x-x_0$=5ins , m_0'=0·002 lb/in-sec)

$\leftarrow u_e$

c."pebbled" (u_e=130 fps , $x-x_0$=5ins , m_0'=0·001 lb/in-sec)

$\leftarrow u_e$

d. unstable (u_e=130 fps , $x-x_0$=5ins , m_0'=0·0045 lb/in-sec)

Figure 4.   Photographs of the Characteristic Interfacial
Structures for a Liquid Film

different characteristic interfacial structures.

"The photographs presented in Figure 4 were taken when the static pressure and the main-stream temperature had values of 220 psia and 1000R, respectively   Flow parameters which were not common to all of the photographs are specified in the appropriate subtitles of Figure 4; they are the mainstream velocity, u_e, the position downstream of the point of liquid injection at which the photographs were taken, $x - x_o$ and the rate of liquid injection per inch of injector slot width, m_o

The interfacial structure presented in Figure 4a is characterized by its extreme smoothness   In that particular photograph there is shown a 1/2 in diameter cylindrical plug which protrudes approximately 0 001 in above the surface. The fortuitous presence of that surface irregularity serves to indicate that a liquid film which has a smooth interfacial structure is, in general, very thin and sensitive to relatively small surface rough-ness   The smooth character of the interfacial structure is apparently due to the fact that the liquid film is so thin and viscous that any disturbances impacted to it as a consequence of turbulent velocity fluctuations in the adjacent gas phase are completely suppressed or "damped out"

The interfacial structure presented in Figures 4b and 4c is quite common and is characterized by its "pebbled" appearance. The small disturbances which are evident on the

surface of the liquid film are apparently a consequence of turbulent velocity fluctuations in the gas phase flowing past the liquid film. The liquid film is sufficiently thin and viscous that small disturbances which appear on its surface do not amplify and cause film instability. (It should not be implied, however, that there may not exist turbulent stresses in the liquid film.) The difference in the scale of the interfacial disturbances for the two "pebbled" interfaces presented in Figure 4 is due primarily to a corresponding difference in the scale of the turbulence in the adjacent flowing gas; the turbulence scale of the gas phase decreases with increasing gas mass flow rate. That relationship between the gas mass flow rate and the nature of the "pebbled" interfacial structure has been observed previously (3)(4)(5)(6).

The interfacial structure presented in Figure 4d defines the phenomenon of film instability; the latter is characterized by the existence of large-scale disturbances which are turbulent in nature, and which are superimposed on a "pebbled" interfacial structure."

The study of the stability characteristics of liquid films was not a part of the subject investigation. The observed results were, however, correlated to an established stability criterion, namely, the dimensionless liquid flow rate, W^+. Above a certain value of W^+ the longer wavelength waves i.e., two dimensional disturbances appear as shown in Figure 4d. Entrainment of liquid in the gas stream occurs at the crests of these waves. The value of the dimensionless liquid

flow rate at which the larger waves appear is a function of the gas stream Reynolds number for lower values of this Reynolds number. For higher values of the gas stream Reynolds number, however, the value of W^+ for which the larger waves appear becomes more or less constant.

The use of W^+ to correlate the stability of the liquid film is related to the assumption [1][4][7] that the velocity distribution in the liquid film can be related to the law of the wall. In the interpretation of the law of the wall, the flow interior to the liquid film for which y^+ 12 is characterized as being viscous in nature and stable; the flow for which $15 < y^+ < 20$ to 30 is characterized by the presence of both viscous and turbulent effects, while the flow for which y^* 20 to 30 is characterized by being turbulent. The parameter W^* as a stability criterion infers that the first appearance of instabilities correlates approximately to the appearance of turbulence in the film, i.e., approximately $y^* = 15$. The range of the dimensionless liquid flow rate for which instability is incipient is $90 < W^+ < 150$ which corresponds to the range $15 < y^* < 30$, approximately.

The foregoing criterion is useful in predicting the inception of instability, but once instability is present, the surface characteristics of the liquid film displaying the larger waves are influenced by the gas stream conditions. The present investigation was conducted in a regime of instability wherein the gaseous

boundary layer was intimately involved in establishing the surface characteristics of the liquid film as will be shown.

Figure 5 presents a schematic diagram of a liquid film indicating certain characteristic thicknesses defined for the liquid film. The continuous sublayer thickness of the liquid film, δ_B, is the thickness of liquid film immediately adjacent to the wall which is not penetrated by the troughs of the surface waves. The maximum wave amplitude of the interfacial waves, δ_T, is the height of the crests of the instability waves above the boundary wall. The flow mean thickness, δ_f, is the thickness in which the liquid would flow for some specified velocity distribution (laminar or law of the wall) in the film if it were free of surface disturbances. The modal thickness, δ_m, is the distance from the wall at which the wave frequency is a maximum. The difference between the modal thickness and the continuous sublayer thickness, $(\delta_m - \delta_B)$, is termed the net disturbance amplitude.

Figure 6, based on data obtained by Charvonia (7)[*], presents the continuous sublayer thickness, the net disturbance amplitude, the maximum wave amplitude and the flow mean thickness of a liquid film as a function of the gas velocity for the liquid flow rate of

---

[*] The experiments of Charvonia were conducted for vertical downward co-current flow of water and air at near ambient conditions. The diameter of the duct was 2 1/2 inches.
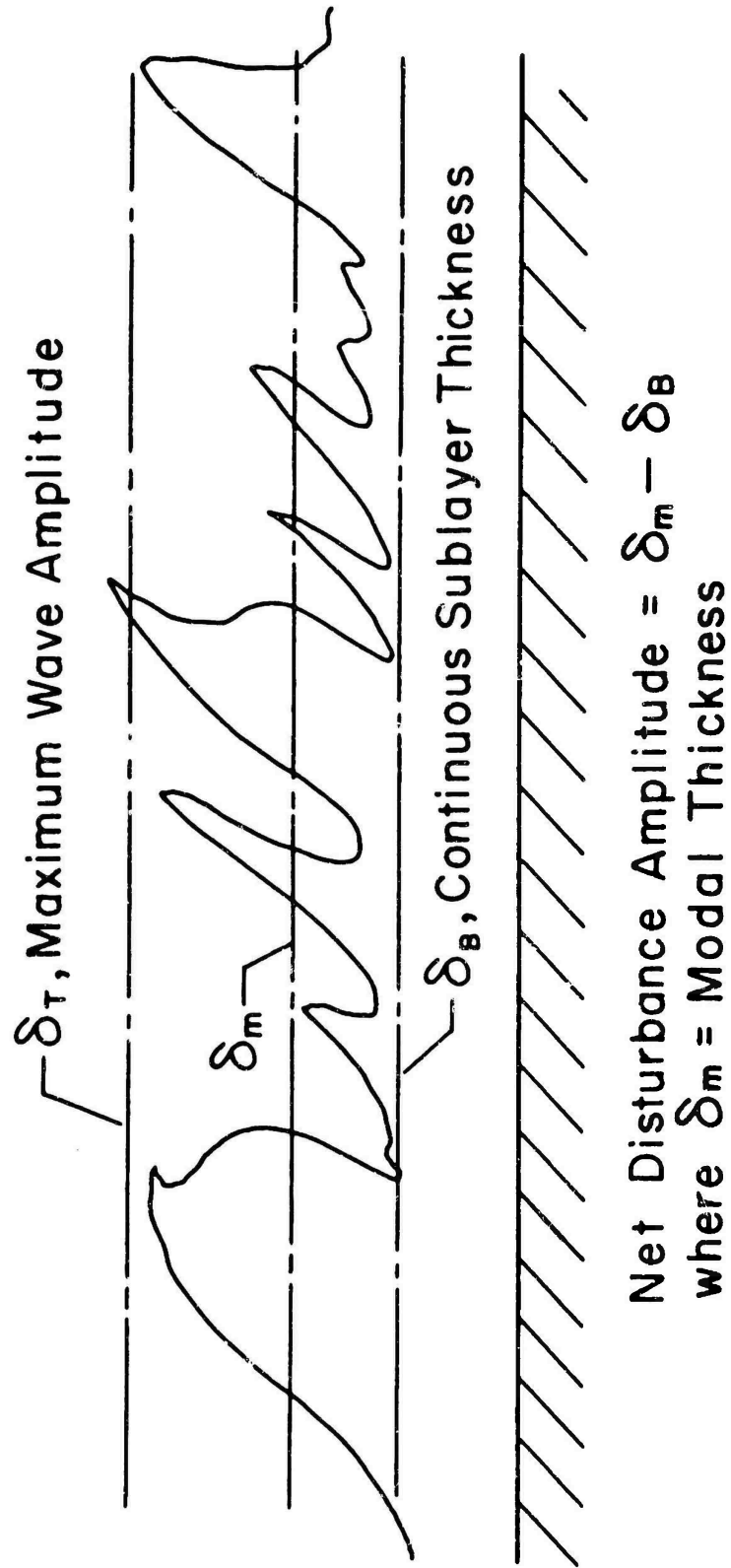
Figure 5. Schematic Diagram of a Liquid Film
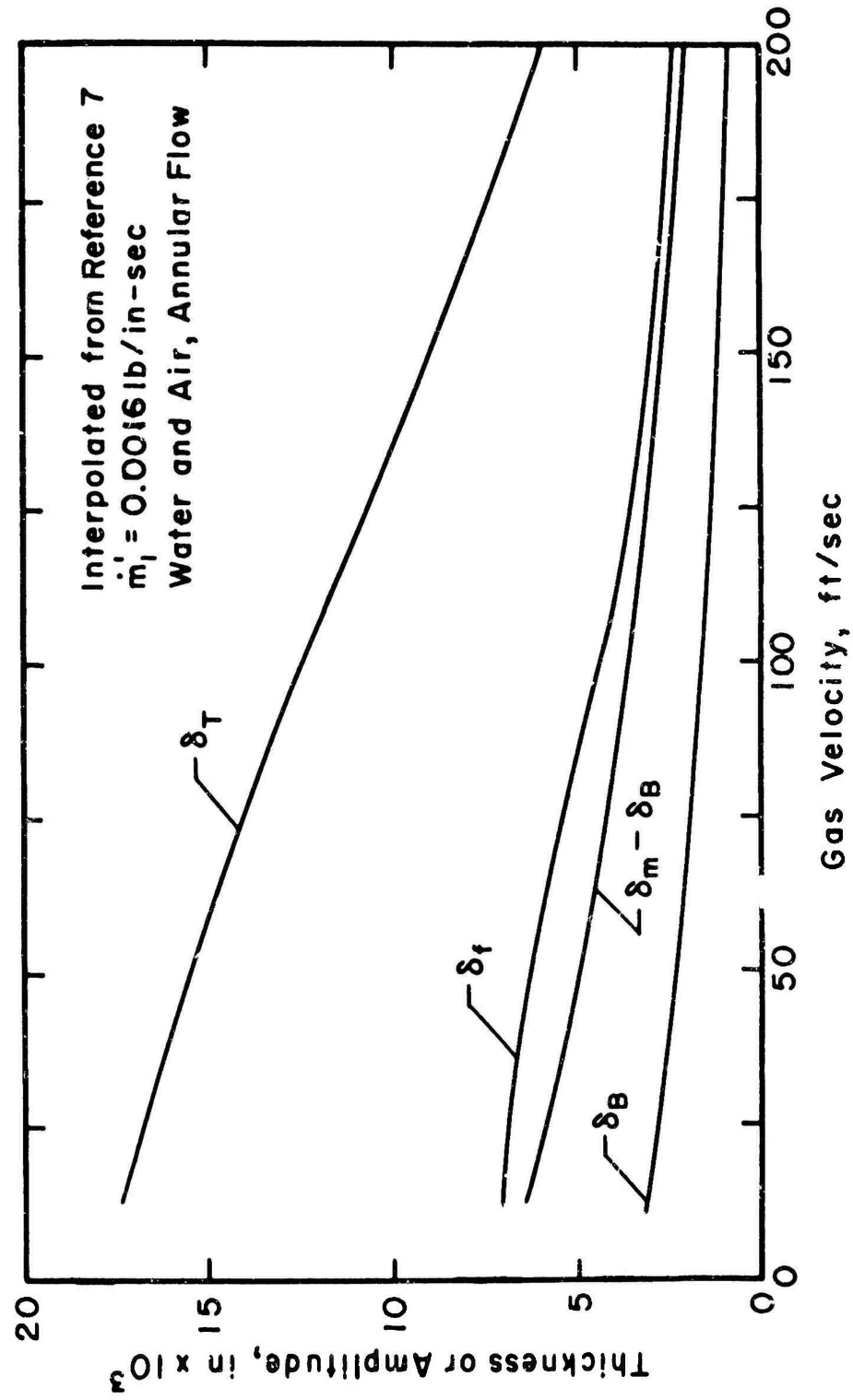
Figure 6. Thickness Parameters for a Film of Liquid as a Function of the Gas Velocity

0.0016 lb/in-sec. The curves were interpolated from the reference data at the above flow rate in order to agree in value with that of the subject investigation. In Charvonia's investigation the liquid film for that particular flow rate was stable, displaying no droplet breaka- way. The values of the various thickness parameters indicated by the curves in Figure 6 must be interpreted as representative The con- tinuous sublayer thickness is approximately 0.002 in. or less for gas velocities in excess of 100 ft/sec. In the same range of gas velocity the net disturbance amplitude varies between approximately 0.002 and 0.004 in. The flow mean thickness varies between 0.003 and 0.004 in. for gas velocity from 100 to 200 ft/sec while the flow mean thickness of the subject investigation was approximately 0.001 to 0.002 in. One interesting point brought out in Figure 6 is the fact that the wave disturbances on the surface of the liquid film can be several times larger than either the flow mean thickness or the continuous sublayer thickness.

Roughness The flow of a gas over a liquid film on which surface waves are present is recognized as being similar to a gas flow over a rough surface (7 through 13) The roughness of the liquid film in the subject investigation was only estimated from the photographic results It is,therefore,worthwhile to establish some estimates based on other sources for qualitative comparison

Gill, et. al. (10) report values of apparent roughness

height for an annular film of water in a 1 1/4 in. diameter tube flowing air.[*] The average gas velocity was varied between 75 and 200 ft/sec while the peripheral liquid flow rate was varied between 0.0021 and 0.014 lb/in-sec. The static pressure and temperature in the tube were near ambient conditions. Entrainment of liquid from the film was present except for the lower liquid flow rates. Although the flow conditions are not equivalent to those of the present investigation in regard to pressure and temperature, the results will be employed for want of more suitable data. The apparent roughness reported in Reference 10 was calculated from pressure loss data measured for the gas flow in the tube. The results were compared in Reference 10 with similar results reported elsewhere (11)(12)(13) and were found to be in relatively good agreement. Figure 7 presents the curve of apparent roughness height, λ, as a function of the relative film thickness, δ_r. The relative film thickness is defined (11) for annular flow as

$$\delta_r = d \left(\frac{\delta_f}{d} - \frac{5}{Re_g} \sqrt{\frac{1}{2c_f}} \right)$$
(2-9)

---

[*] Apparent roughness implies that uniform surface roughness which would yield the same pressure drop in the tube as observed for the liquid film.
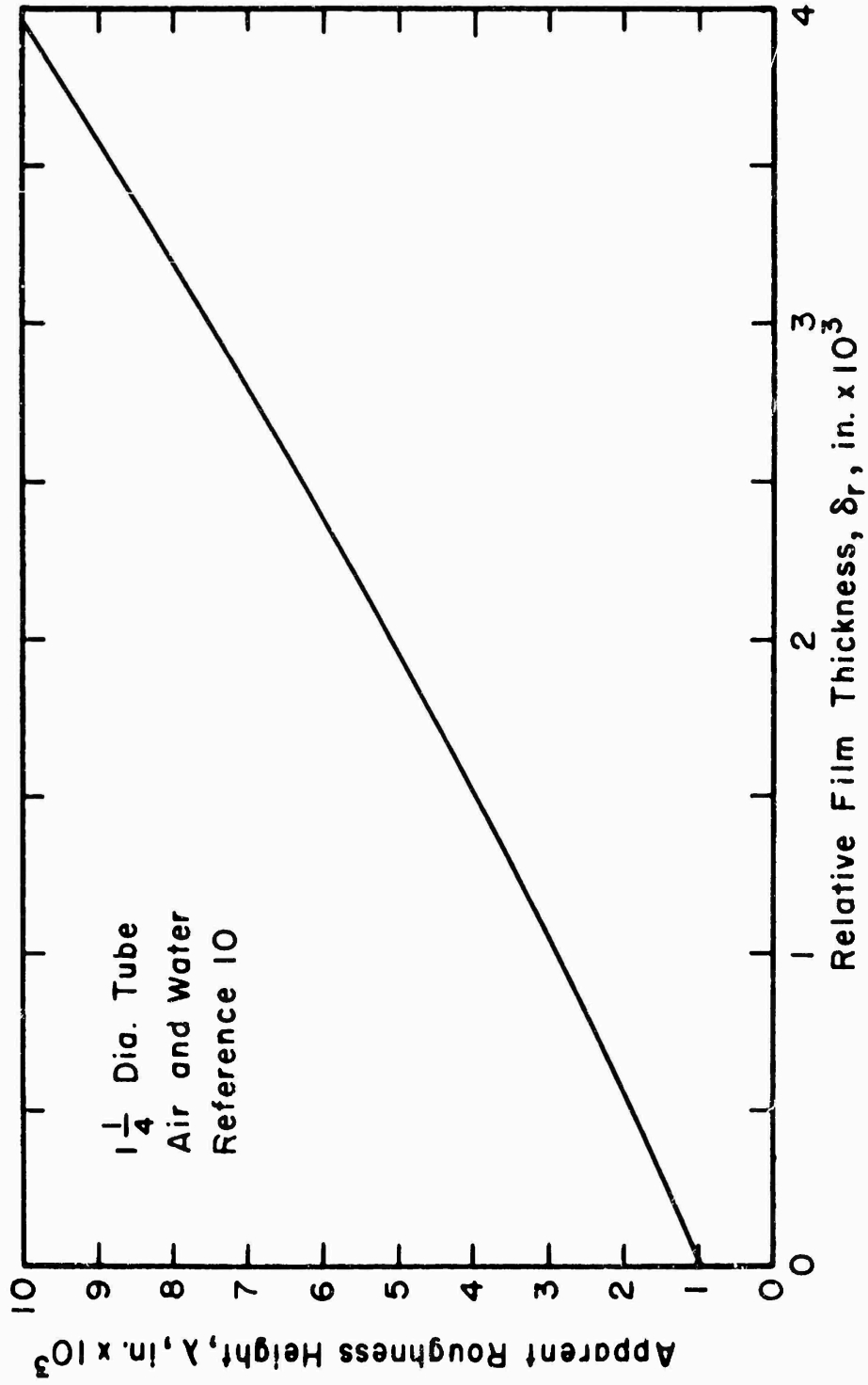
Figure 7. Apparent Roughness Height as a Function of Relative Film Thickness

where

    d = diameter of tube

    δ_f = liquid film thickness

    Re_g = Reynolds number for the gas

    c_f = value of friction coefficient over the dry wall

    $\bar{u}$ = average velocity of gas in the duct

The second term in the parenthesis relates to the thickness of the viscous sublayer in the gas flow over a dry wall. For purposes herein equation 2-9 can be rewritten to eliminate the diameter of the duct by noting that $Re_g = d\,\bar{u}/\nu$. Thus

$$\delta_r = \delta_f - \frac{5\nu}{\bar{u}} \sqrt{\frac{1}{2c'_f}} \qquad (2\text{-}9a)$$

Introducing the values of the parameters pertinent to the subject investigation and substituting the free stream velocity u_e for $\bar{u}$, the relative film thickness is calculated to be approximately $\delta_r = 1$ to 2×10^{-3} in.

Reading from Figure 7 the apparent roughness for a liquid film for which $\delta_r = 1$ to 2×10^{-3} in. is approximately 0.003 to 0.005 in. Charvonia's results for the same liquid flow rate as employed herein, the net disturbance amplitude, $(\delta_m - \delta_B)$, is approximately 0.0025 in. for gas velocities above 150 ft/sec. If the net disturbance amplitude is multiplied by two to

approximate a mean height of the waves on the film, i.e., roughness elements, the result of 0.005 in. is seen to agree well with Gill et. al. (based upon the necessary modifications of equation 2-9). It will be noted that the maximum wave height interpolated from Charvonia's results for m_1 = 0.0016 lb/in-sec at the <u>same</u> <u>surface</u> <u>shear</u> <u>stress</u> as found in the present investigation was 0.006 to 0.007 in.

Provided that the different operating conditions of the present investigation do not fundamentally alter the characteristics of the surface instability, the apparent roughness of the liquid film in the test section may be predicted to be from 0.003 to 0.006 in.

<u>Surface Area</u> The increase of the surface area of the liquid film caused by surface waves is sometimes mentioned in connection with the calculation of heat and mass transfer, i.e., the necessity of knowing what area is involved in the transfer process. Schneiter (14) performed a study of annular two-phase flow in which one of the objectives was to measure the increase in surface area due to the presence of waves. In his survey of the literature he reports the wide divergence of results of both experiments and analysis. The results vary from practically a negligible increase to 150 percent as predicted by one theory and 50 percent as measured in one experiment. On the basis of

his research Schneiter concluded that the increase in surface area of the film due to waves was negligible for stable films (the limit of his investigation).

As to the present investigation the point made by Fulford (15) seems pertinent, namely, that the increase in turbulent mixing caused by the presence of the waves (and certainly here, entrainment) would far overshadow the effect of an area increase in regard to the processes of heat and mass transfer.

Evaporation. The evaporation of the liquid comprising the film occurs in two ways, namely, evaporation from the exposed surface of the film and evaporation of the droplets entrained in the gas flow above the film. Luikov (16)(17) has perhaps identified an effect in the evaporation from the surface of a film which influences the heat and mass transfer processes. The effect is the result of the so-called "dynamic theory of evaporation and condensation". The essence of the hypothesis is the presence of extremely fine liquid droplets in the boundary layer. The droplets referred to are not necessarily those resulting from disturbance instability According to Luikov (16): The basic cause of droplet separation from the exposed liquid surface is the existence of point condensation and the interaction of the gaseous stream with the liquid surface (entrainment). According to the dynamic adsorption

33

theory of De Bur, the evaporation process is a dynamic desorption
and sorption process. The liquid molecules not only leave the
surface (evaporation) but also continuously return (condensation);
thus the evaporation rate (net) is proportional to the difference
between these two molecular streams

Evaporation of droplets in the boundary layer (whether
produced by condensation or entrainment) is termed volumetric
evaporation. Volumetric evaporation provides a source for
vapor and a sink for heat It is hypothesized (by Luikov) that
volumetric evaporation intensifies the process of heat exchange
in evaporation. In evaporation there is a many-fold increase in the
volume of the material while in condensation there is a corresponding
decrease in the volume of the material These two processes
disrupt the structure of the boundary layer, and particularly, the
viscous sublayer if it exists, i e., an effect analogous to
turbulence

If the foregoing hypothesis is correct, the following
comments are made relative to the present investigation: (1) the
physical situation investigated herein supplies all the require-
ments for volumetric evaporation, and (2) the magnitude of the
effect of volumetric evaporation compared to other disrupting
influences is not known

2.4 The Boundary Layer

In the present section are presented the basic differential equations for the boundary layer which take note of the presence of an unstable evaporating film of liquid. The aforementioned equations are compared with a similar set of equations written for the boundary layer above a rigid porous plate with mass addition at the wall (simple mass addition). The result of this comparison is a delineation of the basic differences in the two cases, and hence, a clearer understanding of the influence of the liquid film on the boundary layer[*].

The remainder of the section is devoted to a discussion of the description of the turbulent boundary layer and the various interactions between the gas stream and the liquid film.

---

[*] The use of the example of transpiration cooling through a porous wall is employed here, first because much work has been performed in this area and its description is well documented (Reference 18 lists 97 papers dealing with transpiration cooling), and second, because it bears the similarity of surface mass transfer to the case of the evaporating liquid film. The intention is not to eventually show that the evaporation of a liquid film and porous wall cooling are the same in physical terms. Quite to the contrary, the present investigation as well as others (17)(19) show there is a significant difference between the two cases insofar as transfer coefficients are concerned.

Estimates of the order of magnitude of the various interactions on the heat and momentum transfer coefficients are made with respect to the same coefficients for flow over a dry wall.

2.4.1 The Boundary Layer Equations

The assumptions applicable to the most general case of gas boundary-layer liquid film flow to be discussed in this and subsequent sections are:

1. Two-dimensional steady flow of a turbulent boundary layer.

2. There is no axial static pressure gradient, i.e., constant pressure flow.

3. The boundary layer flow is compressible but no effects associated with high speed flow such as frictional dissipation are present and the specific heat of the gas is constant.

4. Heat transfer is from the higher temperature gas stream toward the liquid film or wall

5. There are no radiation effects

6. The vapor from the liquid film (or other mass addition) and the gas in the free stream are the only two components present.

7. A portion of the liquid film is entrained as droplets in the boundary layer.

In regard to assumptions 3 and 6, the change in property values through the boundary layer in the subject investigation was due

principally to a variation in gas temperature in the boundary layer
as opposed to the presence of vapor (the partial pressure of the vapor at the
at the <u>surface</u> of the film was 12 percent of the free stream static
pressure). Hence, throughout the present discussion mixture
properties are not taken into account and the gas in the boundary
layer is treated as if it were air.

In regard to assumption 7, the presence of entrained drop-
lets in the boundary layer is not treated quantitatively but the
qualitative aspects of such a phenomenon are examined relative to
the boundary layer.

The equation of motion governing the boundary layer is (see
Reference 20 for basic equations)

$$\rho u \frac{\partial u}{\partial x} + \rho v \frac{\partial u}{\partial y} = \frac{\partial}{\partial y} \left[\mu \frac{\partial u}{\partial y} + \epsilon \frac{\partial u}{\partial y} \right] + F_1 \qquad (2\text{-}10)$$

where

ϵ = eddy viscosity

F_1 = a term expressing the influence of form drag of the
entrained droplets and the momentum deficit caused
by the vapor eminating from the droplets as evaporation
occurs

The equation of sensible energy is

$$\rho u \, \frac{\partial h}{\partial x} + \rho v \, \frac{\partial h}{\partial y} = \frac{\partial}{\partial y} \left\{ \left[\frac{\mu}{P} + \frac{\epsilon}{P_t} \right] \frac{\partial h}{\partial y} \right\}$$

$$+ \frac{\partial}{\partial y} \left\{ \left[\frac{k}{c_p} \, (L - 1) + \frac{\kappa}{c_p} (L_t - 1) \right] (h_v - h_g) \, \frac{\partial C_v}{\partial y} \right\}$$

$$+ \, Q_1 \qquad\qquad\qquad (2-11)$$

where

    h = sensible enthalpy of the gas-vapor mixture

    L = laminar Lewis number, $\dfrac{c_p \rho D_{vg}}{k}$

  D_{vg} = binary diffusion coefficient of vapor into the gas

    κ = eddy conductivity

  L_t = turbulent Lewis number, $\dfrac{c_p \; \rho D_t}{\kappa}$

  C_v = mass fraction of vapor, ρ_v / ρ

  Q_1 = a term expressing the influence of the volumetric

        absorption of heat by the entrained droplets

In the present case it would be most direct at this point to eliminate the next to the last term of equation 2-11 by observing: (1) $L \approx L_t \approx 1$ and (2) in the present case the maximum mass fraction of vapor (which occurs at the surface of the liquid film) is relatively low. Hence, the bracketed term in equation 2-11 may be assumed negligible. Thus, equation 2-11 now becomes

$$\rho u \; \frac{\partial h}{\partial x} \; + \; \rho v \; \frac{\partial h}{\partial y} \; = \; \frac{\partial}{\partial y} \; \left\{ \left[\frac{\mu}{P} \; + \; \frac{\epsilon}{P_t} \right] \frac{\partial h}{\partial y} \right\} \; + \; Q_1 \qquad (2\text{-}11a)$$

The equation for the concentration of vapor is

$$\rho u \; \frac{\partial C_v}{\partial x} \; + \; \rho v \; \frac{\partial C_v}{\partial y} \; = \; \frac{\partial}{\partial y} \left[\rho D_{vg} \; \frac{\partial C_v}{\partial y} \; + \; \rho \; D_t \; \frac{\partial C_v}{\partial y} \right]$$

$$+ \; W_v \qquad\qquad (2\text{-}12)$$

W_v = a term expressing the influence of the volumetric generation

of vapor by the entrained droplets

The equation of continuity for the gas-vapor mixture is

$$\frac{\partial(\rho u)}{\partial x} \; + \; \frac{\partial(\rho v)}{\partial y} \; = \; W_v' \qquad\qquad (2\text{-}13)$$

where

W_v' = contribution of mass to the gas-vapor mixture by the

evaporation of the entrained droplets

The boundary conditions placed on the foregoing set of equations,
as dictated by the physical situation described in Section 2.2, are:

at $x - x_0 \leq 0$, upstream of the liquid injector

$y = 0$: $u = 0$, $\tau = \tau_{sd}$, $h = h_e$, $C_v = (C_v)_e$

$y \geq \delta$: $u = u_e$, $\tau = 0$, $h = h_e$, $C_v = (C_v)_e$

at $x = x_0 \geq 0$, downstream of the liquid injector

$y = 0$: $u = u_{sf}$, $\rho v \qquad (\rho v)_s = \dot{m}_s''$, $\tau = \tau_{sf}$

$$h = h_f, \quad C_v = (C_v)_s$$
$$y \gtreqless \delta, \Delta: \quad u = u_e, \quad \rho v = 0, \quad \tau = 0, \quad h = h_e$$
$$C_v = (C_v)_e$$

where

τ_{sd} = shear stress at the wall for a dry wall with no mass transfer

τ_{sf} = shear stress at the surface of the liquid film

u_{sf} = velocity of the surface of the liquid film

$(\ )_e$ = free stream conditions

The terms relating to entrainment which appear in equations 2-10 through 2-13 bear the following comments. First, all four terms F_1, Q_1, W_v, and W_v' appear in the equations proper as opposed to being boundary conditions, and second, all four terms are functions of both x and y. Although a functional representation of these terms is a relatively straight forward matter, the explicit x-y dependence must be known before their effect on the corresponding boundary layer profiles can be determined. The x-y dependence was not determined experimentally in the subject investigation and is not derivable from an analytical approach. Hence, the influence of entrainment on the boundary layer profiles can only be discussed qualitatively.

The differential equations for the boundary layers of velocity, enthalpy and concentration above a porous wall with mass addition

are the same as equations 2-10 through 2-13 except that (1) no
analogous terms appear accounting for the entrainment of liquid,
and (2) the boundary condition in $x-x_o \leq 0$ at $y = 0$ of $u = u_{sf}$
becomes $u = 0$. Another difference between two cases not explicit
in the boundary layer equations or the boundary conditions is the
increase in surface roughness associated with gas flow over a
liquid film. Finally, the mechanism of evaporation of liquid
from a free surface has no direct analogy in porous wall cooling
with gas where no phase change occurs. The four differences
just noted between the physical situations of the evaporating
liquid film and porous wall cooling with a gas are the principal
ones.

At this point the following hypothesis will be given
relative to the comparison of the liquid film and porous wall
cooling. If it is accepted that, for steady unchanging free
stream conditions, the interactions occurring at the wall in
the two cases under consideration are reflected in the boundary
layer parameters, then any difference in the boundary layer
parameters reflects the influence of one or a combination of
the four differences in the two cases as presented in the previous
paragraph. Only one of the four differences noted was associated
with the outer regions of the boundary layer, namely, entrainment.
The remaining three differences are all associated with surface
characteristics. The influence of the aforementioned differences

on the boundary layer and transport mechanisms is discussed in sub-
sequent sections. As a basis for the subsequent discussion the
following characteristics associated with porous wall cooling are
noted (18)(21)(22)(23):

1. The description of and the correlations applicable to the
boundary layer profiles over a porous plate with mass addition
(gas) are not substantially different from the description and
correlations pertinent to the boundary layer profiles over a
smooth flat plate.

2. In the presence of heat transfer and simple mass addition
the velocity and temperature boundary layers are similar in shape.

3. The Reynolds analogy relating the momentum and heat
transfer coefficients is substantially unchanged from that Reynolds
analogy applicable to a smooth flat plate.

2.4.2 The Velocity Boundary Layer and Friction Coefficient
Definitions. Two characteristic thicknesses associated with
the velocity boundary layer are the disturbance thickness or simply,
thickness, and momentum thickness. These two parameters are defined
as usual for a compressible boundary layer as

disturbance thickness

$$\delta = y \text{ for which } u = 0.99 \, u_e \qquad (2\text{-}14)$$

and momentum thickness

$$\delta_2 = \int_0^{\infty,\delta} \frac{\rho u}{\rho_e u_e} \left(1 - \frac{u}{u_e}\right) dy \tag{2-15}$$

The characteristic lengths of x, the distance measured in the direction of flow from the starting point of the boundary layer, and momemtum thickness, δ_2, can be incorporated in Reynolds numbers. Thus,

$$Re_x = \frac{xu_e}{\nu_e} \tag{2-16}$$

and

$$Re_{\delta_2} = \frac{\delta_2 u_e}{\nu_e} \tag{2-16a}$$

where

ν_e = kinematic viscosity evaluated for free stream conditions.

The shear stress at the wall or surface, τ_s, is incorporated into the skin friction coefficient[*]

---

[*] The friction coefficient and Stanton number for flow over a liquid film are defined herein on the basis of the free stram velocity and not the relative velocity between the gas and the surface of the liquid.

$$c_f = \frac{2\,\tau_s}{\rho_e u_e^2} \qquad\qquad (2\text{-}17)$$

If the <u>local</u> value of shear stress is employed then equation 2-17

gives the <u>local</u> friction coefficient, and if an average value of

the shear stress over same increment Δ is used, then equation 2-17

gives an <u>average</u> <u>local</u> friction coefficient. If the average value

of τ_s is used based on the length x measured from the start of

the boundary layer, then equation 2-17 gives the <u>overall</u> friction

friction coefficient.

<u>Integral Momentum Relation</u>. For the same assumptions

presented in Section 2.4.1, the equation of motion, equation 2-10,

may be rewritten for the case of no entrainment as

$$\rho\, u\, \frac{\partial u}{\partial x} + \rho v\, \frac{\partial u}{\partial y} = \frac{\partial \tau}{\partial y} \qquad\qquad (2\text{-}18)$$

where the right hand side of equation 2-10 has been contracted

to a single term and entrainment has been neglected. Equation

2-18 is subject to the boundary conditions

$$\text{at } y = 0: \quad u = 0, \quad \rho v = (\rho v)_s = \dot{m}_s'', \quad \tau = \tau_s$$

$$\text{at } y = \delta \quad u = u_e, \quad \rho v = 0, \quad \tau$$

Taking into account the above boundary conditions and the equation

of continuity, equation 2-18 can be integrated to obtain the integral momentum equation in the form desired herein[*]. Thus

$$\frac{d\delta_2}{dx} - \frac{\dot{m}_s''}{\rho_e u_e} = \frac{\tau_s}{\rho_e u_e^2} \qquad (2\text{-}19)$$

where δ_2 is defined by equation 2-15. The right side of equation 2-19 can be rewritten with the aid of equation 2-17 as

$$\frac{\tau_s}{\rho_e u_e^2} = \frac{c_f'}{2} \qquad (2\text{-}19a)$$

where c_f' = local friction coefficient

It should be noted that equation 2-19 is applicable at any length, x, along the flat plate on which the boundary layer is formed, i.e., no boundary conditions containing x are prescribed. Further, equation 2-19 is applicable for compressible flow with heat and mass transfer at the wall, but only for constant pressure.

---

[*] The application of equation 2-19 to the liquid film does not take into account the surface velocity of the film. Equation 2-17 and the right hand side of equation 2-19 are, however, consistent in the use of the free stream velocity, and hence, relate to the same surface shear stress. The value of the mass transfer parameter, $\dot{m}_s''/\rho_e u_e$, was more than an order of magnitude less in the subject investigation than the other two terms of equation 2-19. As a result, the use of the free stream velocity or the relative velocity of the gas with respect to the liquid for this term is of no significance numerically.

Although the derivation of equation 2-19 neglected the influence of entrainment, a derivation based on a control volume of the integral momentum equation can be made which includes an entrainment term (see Reference 24 for a representative control volume derivation). Such a derivation shows that the influence of entrainment on the growth of the momentum thickness is analogous to an additional surface shear stress. Hence, the integral momentum equation presented in equation 2-19 remains valid except that the term τ_s must be thought of as an "effective" surface shear stress including the effects of entrainment.

Velocity Profiles. The velocity profile in a turbulent boundary layer is subject to correlation by several different methods. The two methods which will be employed herein are: (1) correlations based upon the friction velocity, u_τ, and (2) the power law relation.

In the correlation of the velocity profile by the first method the boundary layer is divided into three regions. These three regions are: (1) the viscous sublayer which is immediately adjacent to the wall, (2) the wall region which extends from the edge of the viscous sublayer to approximately 0.10 to 0.20 the thickness of the boundary layer, and (3) the outer region or wake region which extends outward from the wall region to incorporate the remainder of the boundary layer.

Figure 2 in Section 2.3.1 presents the universal law of

the wall for an incompressible turbulent boundary layer on a smooth

surface. Figure 8 presents the generalized velocity distribution or

the law of the wall for a compressible turbulent boundary layer on

a smooth surface. The curves presented were taken from Deissler

and Loeffler, Reference 25. The dimensionless velocity parameter,

u^+, and the dimensionless distance from the wall, y^+, are defined as

$$u^+ = \frac{u}{(\tau_s/\rho_s)^{1/2}} = \frac{u}{u_\tau} \qquad (2\text{-}20)$$

and

$$y^+ = \frac{y(\tau_s/\rho_s)}{\nu_s} = \frac{yu_\tau}{\nu_s} \qquad (2\text{-}20a)$$

for compressible flow.

The symbol β appearing in Figure 8 is termed the heat transfer

parameter and is written as

$$\beta = \frac{q_s u_\tau}{c_p T_s \tau_s} \qquad (2\text{-}21)$$

where q_s = heat flux at the surface, B/ft^2-sec. A positive value of

β implies heat addition to the boundary layer and a negative value

of β implies heat loss (cooling) from the boundary layer. The

three curves appearing in Figure 8 show the representative influence
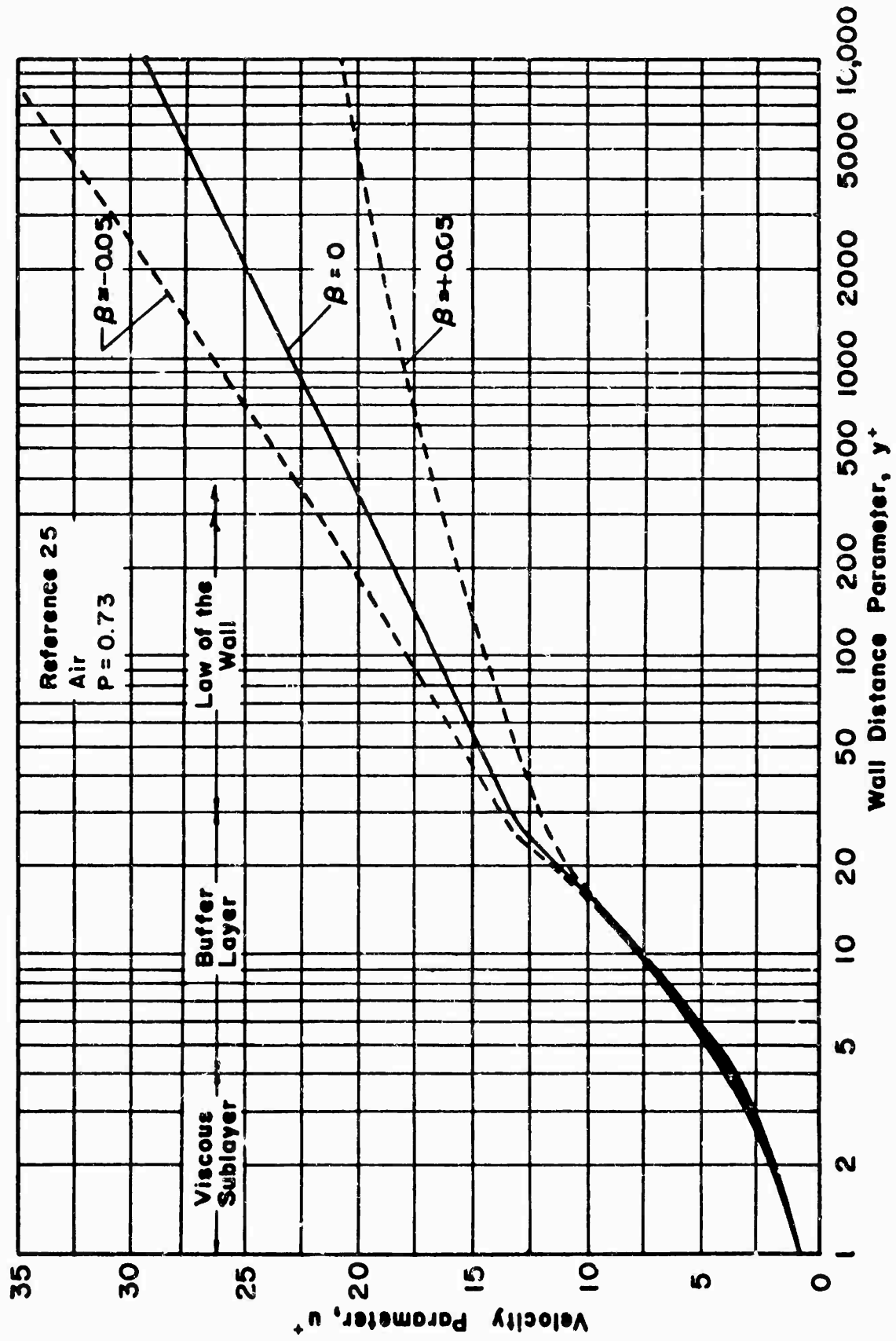
Figure 8. Generalized Velocity Distribution for a Compressible Turbulent Boundary Layer on a Smooth Surface

of heat transfer on the law of the wall profile. The viscous sublayer
is represented by the equation

$$u^+ = y^+ \qquad (2\text{-}22)$$

and it extends to $y^+ = 5$ for the adiabatic case. The law of the
wall extends from the viscous sublayer outward to $y^+ = 1000$ to
3000, with y^+ increasing for increasing Reynolds number.

The law of the wall for the adiabatic boundary layer was
employed herein to judge the accuracy of the measurements ob-
tained in the boundary layer over the test plate in the subject
investigation. Of the parameters appearing in equations 2-20 and
2-20a, the velocity, u, the distance above the surface, y, and
the shear stress, τ_s, were experimentally derived parameters.
Correlation of the boundary layers measured above the wetted
test plate further incorporated the heat flux, q_s.

Figure 9 presents the <u>velocity</u> <u>defect</u> <u>parameter</u> for
turbulent boundary layers at constant pressure as a function of
the ratio of the distance from the wall to the boundary layer
thickness (27). The curve is termed the universal velocity pro-
file for a turbulent boundary layer. The correlation represented
by the curve of Figure 9 is applicable to the correlation of the
outer region of an isothermal boundary layer beyond the extent of
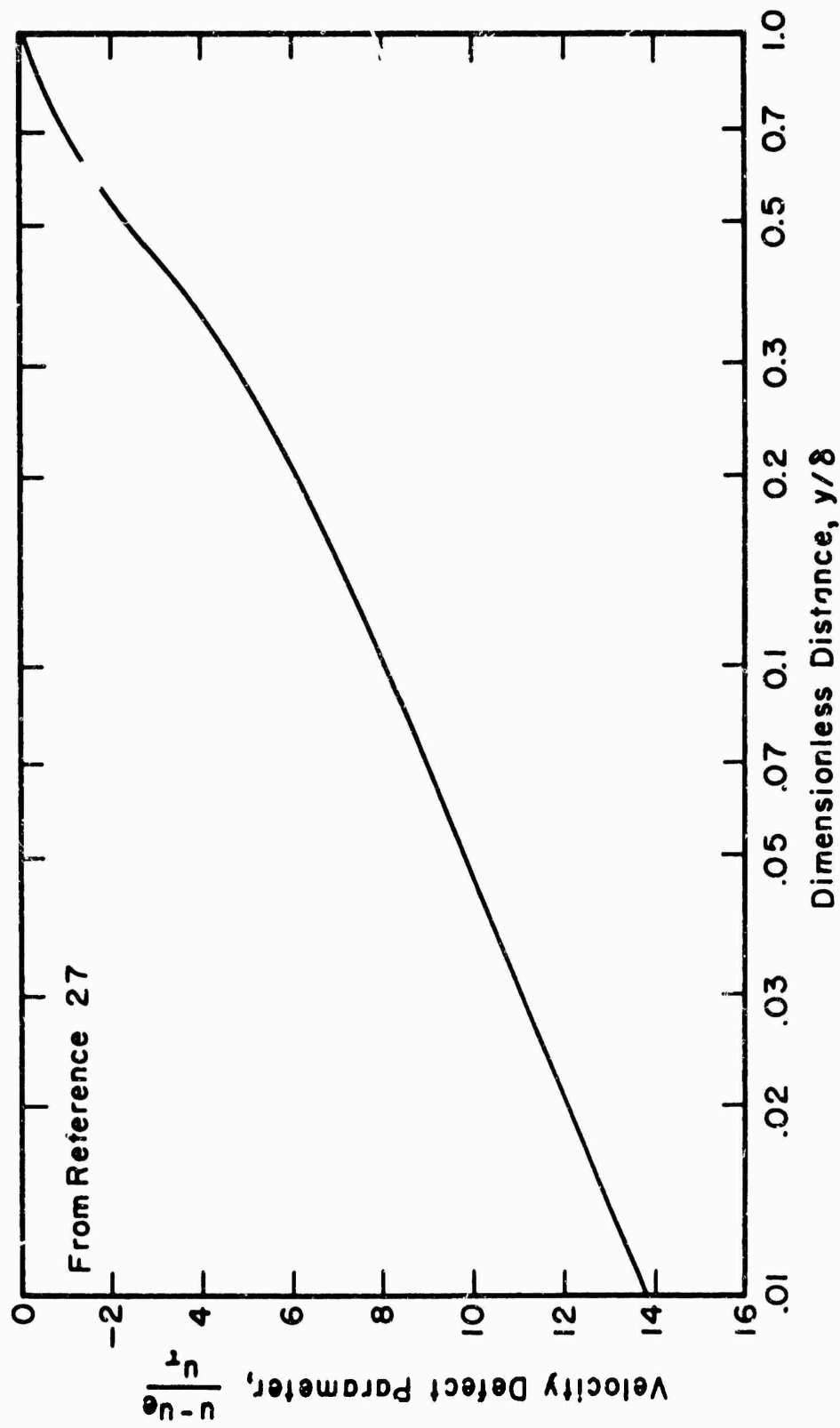
Figure 9. Universal Velocity Profile for a Turbulent Boundary Layer in Constant Pressure

the law of the wall (the curve of Figure 9 also overlaps a portion of the law of the wall).

Table 2, reproduced here from Reference 2, presents the values representative of the thickness or extent of the various regions relative to the thickness of the boundary layer at several Reynolds numbers for incompressible flow. The values shown in Table 2 are approximately correct for the boundary layers studied in the present investigation at a Reynolds number of 10^7.

Table 2

Values of the Thickness Ratios for an Incompressible Turbulent Boundary Layer for Various Length Reynolds Numbers on a Flat Plate (1/7th power law)

Re_x	Viscous sublayer δ_{lam}/δ	Buffer layer δ_{buf}/δ	Law of the Wall δ_{lw}/δ
10^5	0.025	0.152	-
10^6	0.005	0.030	1.000
10^7	0.001	0.006	0.201
10^8	0.0002	0.001	0.040
10^9	0.00004	0.0002	0.008

$\delta = 0.4$ in., $Re_x = 10^7$ in subject investigation. The "thinning down" of the various regions for an increase in the Reynolds number is quite apparent. Reynolds numbers of the order of $5 \cdot 10^6$ to 10^7 are representative of the values encountered

in the present investigation.

Turning now to the power law correlation for the velocity
profile this well known relation is

$$\frac{u}{u_e} = (\frac{y}{\delta})^{\frac{1}{n}} \tag{2-23}$$

The exponent 1/n varies between one third and one tenth
(constant pressure flow) depending on the surface characteristics
of the wall and the Reynolds number. For a single appropriate
value of the exponent equation 2-23 may correlate as much as
99 percent of a boundary layer, failing to do so only very close
to the wall. Such a range includes the entire outer region as
well as much of the wall region of the boundary layer. Since
virtually all constant pressure turbulent boundary layers can
be correlated by equation 2-23, the power law relation offers
not only a convenient representation of experimental data but
also suffices to evaluate the scatter of such data.

2.4.3 Influence of Various Wall Effects on the
Velocity Profile and the Friction Coefficient

Roughness Effects. Where a viscous sublayer is present
the shear stress and heat flux at the wall are given as

$$\tau_s = \mu(\frac{du}{dy})_{y=0} \tag{2-24}$$

and

$$q_s = -k\left(\frac{dT}{dy}\right)_{y=0} \tag{2-24a}$$

The magnitude of the shear stress and heat flux are dependent on
the molecular properties of viscosity and thermal conductivity.
If the viscous sublayer is not present to act as a buffer to the
adjacent turbulent region, then the magnitude of the shear
stress and heat transfer will increase in general. The increase
arises from the eddy contributions to the viscosity and thermal
conductivity. The relative thinness of the viscous sublayer
as noted in Table 2 makes this region susceptible to the effects
of surface roughness, and this in turn, leads to an influence
on the transport processes and the velocity profile in the
boundary layer.

In dealing with the influence of a uniform surface roughness
on the velocity boundary layer and the corresponding skin friction,
it is necessary to consider three "regimes" of roughness. The
three regimes are described by the magnitude of the roughness
parameter defined as

$$\frac{k_r u_\tau}{\nu} \tag{2-25}$$

where

k_r = effective height of the roughness protrusions.

For roughness generated artifically by sand glued to the inside

of a pipe the regimes of roughness are defined as follows (28):

1. Hydraulically smooth regime:

$$0 \leq \frac{k_r u_\tau}{\nu} \leq 5 \qquad (2-25a)$$

The size of the roughness is so small that all protrusions

are contained within the viscous sublayer.

2. Transition regime:

$$5 \leq \frac{k_r u_\tau}{\nu} \leq 70 \qquad (2-25b)$$

Protrusions extend partly outside the viscous sublayer and the

additional resistance as compared with the smooth wall is mainly

due to form drag experienced by the protrusions in the boundary

layer.

3. Completely rough regime:

$$\frac{k_r u_\tau}{\nu} > 70 \qquad (2-25c)$$

All protrusions reach outside the viscous sublayer and by far the

largest part of the resistance to flow is due to form drag which

acts on them.

The ratio of the height of the roughness elements, k_r, to the radius the pipe is termed the <u>relative</u> <u>roughness</u>. The corresponding definition for the case of rough plates is the ratio of k_r to the thickness of the boundary layer δ. Then, the foregoing delineation of the regimes of roughness in pipes is applicable to flow over rough flat plates if relative roughness is based on k_r/δ.

The roughness generated by the surface disturbances on a liquid film is amenable to treatment by the roughness criteria just discussed provided some suitable value of k_r can be obtained (see Section 2.3.2).

The influence of surface roughness on the shape of the velocity profile and on the magnitude of the friction coefficient is well established (27)(28). The friction coefficient for a particular boundary layer on a flat plate is unaffected by roughness so long as the flow is hydraulically smooth. The friction coefficient increases, however, as the effect of the roughness elements is felt outside the viscous sublayer. Where this effect is present, the influence of the roughness elements on the boundary flow is such as to increase the friction coefficient and cause the velocity profile to become less full, all other variables constant. The recession of the velocity profile, which is caused by the increased friction coefficient, is manifest by the decrease of n in the exponent of the power law distribution.

The relative roughness of the liquid film in the subject investigation can be predicted qualitatively from the estimate of surface roughness presented in Section 2.3.2. Assuming a surface roughness, k_r of 0.005 in. and a buffer layer thickness of 0.003 in. (for which $\frac{yu_\tau}{\nu} = 30$) based on Table 2 for a Reynolds number of 10^7, the value of the roughness parameter, $\frac{k_r u_\tau}{\nu}$, is approximately 50. This corresponds to the transition regime of roughness. The increase in the friction coefficient at the limit of the "rough regime" at $\frac{k_r u_\tau}{\nu} = 70$ is approximately 65 percent for incompressible flow at the nominal Reynolds number of 10^7 of the subject investigation (28). Hence, the increase in the friction coefficient due to surface roughness of the liquid film can be estimated to be approximately 40 to 50 percent based on the ratio of the predicted value of $\frac{k_r u_\tau}{\nu}$ for the liquid film to the value of $\frac{k_r u_\tau}{\nu}$ for the fully rough regime.

Figure 10 presents the influence of the roughness parameter, $\frac{k_r u_\tau}{\nu}$, on the law of the wall for incompressible flow. As the value of the roughness parameter increases the law of the wall shifts to lower values of the dimensionless velocity parameter but remains parallel to the law of the wall for a smooth wall. The amount of the shift of the curve for the previously predicted roughness parameter of 50 is seen to be significant.

An investigation of annular flow with a hot gas in which the friction coefficient was measured was performed by Mezey (30). Mezey reports results obtained for annular film flow of water in a 1.5 in.
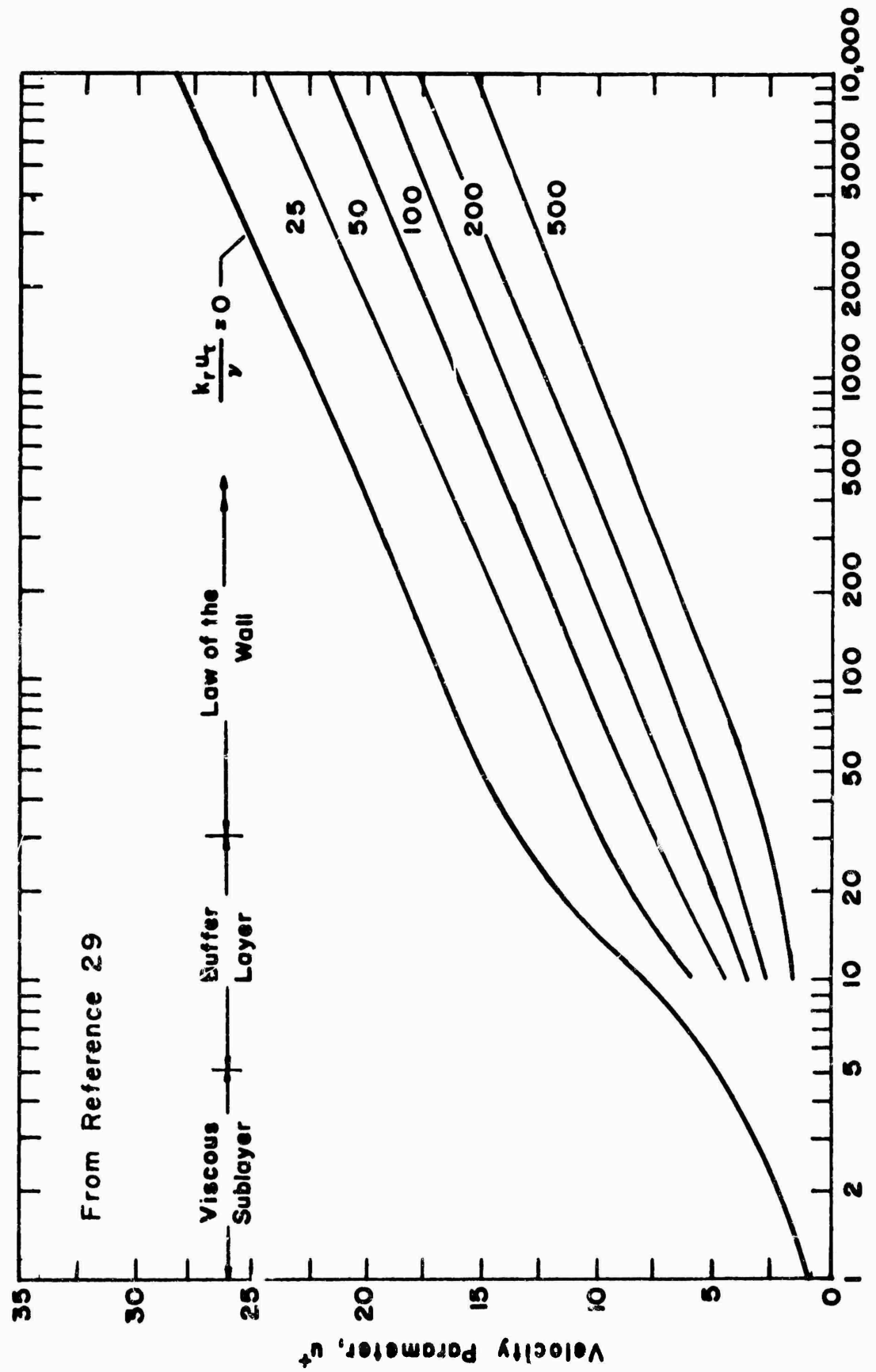
Figure 10. Influence of Surface Roughness on the Law of the Wall

diameter tube in co-current flow of heated air. The static pressure was varied from 1 to 2 atm, air velocity from 40 to 207 ft/sec and air temperature from 104 to 355 F. Entrainment was present in a portion of the investigation. For an air Reynolds number of 10^5 which is approximately one-third the equivalent value of the subject investigation and an air temperature of 314F, Mezey reports an increase in the friction coefficient for the liquid film compared to the dry tube of from 10 to 60 percent for an initial dimensionless liquid flow rate, W^+, from 30 to 120. Entrainment was reported for those values of W^+ in excess of 80 or 90 for the aforementioned conditions. Mezey noted one further result of significance relative to the subject investigation, namely, that the ratio of the wet wall to the dry wall friction coefficient decreases with an increase in the temperature of the air for a constant gas Reynolds number and dimensionless liquid flow rate.

Discontinuous Surface Roughness. Related directly to the previous topic of roughness is the aspect of a stepwise change in surface roughness found in the present investigation. The flow leaves the smooth surface of the lead section and enters the test section where the surface of the film is rough. For the transition from the smooth to the rough wall the variation in shear stress in the boundary layer has the following characteristics: (1) the shear stress at the wall increases

stepwise to almost the value which will be identified with the fully developed flow further downstream, and (2) the shear stress adjusts to the new value at the wall by increasing from the wall outward as the flow proceeds downstream, finally achieving a new distribution at some location downstream. The preceding two points can be expressed in an equation for flow in a channel after Jacobs as summarized in Reference 28. Thus,

$$\tau(x,y) = \{\tau_{sm} - (\tau_{sm} - \tau_r)e^{-11.6^{y/}x}\} \frac{h-y}{h} \qquad (2\text{-}26)$$

where

τ_{sm} = shear stress for the flow in the smooth lead
      section

τ_r = shear stress for the flow in the rough section

y = distance from the wall

h = height of the channel

A qualitative estimate of the length required for a boundary layer to adjust to a stepwise change in surface roughness can be obtained from equation 2-26 by setting h equal to δ. If this is done, complete adjustment of the shear stress distribution is achieved at a length downstream of the stepwise change of approximately $x = 20\delta$. This length corresponds to approximately 8 inches downstream of the liquid injector slot in the subject investigation.

In the completely rough regime in incompressible flow the overall friction coefficient is given by (28)

$$c_f = (1.89 + 1.62 \log \frac{x}{k_r})^{-2.5} \tag{2-27}$$

The similar expression for the overall friction coefficient for flow over a smooth flat plate (turbulent from the leading edge) is

$$c_f = 0.455(\log Re_x)^{-2.58} \tag{2-28}$$

On comparing equation 2-26 to equation 2-28 it can be seen that as the roughness increases from hydraulically smooth to completely rough, the friction ccefficient becomes a function of the roughness of the wall as expressed by k_r as well as a function of the history of the flow as expressed by the Reynolds number or x. The foregoing fact is of consequence in the present investigation where an initial boundary layer was formed over a smooth plate and the boundary layer was subsequently subjected to the influence of the surface roughness of the liquid film. The above indicates that caution must be exercised in relating the friction coefficient associated with the flow over the liquid film to the Reynolds number based on an overall length of flow where a stepwise change in surface roughness is present.

Heat Transfer Effects. The friction coefficient (and hence, the velocity profile) is influenced by the temperature profile in

the boundary layer through compressibility effects. The magnitude of the influence in turn depends not only upon the temperature ratio across the boundary layer but also on the ratio of the thickness of the velocity boundary layer to the thickness of the temperature boundary layer, δ/Δ. Reference 31 presents in tabular form the ratio of the local friction coefficient for flow with heat transfer to the local friction coefficient for isothermal flow for low Mach numbers at large Reynolds numbers and affinely similar 1/7 profiles of velocity and temperature. At the value of the ratio of surface temperature to free stream temperature of the subject investigation, namely 0.75, the increase in the friction coefficient is approximately 12 percent for δ/Δ ratios of 1 to 5. The latter range of thickness ratios includes that range encountered in the subject investigation. The predicted relative magnitude of the influence of heat transfer on the friction coefficient is seen to be approximately 25 percent of the corresponding influence predicted for surface roughness.

Mass Addition due to Evaporation. It was noted previously that the case of simple mass addition is quite well documented both analytically and experimentally. The value of friction coefficient decreases as the magnitude of the mass addition increases. The velocity profile tends to become less full (power law n decreases) and near the wall the velocity gradient becomes less than for a flow over the same surface without mass addition.

The magnitude of the mass addition due to evaporation of the liquid film in the subject investigation was relatively small. In the momentum integral equation, equation 2-19, the magnitude of the $\dot{m}_s''/\rho_e u_e$ was approximately an order of magnitude or more, less than the right hand side of the equation. If the evaporative mass addition influences the friction coefficient for the flow over the liquid film to the same extent as the same mass flux in simple mass addition would, then the friction coefficient would be reduced approximately 5 percent or less. The corresponding influence on the velocity profile beyond the wall region would be slight. It should be noted, however, that the addition of mass by evaporation from the rough surface of the liquid film which also has a surface velocity may present a situation entirely different from that of simple mass addition (see Evaporation, Section 2.3.2).

Entrainment. The drag effects on the boundary layer caused by entrained liquid result in an apparent increase in the friction coefficient as was noted in the discussion of the integral momentum equation. The velocity profile responds by receding as with an increase in surface roughness but the recession of the velocity profile is dependent on the x-y distribution of the entrained liquid.

2.4.4 The Temperature Boundary Layer and the Stanton Number

Definitions. Analogous to the defining of characteristic

thicknesses in the velocity boundary layer, two characteristic

thicknesses associated with the temperature boundary layer are:

thickness of temperature boundary layer

$$\Delta = y \text{ for which } T = 0.99 \ T_e \qquad (2\text{-}29)$$

and enthalpy-deficit thickness

$$\Delta_2 = \int_0^{\infty, \Delta} \frac{\rho u}{\rho_e u_e} \ (1 - \frac{h - h_e}{h_s - h_e}) \ dy \qquad (2\text{-}30)$$

For the assumption of constant specific heat and a single

constituent gas the enthalpy terms of equation 2-30 can be

represented by their corresponding temperature.

The Stanton number is

$$S = \frac{q_s}{\rho_e u_e c_p (T_e - T_s)} \qquad (2\text{-}31)$$

If the heat flux term in equation 2-31 represents the local heat

flux, then the corresponding Stanton number is the local Stanton

number, S_x. Similarity, if the heat flux term represents the average

value over some increment of flow length, then equation 2-31 gives

an average Stanton number, $\overline{S}$.

Integral Energy Relation. In a manner similar to that

described for the integral momentum equation, the energy equation

for the boundary layer, equation 2-11a, may be integrated subject to the assumptions of Section 2.4.1 to obtain the <u>integral energy equation</u>. Thus (31)

$$\frac{d\Delta_2}{dx} + \Delta_2 \left[\frac{1}{\Delta T} \left(\frac{d(\Delta T)}{dx} \right) \right] - \frac{\overset{\circ}{m}_s''}{\rho_e u_e} = $$

$$\frac{q_s}{\rho_e u_e c_p (T_e - T_s)} \tag{2-32}$$

The bracketed term on the left hand side of equation 2-32 accounts for a changing temperature potential with length. The right hand side of equation 2-32 is recognized to be the Stanton number. Like the integral momentum equation, the integral energy equation above is applicable for compressible flow with mass transfer but is restricted herein to a constant pressure and low speed flow.

The integral energy equation relates the change in the enthalpy-deficit thickness to the Stanton number. The enthalpy-deficit thickness can be determined experimentally, and hence, equation 2-32 written in finite difference form can be employed to determine the Stanton number once values have been ascribed to the second and third terms on the left hand side of equation 2-32. This technique was employed to evaluate the data obtained in the subject investigation.

<u>Temperature Profiles</u>. Two correlations applied herein to the temperature profiles are: (1) a dimensionless correlation

analogous to the law of the wall for the velocity profile, and (2) the power law relation.

Figure 11 presents the dimensionless temperature parameter for the temperature boundary layer as a function of the dimensionless distance from the wall for a smooth surface. The curves presented were taken from Deissler and Loeffler, Reference 25. The dimensionless temperature parameter, T^+, is defined as

$$T^+ = \frac{(T_s - T)c_p \tau_s}{q_s u_\tau} = \frac{1 - \frac{T}{T_s}}{\beta} \tag{2-33}$$

where β is defined in equation 2-21. The dimensionless distance from the wall, y^+, is defined by equation 2-20a for compressible flow. The three curves in Figure 11 display the influence of heat transfer on the dimensionless temperature profile. The profiles in Figure 11 have corresponding regions based on y^+ similar to the viscous sublayer, the buffer layer and the law of the wall.

The dimensionless profile of Figure 11 was employed to correlate the temperature profiles measured above the wetted test plate. As in the case of the law of the wall such a correlation involves several experimentally determined parameters and thus, affords a check on the consistency of the experimental data.

The power law correlation for the temperature profile is defined as

$$\frac{T - T_s}{T_e - T_s} = (\frac{y}{\Delta})^{\frac{1}{n}} \tag{2-34}$$
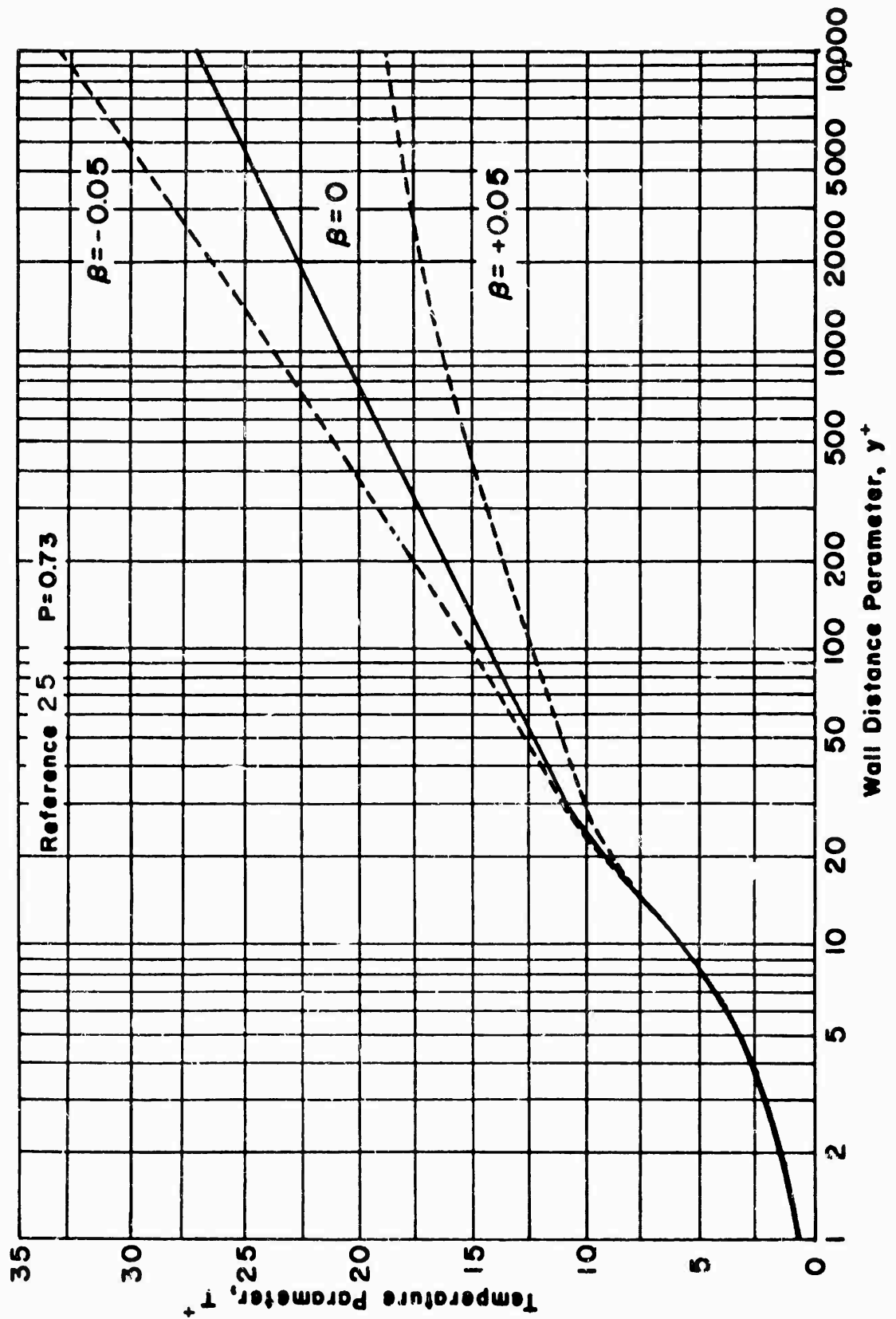
Figure 11. Generalized Temperature Distribution for a Compressible Turbulent Boundary Layer on a Smooth Surface

The properties and uses of the power law expressed by equation 2-34 are quite analogous to those discussed for the same correlation applied to the velocity in Section 2.4.2 and will not be repeated here.

2.4.5 Influence of Various Effects on the
Temperature Profile and the Stanton Number

Reynolds Analogy. The Reynolds analogy relates to the fact that the transport mechanisms involved in momentum, heat and mass transfer are similar when such transfer processes are occurring. The similarity is present in the relationship of the magnitudes of transfer coefficients to one another and also to the shape of the appropriately defined profiles of velocity, temperature and concentration in the flow field. In the subject investigation it is the relationship between the momentum and heat transfer processes which is of principal interest since these were evaluated experimentally for the unstable liquid film.

The direct correspondence between the friction coefficient and the Stanton number by Reynolds analogy is

$$\frac{c_f'}{2} = S_x \tag{2-35}$$

for $P = P_t = 1$.

Equation 2-34 is, in general, not exactly valid, the Stanton number being greater or less than indicated depending on the flow

situation (excluding restrictive cases such as adiabatic flow).
Nevertheless, equation 2-35 displays a remarkable degree of agree-
ment in a wide variety of flow situations. The validity of Reynolds
analogy for the case of gaseous flow over an unstable liquid film
was examined in the subject investigation. The identification
of such validity in any unusual flow situation is most informative.
The validity of Reynolds analogy in the unusual flow implies that
the description of the transport mechanisms is not substantially
different from the description of the same transport mechanisms
in other flow situations wherein Reynolds analogy is known to be
valid.

With respect to the velocity and temperature profiles in
the boundary over the liquid film Reynolds analogy, if it is
present, implies that the influence of a certain effect such as
heat transfer on one profile will be similarly reflected in the
other profile. The generalized velocity and temperature distri-
bution presented in Figures 8 and 11 display the similar influence
of heat transfer. In the subject investigation, however, certain
aspects of the flow were different from say, those associated with
the flow of a gas over a smooth isothermal plate, a case where the
direct Reynolds analogy is approximately valid. Two principal
differences, the effect of which on Reynolds analogy will be noted,
were the discontinuity in surface temperature occurring at the
injector slot and the surface roughness of the liquid film. The
results of studies relative to these two effects are available and

permit some discussion relative to the subject investigation. The
influence of the finite velocity of the surface of the liquid film
on Reynolds analogy and the corresponding influence on predictions
based on the analogy has apparently not been established.

Roughness. The influence of surface roughness on the heat
transfer coefficient is such as to cause it to increase as the
friction coefficient does but at a lower rate. The rate of heat
transfer immediately adjacent to a surface, no matter how irregular
the surface may be, is dependent on a molecular property of the
fluid, i.e., thermal conductivity. On the other hand shear stress,
augmented by roughness, is transmitted to the surface as a form
drag on the roughness element. Hence, it would be expected that
the expression of Reynolds analogy as given by equation 2-35
would show a divergent trend for increasing surface roughness.
Such an effect has been identified (32). The magnitude of the
effect is, however, relatively small for flow regimes from
transition to fully rough flow.

Discontinuous Wall Temperature. The problem of heat trans-
fer in a turbulent flow over a smooth surface having a stepwise
discontinuity in surface temperature has been examined both
analytically and experimentally (33)(34)(35).

The results of such work indicate that for the incompressible
flow of air with a uniform free stream velocity the Stanton number
for the flow with a stepwise discontinuity can be related to the
Stanton number for flow over a surface of constant temperature

through a length ratio. The length ratio is the ratio of the length
of flow before the temperature discontinuity to the total length
of flow. The expression correlating the work of Reynolds et al (35),
in terms of the present nomenclature is

$$\frac{S}{S_i} = \left[1 - \left(\frac{x_o}{x}\right)^{\frac{9}{10}} \right]^{-\frac{1}{9}} \tag{2-36}$$

where x_o = length of lead section

   x = total length of flow

   $x_o + (x - x_o)$

   S = Stanton number for stepwise change in wall
   temperature

   S_i = Stanton number for constant wall temperature

Equation 2-36 shows that the value of the Stanton number after the
surface temperature discontinuity is greater compared to the Stanton
number for a constant surface temperature. This result is due to
the fact that the temperature boundary layer after the discontinuity
is thinner than if it had started growing at the initiation of the
boundary layer and subsequently grew over a constant temperature
surface. As a result the temperature gradients through the tempera-
ture boundary layer are steeper and the heat transfer is greater
than it would be for the flow over a constant temperature surface.

In the subject investigation the length of the lead section
was 18 in. while the length of the test plate was 22 in. For the
foregoing dimensions equation 2-36 predicts an average increase

of approximately 20 percent in the overall Stanton number in the test
section as a result of the temperature discontinuity caused by the
injection of the liquid film. It will be noted that the temperature
discontinuity does not lead to a co responding increase in the
friction coefficient. For incompressible flow the velocity profile
is not coupled to the temperature profile. Further, in Section
2.4.3, it was noted that the increase in the coefficient of
friction caused by heat transfer from the compressible gas was
only weakly dependent on the ratio of the thicknesses of the
velocity and temperature boundary layers.

The temperature profiles in the boundary layer after the
temperature discontinuity are thinner but fuller than the
corresponding temperature profiles in the boundary layer over
an isothermal plate. The temperature profiles measured by
Reynolds et al (35) after a stepwise increase in wall temperature
correlated to a 1/8 to 1/7 power law distribution whereas the
temperature profiles measured over a constant temperature wall
were correlated to a 1/5.6 power law distribution, both cases for
the same values of Reynolds number. The aforementioned variation
in the shape of the profiles represents as much as 10 percent
variation in the dimensionless temperatures observed in the two
boundary layers.

2.4 Summary

The preceding discussion presented a description of the inter-
actions between a liquid film and a moving stream of gas which bears
on the subject investigation. The material presented contained
predictions and some numerical estimates of the influence of certain
effects associated with the liquid film on the velocity and tempera-
ture profiles in the boundary layer and the derived parameters of
friction coefficient and Stanton number. The principal points are
summarized as follows:

1. There exists some length downstream of the point of
liquid injection in which the gas flow and liquid film adjust to
each other.

2. The temperature of the liquid film achieves some
equilibrium value determined by the fluid mechanic and thermodynamic
conditions of the flow. The value of the temperature predicted for
the subject investigation was approximately 250F.

3. The unstable surface of the liquid film acts as a rough
surface with respect to the gas. The predicted height of the
apparent roughness of the liquid film was 0.003 to 0.006 in.; these
values being two or three times greater than the flow mean thickness
of the liquid film.

4. The influence of entrained liquid in the boundary layer
cannot be stated quantitatively.

5. Comparing the gas and liquid film flow of the subject
investigation with the case of simple mass addition through a
porous plate it was noted that for the latter there exists (1) no
entrainment, (2) no surface roughness, (3) no evaporation, and

(4) no surface velocity.

6. The dimensionless velocity and temperature profiles measured over the wetted test plate should correlate to a power law distribution and to the law of the wall in a manner prescribed by the surface conditions.

7. The temperature profile measured over the wetted test plate should be fuller than the velocity profile as a result of the temperature discontinuity at the point of injection of the liquid film. Further, as a result of the temperature discontinuity the Stanton number for the wetted test section could reflect an approximate 20 percent increase relative to that value for an isothermal plate.

8. The friction coefficient would increase in the presence of the liquid film due to the presence of surface roughness and heat transfer, and decrease due to the presence of mass transfer. The magnitudes of the influences of the foregoing effects on the friction coefficient relative to that for a smooth dry adiabatic wall were estimated to be +40 to 50%, + 10% and less than -5%, respectively.

3. EXPERIMENTAL RESULTS

The objectives of the experimental investigation of the flow of an unstable evaporating film of liquid and a moving stream of hot gas as discussed herein were as follows:

1. To examine the surface characteristics of the liquid film both visually and photographically, and to measure the temperature of the liquid film.

2. To determine the velocity and temperature profiles in the gaseous boundary layer above the liquid film.

Section 3.1 presents a brief description of the experiments and of the experimental procedures Section 3.2 presents the results of the film characteristics experiments; Section 3.3 presents the results of the boundary layer measurements.

3.1 Description of Experiments and Experimental Procedure

3.1.1 Film Characteristics Experiments

The film characteristics experiments were conducted as an exploratory study designed to reveal the nature and description of the liquid film, and were not designed to be the basis of a formal parametric study. The information obtained was subsequently applied to establishing the experimental procedure associated with the boundary layer measurements. Considerable

effort was directed toward establishing uniform injection of liquid so as to obtain the uniform coverage of the test plate by the liquid, followed by an even, well defined location or region of film termination at some distance downstream of the liquid injector.

Figure 1,in Section 2,presents a schematic diagram of the flow channel in which the experiments were conducted. The test plate on which the liquid was injected as a thin film was 4 in. wide by 22 in. long. The test section was preceded by an 18 in. long lead duct (following the final set of turbulence grids). The liquid film was injected tangentially onto the test plate by a spanwise slot located at the fore end of the test plate. The liquid film covered the entire length of the central portion of the test plate.

The general procedure followed during an experiment was to allow the apparatus to reach thermal equilibrium at a fixed temperature (hot or cold), for a fixed total pressure, and a fixed flow rate of the gas. The principal variable was the liquid flow rate which could be set at several constant values, each for a period of time to permit observation. After several liquid flow rates had been run at a fixed gas flow point, the gas flow rate through the test section (and hence, gas velocity) was changed by increasing or decreasing the nozzle area. The total temperature (in hot flow) and total pressure were again adjusted to the previous values. After thermal equilibrium had again been established another series of liquid flow rates would be run. In some experiments the total pressure was varied as a parameter but such variation was infrequent.

For any one run point in which all of the flow parameters were
stationary the following measurements and observations could be made.

1. The distribution of the temperature in the test plate as
measured by 38 imbedded thermocouples and 16 spotwelded thermocouples
located on the bottom (external side) of the test plate, and 7
thermocouples located in the manifold cavities of the liquid
injector.

2. The temperature of the liquid film as measured by a thermo-
couple mounted flush with the wetted surface of the test plate.

3. Visual observation through the viewing ports of the
coverage of the film, the location of dry spots, the weaving of
the film back and forth spanwise, and the termination of the film.

4. Photographic observation through the viewing ports of
the instantaneous configuration of the surface of the liquid film
in the field of view of the camera.

All of the observations and measurements were coordinally known
with respect to the distance measured longitudinally from the liquid
injector, i.e., the parameter $x - x_o$

3.1.2 Boundary Layer Measurements

The measurement of the profiles of velocity and temperature in
the boundary layers was directed toward a quantitative determination
of these parameters. The configuration of the apparatus was the
same as in the film characteristics experiments except for the
presence of the boundary layer probe in the test plate. The probe
was located on the centerline of the test plate, being inserted
selectively through one of eight removable plugs located along the

centerline of the test plate. Unlike the film characteristics experiments, during all of the boundary layer measurements reported herein the apparatus was operated at one running point, termed the nominal operating point. Table 1, Section 1, presents the flow conditions of the nominal operating point. The liquid flow rate was 0.0065 lb/sec. or 0.0016 lb/in-sec. A measurement set consisted of a velocity and/or temperature profile determined at a fixed distance downstream of the liquid injector at the nominal operating point.

In the investigation four measurement sets were taken for the wetted test plate at the one liquid flow rate and three measurement sets were taken for the dry test plate, all seven being for the same nominal gas flow conditions. Table E.1, Appendix E, summarizes the operating data for the apparatus for the seven measurements sets. The boundary layer profiles as a function of the axial distance along the test section were ensemble data collected in several test runs with the apparatus at the nominal operating point. The last column in Table E.1 presents the deviation of the operating conditions of the apparatus during a particular run from the nominal operating conditions for which the ensemble data are reported herein

The general procedure for obtaining the boundary layer data for the wetted test plate and dry test plate was the same in both cases. The probe was located at a particular axial position and a sufficient number of runs were made in order to describe the boundary layer at that particular location. The probe was then moved to a different location. The axial positions of the probe

were the same for both the wet and dry plate experiments except no

measurement was made at $x - x_0 = 5$ in. for the dry plate.

The parameters measured during any particular experiment

included all the parameters necessary to specify the data shown

in Table E.1 (see also Appendix B) and the following:

1. The height of the sensing elements of the probe head

as indicated by the probe position determination system (see

Appendix B).

2. The static pressure and the differential velocity

pressure measured at the probe head as indicated by pressure

transducers.

3. The total temperature measured by the thermocouple

on the probe head.

4. The temperature distribution in the test plate.

The further description of the details of the experimental

apparatus and experimental procedure is presented in Appendices

B and C. The details of the methods of reduction of the data

are presented in Appendix D.

3.2 Results of the Film Characteristics Experiments

3.2.1 Methods of Evaluation and Correlation of Results

Visual Observations. The results of the visual observations

are presented as a verbal description of the characteristics of the

flow of the film observed through the viewing ports in the test

section during the experiments. The aspects of coverage of the

test plate by a liquid film, the appearance of dry spots and the

termination of the liquid film were readily discernable. The liquid film, which was wavy or unstable, appeared whitish as compared to the surface presented by the polished test plate. Any weaving of the film back and forth spanwise across the test section or advancement and recession of the film during termination were detectable by the motion of the film back and forth over alternately wet and dry portions of the plate.

Visual observations of the interfacial structure of the liquid film were not possible because of the motion of the surface of the film (approximately 7 ft/sec). Entrainment of liquid in the gas flow above the film was discernable only if a sufficient number of droplets were present to cause blurring and refraction of the image in the observed area. The detection of the presence of entrainment as just described was not possible in the early stages of instability.

Photographic Observations. The view angle of the camera onto the liquid film was 10° to the test plate and perpendicular to the direction of the flow (see Figure B.10) The depth of field permitted a spanwise width of from 1/2 in to 1 in. of the liquid film to be photographed in focus The characteristics of the illumination incident from the light source (a 3μ sec. strobe unit, see Appendix B) limited the length of the field of view to approximately 1 1/2 in. or less depending on the composition of the image. The photographs taken of the liquid film through the viewing ports presented an instantaneous configuration (3μ sec), i.e., the flow of the film was more or less

completely "stopped". The distance a portion of the film could move
at a surface velocity of 5 ft/sec during the photographic event was
less than 0.001 in.

Figure 12 presents a representative photograph of the appearance
of a liquid film partially wetting the surface of the test plate.
The regions of dry plate are readily discernable from the regions
covered with liquid. The 0.030 in. high dividing fences which appear
in the photograph were helpful in height discrimination of the waves
on the surface of the film. The bright area at the top center of
the photograph is the light incident from a viewing port. The
scale of the photograph is denoted by the insert.

Figure 13 presents two photographs taken during an experiment
in which the head of the boundary layer probe is visible. The
scale of the photograph is defined here from the known dimensions
of the probe head, certain of these dimensions being marked in
the photograph. Study of these photographs indicated that visual
discrimination of a dimension less than about 0.003 in. was not
reliable. The height of the larger instability wave which appears
in Figure 13b can be estimated by noting its appearance next to
the probe elements. The crest noted by the arrow is in line with
the total pressure tube and appears to be breaking over the tube
as judged by the fact that the tip is occluded. From this fact
it may be estimated that the wave was approximately 0.010 in. to
0.020 in. high. The three photographs inserted in the upper
portion of Figure 13b show larger waves sillouetted against a
uniform surface. From the heights of the sillouettes and the

Figure 12. Photograph of the Liquid Film on the Surface of the Test Plate
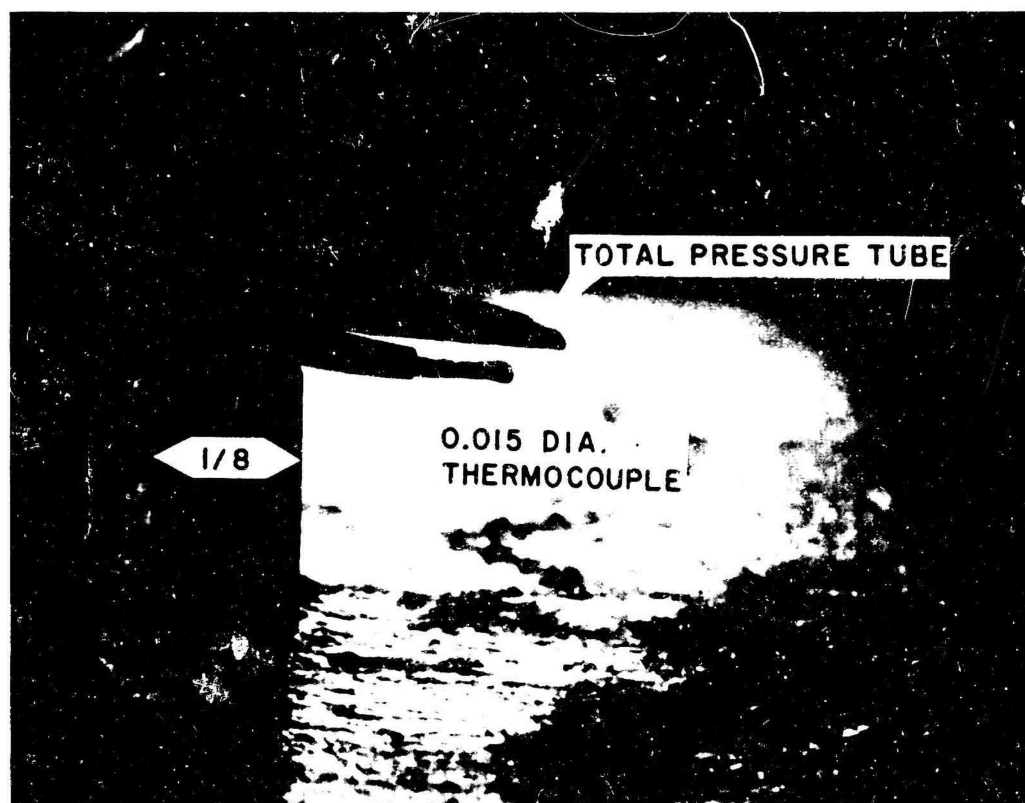
(a)
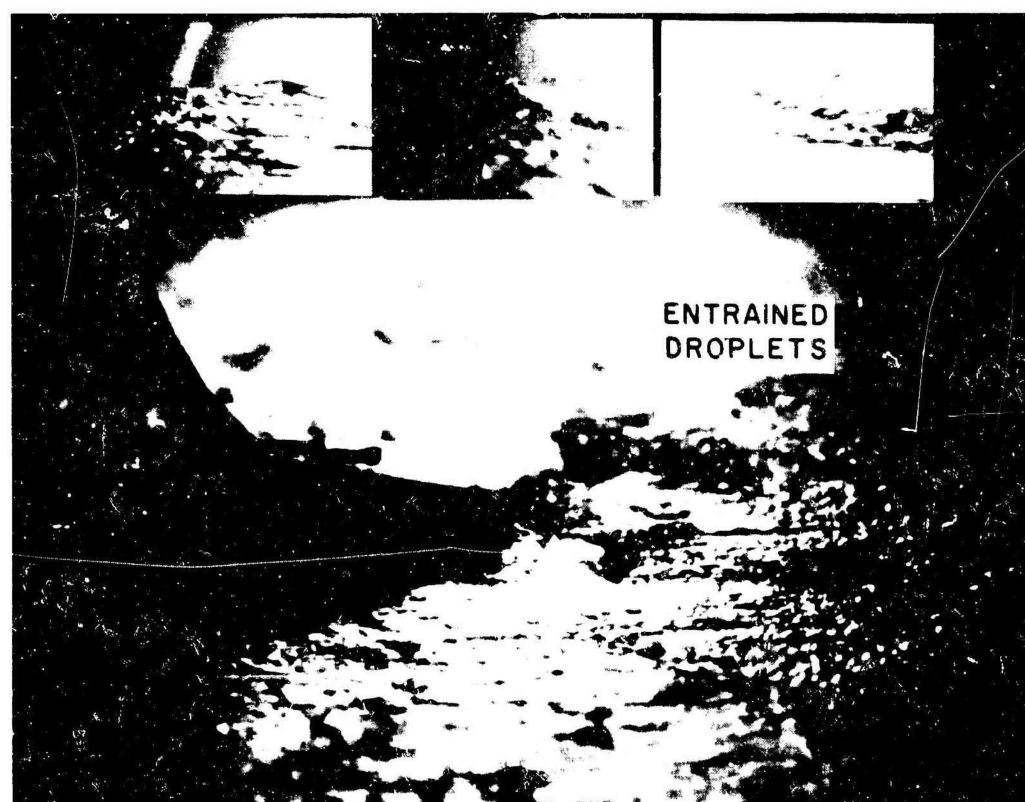
(b)

Figure 13. Photograph of the Boundary Layer Probe
in the Presence of a Liquid Film

scale of the photographs the three waves appear to have a height of approximately 0.008 to 0.010 in.

The liquid entrained as droplets above the liquid film appeared in several ways in the photographs. Figure 14 presents two photographs in which liquid droplets appear. In the upper photograph the droplets appear as short white streaks against the darker background. The streaks were produced by the highlight of the illumination off of the droplet. The droplets well above the film were moving substantially faster than the surface of the liquid film, hence, the blurred effect. The lower photograph shows two droplets of spherical shape. The appearance of these readily identifiable droplets was helpful in identifying the appearance of droplets immediately adjacent to the liquid film where the advantage of a dark or uniform background was not present. Referring to the photographs of Figure 13, the characteristic spherical images similar to those of Figure 14 can be seen above and just ahead of the total pressure tube in the lower photograph.

Dimensionless Stability Correlation   The application of dimensionless stability criteria to the present investigation was done in a comparative manner. The actual condition of a particular liquid film, i.e., stable or unstable, was determined from photographs. The dimensionless stability criteria such as the dimensionless liquid flow rate, W^*, or liquid Reynolds number have not been correlated to stability conditions for the liquid
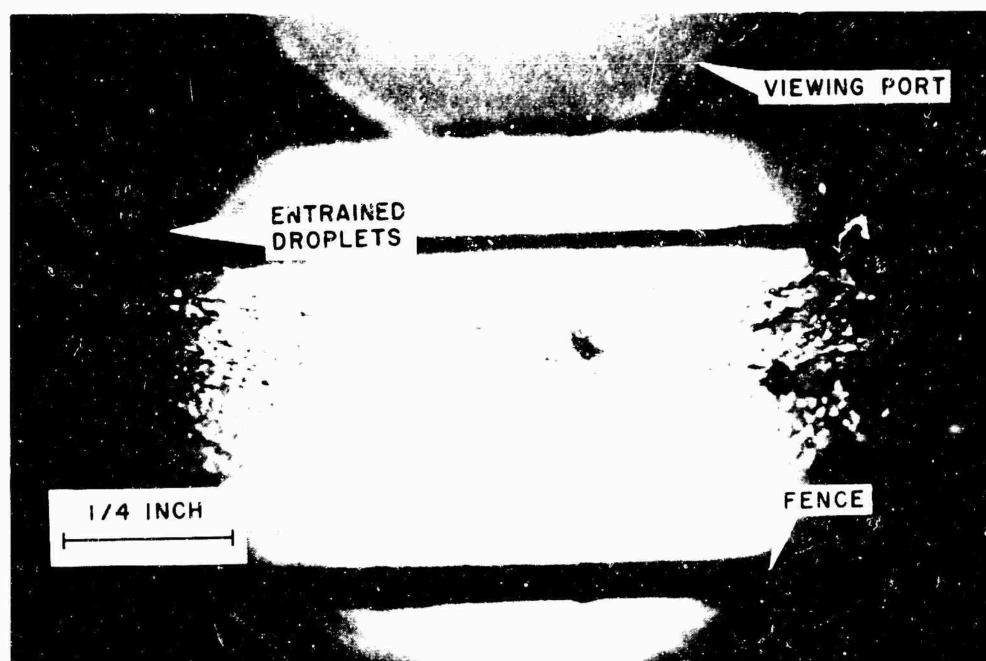
Figure 14. Photographs of Entrained Liquid Droplets above an Unstable Film

films found in the present investigation, i.e., with an elevated free stream pressure and surface mass transfer. Table 3 presents the values of the dimensionless liquid flow rate for the various regimes of film stability for the higher range of gas stream Reynolds number.

Table 3

Film Stability Based on W^+

Value for Stable Film	Value for Incipient Instability	Value for Unstable Film
$W^+ < 90$	$90 < W^+ < 120$	$W^+ > 120$ to 150

The values of the dimensionless liquid flow rate presented in Table 3 for the liquid film could only be computed for the flow a short distance downstream of the liquid injector where the flow rate of liquid in the film was substantially the injected flow rate. The rate of evaporation of liquid from the film was not known as a function of length, and hence, the local liquid flow rate at any axial position on the test plate was not known

Roughness. Only one technique was applied to obtain _estimates_ of the height of the waves as they appeared in a photograph. That technique was noted earlier in this section, namely, when a wave structure appeared in coincidence with a dimensional element such as a probe element or test section divider fence. The estimates of wave height for films wherein dimensional elements did not appear were made by comparing the shadows cast by such waves with

the shadows cast by either a dimensional element or wave near a dimensional element.

Film Temperature. The temperature of the liquid film was indicated by three separate measurements with thermocouples. These measurements were:

1. The reading of a thermocouple installed in a plug and mounted flush with the test section surface.

2. The average of the readings of the thermocouples imbedded less than 0.030 in. below the wetted surface of the test plate.

3. The reading from the total temperature thermocouple on the probe head when the thermocouple was in contact with the liquid film.

The results of the foregoing measurements were correlated to the Gater-Knuth results summarized in Figure 3, Section 2.2.

Velocity of the Surface and the Flow Mean Thickness of the Film The velocity of the surface of the liquid film was calculated assuming (1) the film flowed at its flow mean thickness, δ_f and (2) the velocity profile through the film was linear. Thus, from Newton's law of friction

$$\tau_s = \mu_1 \frac{du}{dy} = \mu_1 \frac{\mu_s}{\delta_f} \tag{2-37}$$

where μ_s = surface velocity of the film   The flow mean thickness is given by equation 2-5 as

$$\delta_f = \left[\frac{2\,\dot{m}_1 \nu_1}{\tau_s}\right]^{1/2} \tag{2-5}$$

The liquid flow rate was measured and the shear stress, τ_s, was derived from the measured velocity profiles in the boundary layer.

3.2.2 Results of the Film Characteristics Experiments

<u>Formation of the Film, Coverage of the Test Plate and Termination of the Film</u>. The exploratory experiments conducted using air at approximately 500R employed the liquid injector configuration A shown in Figure 15. The coverage of the plate was observed visually.[*]
Water formed a film immediately after injection and covered the plate entirely for flow rates greater than 0.003 lb/sec. The coverage of the plate was complete for liquid flow rates substantially lower than were subsequently determined as necessary for complete coverage of the plate in hot flow (approximately $\dot{m}_1 = 0.006$ lb/sec). Except for the appearance of entrainment at the higher liquid flow rates no indication of difficulty was revealed relative to the formation of a film and subsequent coverage of the plate by water at the flow rates to be used in hot flow.

The film formation and coverage experiments conducted using Freon 113 as the liquid in cold flow were unproductive. Interfacial

---

[*] The photographic system employed later in the investigation was not developed at the time the exploratory cold flow experiments were conducted.

instability was so severe at the nominal flow velocity and pressure
that no film could be observed beneath the fog of entrained droplets
above the test plate.

The exploratory cold flow experiments did reveal that the
simple inclined slot employed in the liquid injector was not
satisfactory with respect to injecting the liquid onto the test
plate. Severe entrainment of the liquid in the gas stream resulted
at the first contact between the two fluids. Figure 15 presents
sectional drawings of four configurations of liquid injectors
investigated. In all four configurations the liquid was supplied
from beneath the test plate to a manifold which discharged into
the injector slot. The differential injection pressure between
the manifold and the slot where the liquid was injected onto the
plate was in all cases very much less than the total pressure
in the test section. The deficiency of the first configuration
has already been noted. The second configuration employed a
cantilevered overhung lip which injected the liquid tangentially
onto the test plate and parallel to the direction of gas flow.
The vertical width of the injection slot was approximately
0.010 in. This width, however, could not be maintained con-
stant across the 4 in. span of the test section. As a result the
liquid was injected at a non-uniform rate across the span of the
slot, the local injected flow rate being a function of the local
slot height. The effect of the non-uniform injection
characteristics were observable in the coverage of the test
plate in both hot and cold flow. The third configuration was

CONFIGURATION   RESULTS

GAS FLOW   ⌐LIQUID FILM

(A) SEVERE ENTRAINMENT
AT THE POINT OF
CONTACT BETWEEN
GAS AND LIQUID

TEST
PLATE

⌐MANIFOLD
LIQUID

⌐OVERHUNG
LIP

(B) LESS ENTRAINMENT;
POOR DISTRIBUTION
OF LIQUID

⌐WIRE
GAUZE

(C) MORE UNIFORM
DISTRIBUTION

(D) BEST DISTRIBUTION

SEVEN SEPARATE
CONTROL VALVES
AND PARTITIONED
MANIFOLD
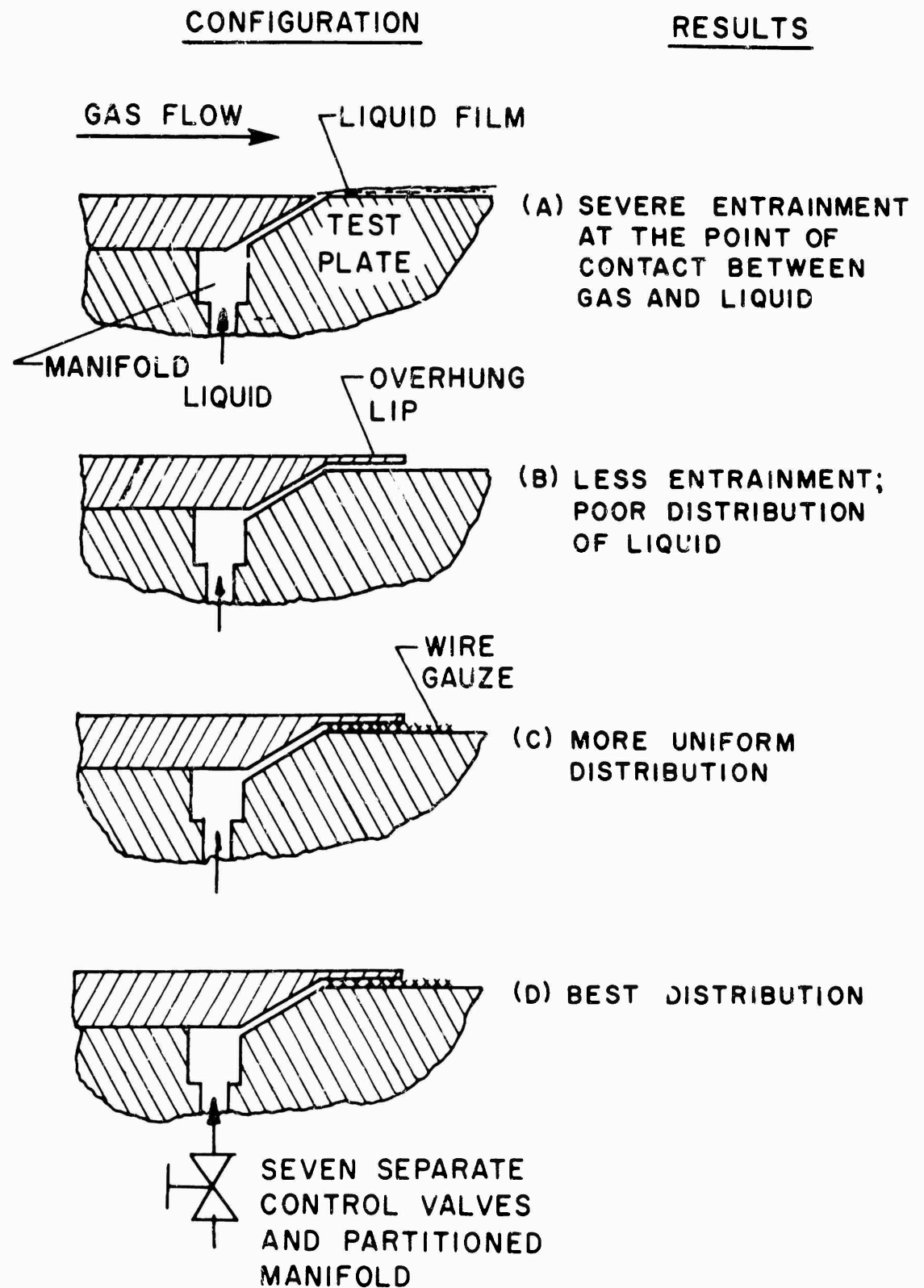
Figure 15. Four Configurations of Liquid Injectors

a modified version of the second configuration. A strip of 100 mesh brass gauze, 4 in. x 3/8 in., was inserted underneath the overhung lip and the lip was sprung so as to bear down on the gauze. The presence of the gauze established a uniform spanwise vertical height for the injector slot. The configuration produced a more uniform distribution of the injected liquid than the previous two configurations but the experiments revealed that some non-uniformity still remained. The fourth and final configuration of injector to be investigated incorporated a partitioned manifold. The partitions divided the original manifold into seven smaller manifolds each isolated from the adjacent ones. The flow rate of liquid supplied to each smaller manifold was controlled by a precision needle valve. This latter configuration permitted the adjustment of the spanwise flow distribution in order to produce the most satisfactory coverage of the test plate by the liquid. The configuration of injector just described was employed throughout the remainder of the investigation.

The aspects of the coverage of the test plate by the liquid and the subsequent termination of the film resulting from complete evaporation of the liquid during hot flow were intimately related. Termination of a film in the present investigation was defined to be the substantial disappearance of a film over a distance between two viewing ports or 3 in. It was desired that the film be uniform in coverage of the test plate and free of dry spots for the axial length up to the inception of the termination. In this way a definite "liquid length" could be established and subsequently

could be related to heat and mass transfer phenomena. It was determined after numerous experiments that termination of the liquid film in the desired manner was not possible in general and certainly not on a reproducible basis. Figure 16 presents four photographs representative of the various modes in which the liquid film was observed to teminate. In Figure 16a the film broke away from the divider fences and subsequently formed a channel in the central portion of the test plate. Figure 16b reveals how two such channeled streams appeared. Figure 16c shows the liquid persisting along the divider fences and evaporating in the central portion of the test plate. The last photograph in Figure 16 shows a liquid film terminating more or less uniformly in the center of the test plate but with liquid persisting along the divider fences. The photograph reveals how the film terminated in long thin streamers, i.e., termination, when it occurred, was by no means abrupt.

The condition of the surface of the test plate, i.e., cleanliness and small roughness elements (blurrs and slight protrusions or depressions of the flush mounted plugs) also influenced the termination. Cleaning of the test plate with solvent prior to an experiment delayed the occurrence of film breakaway from the fences but did not alter the eventual results When the film was thin near the inception of termination, a single roughness element of less than 0.001 in. in height was sufficient to initiate the beginning of a dry spot which would enlarge in the downstream direction.

Figure 17 presents a photograph of a film formed with Freon
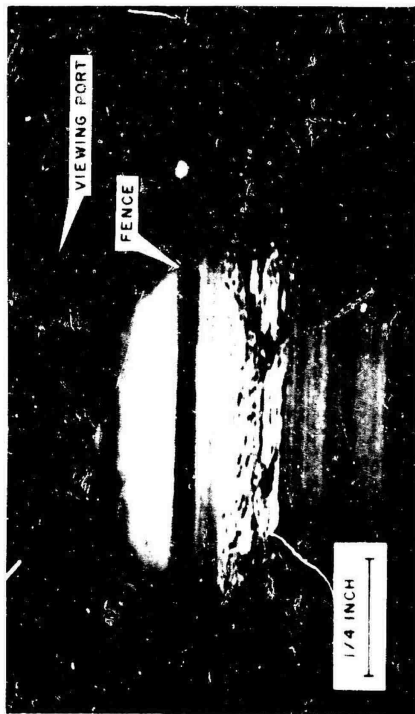
(A) CHANNELLING IN THE CENTER OF THE TEST PLATE

(B) DUAL CHANNELLING

(C) PERSISTING ALONG THE FENCES
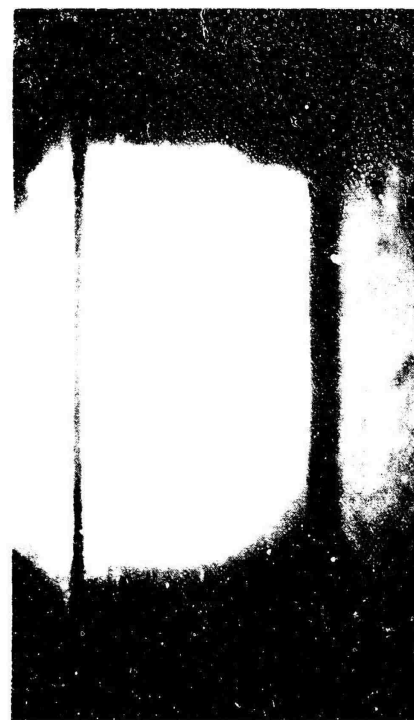
(D) COMBINATION OF IRREGULAR FLOWS

Figure 16. Photographs of the Modes of Termination of the Liquid Film

92

Figure 17. Photograph of a Liquid Film of Freon 113

113 at a position 3 inches from the injector slot in hot flow.

Although the flow rate of Freon was quite large, being several times

more than the flow rate of water required to cover the entire length

of the test plate, only a short film could be established. At lower

flow rates no visible film was found at all. Further, the photo-

graph shows that the Freon film was completely unstable.

Stability and Entrainment. The characteristic interfacial

structures exhibited by the liquid films in the present investigation

were presented in Figure 4 and were discussed in Section 2.3.2.

These will serve as a background for the present discussion.

Figure 18 presents photographs of what was considered a

stable liquid film at four positions along the test section, $x - x_0 =$

3, 9, 12 and 18 in. The liquid flow rate in these photographs

was 0.006 lb/sec at the injector slot. The flow velocity, u_e, was

50 ft/sec, the total pressure, ρ_e, was 200 psia and the total

temperature, T_e, 980R. The value of the dimensionless liquid flow

rate, W^+, was between 80 and 120 computed for the total liquid flow

rate. A value of $W^+ > 90$ implies the liquid film is incipiently

unstable. Figure 18 reveals a more or less uniform coursely mottled

surface present on the liquid film. The few larger waves appearing

in three of the four photographs display no visible entrainment at

the crests. No other indication of entrainment appears elsewhere.

Figure 19 presents photographs of an unstable liquid film

at three positions along the test section, $x - x_0 = $ 3, 6 and 15 in.

The flow conditions at which the photographs were obtained were the

nominal operating conditions at which the four measurement sets of

ue= 50 ft/sec
Pe = 200 psia
Te= 980R
$W_{int}^+ \cong$ 80 to 120
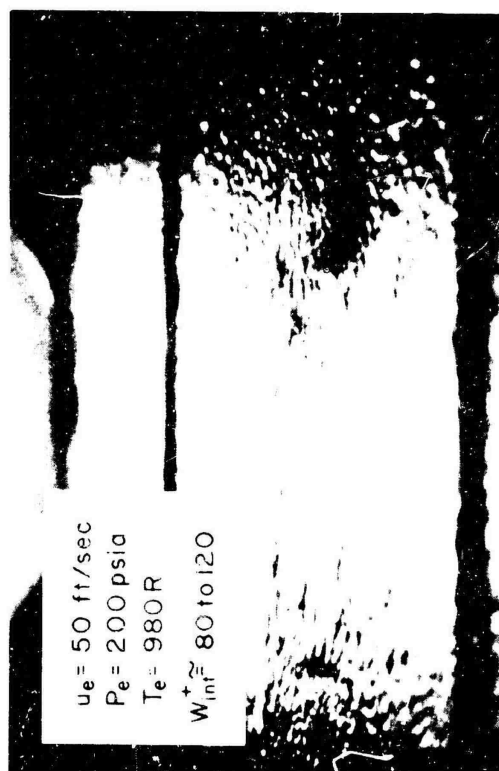
(a) x−x₀ = 3in.

(b) x−x₀ = 9in.

(c) x−x₀ = 12in.

(d) x−x₀ = 18in.

Figure 18. Photograph of a Stable Liquid Film

(a) $X - X_0 = 3$ in.

(b) $X - X_0 = 6$ in.

(c) $X - X_0 = 15$ in.

Figure 19. Photograph of an Unstable Liquid Film at the Nominal Operating Conditions

the boundary layer data were obtained, namely u_e = 100 ft/sec, P_e = 250 psia, T_e = 980R and $\dot{m}_1$ = 0.0016 lb/in-sec or $\dot{m}_1$ = 0.0065 lb/sec. The corresponding value of the dimensionless liquid flow rate was $W^+ \cong$ 130. The surface of the film was broken up by instability waves, the frequency of their appearance and their width being noticably greater than the few larger waves which appeared on the stable film shown in Figure 18. Entrainment of liquid droplets above the film is observable in the second photograph taken 6 in. downstream of the injector slot. The entrainment of droplets just above the film is detectable in the first photograph taken 3 in. downstream of the injector slot. The photograph taken 15 in. downstream of the injector slot shows some entrainment but less than was noted in the second photograph.

Figure 20 presents three photographs at $x - x_0$ = 15 in. for liquid flow rates of $\dot{m}_1$ = 0.0016, 0.0032, and 0.0048 lb/in-sec for the nominal gas flow conditions of the boundary layer measurements. The first photograph is repeated from the previous Figure 19. The sequence of photographs in Figure 20 shows the increasing severity of the instability and liquid entrainment with increasing liquid flow. The comparison of photographs in Figures 18, 19, and 20 indicate the qualitative extent or degree of the unstable film for which the boundary layer measurements were obtained.

Roughness. Estimates were made of the heights of several of the larger waves appearing in the photographs. One estimate was obtained from the coincidence of a larger wave and a probe

$u_e = 100 \, ft/sec$
$P_e = 250 \, psia$
$T_e = 980 \, R$
$x - x_0 = 15 \, in.$

$\dot{m}_l' = 0.0016 \, lb/in.-sec$
$W_{inf}^+ = 110 \, to \, 150$

(a)

$\dot{m}_l' = 0.0032 \, lb/in.-sec$
$W_{inf}^+ \cong 220 \, to \, 300$

(b)

$\dot{m}_l' = 0.0048 \, lb/in.-sec$
$W_{inf}^+ = 330 \, to \, 450$
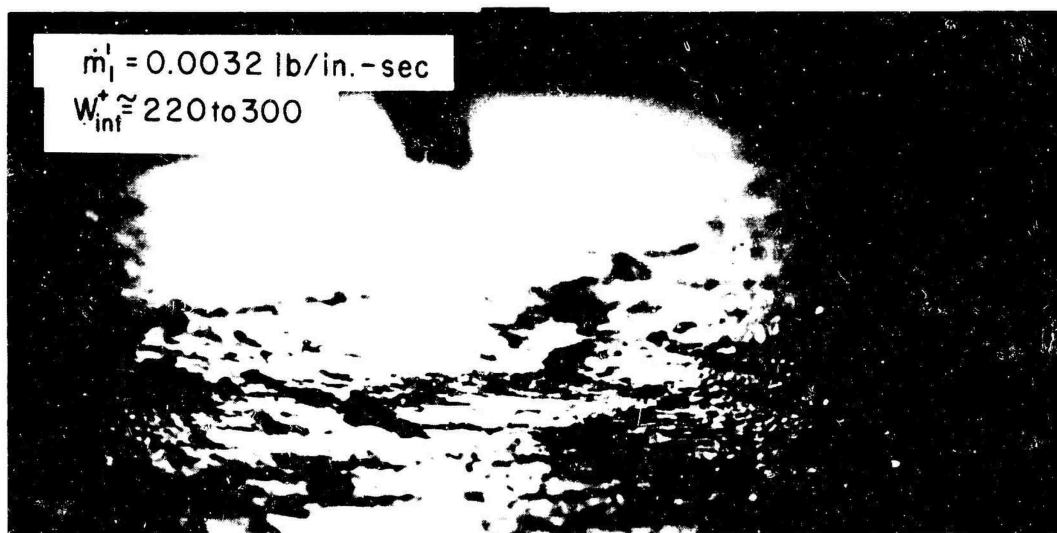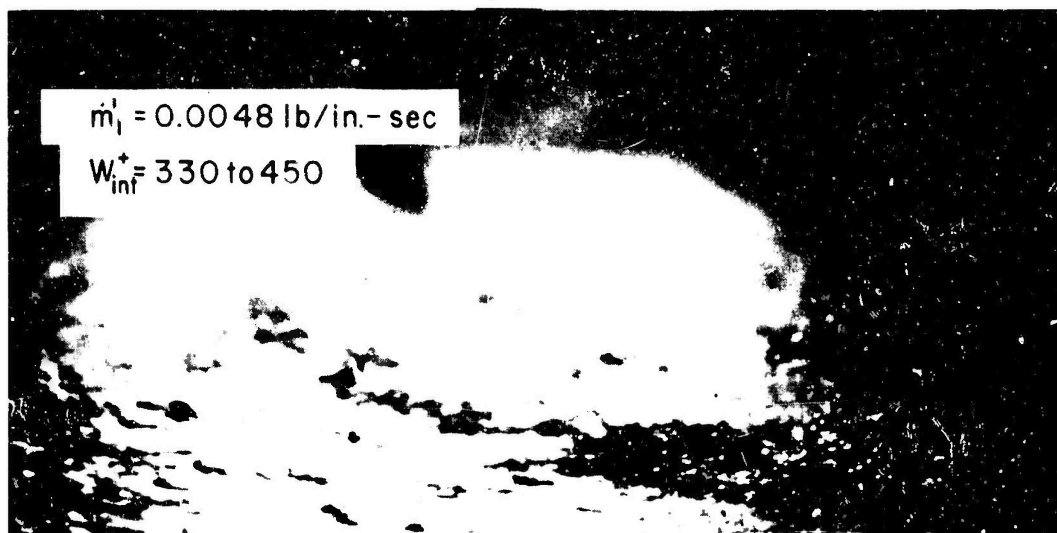
(c)

Figure 20. Photographs of Unstable Liquid Films at Three Liquid Flow Rates

element as shown in Figure 13. That wave was estimated to be between 0.010 and 0.020 in. high. The sillouetted waves inserted in Figure 13 were estimated at approximately 0.008 to 0.010 in. An estimate was obtained by the comparison of the projected shadow of the fences with projected shadow of the wave in Figure 18 at $x - x_0 = 12$ in. The wave front is diagonal to the direction of view in the center of the photograph and is composed of five smaller wave structures. By comparison of the shadows cast by the five smaller wave structures with the shadows cast by the 0.030 in. high fences, the wave was estimated to be 0.015 in. high. The latter estimate led to the further estimate that based on the comparison of the dimensions of the shadows cast by the smaller waves covering the remainder of the film with the shadow cast by the larger wave, the height of the smaller waves was on the order of magnitude of 0.005 in. or less.

Film Temperature. Table 4 lists representative results of the measurement of the film temperature by means of the flush mounted thermocouple, the total temperature thermocouple on the probe and the thermocouples in the test plate. In the last column appears the value predicted by the Gater-Knuth correlations as obtained from Figure 3.

Table 4

Results of Film Temperature Measurements

Total Pressure psia	Total Temperature, F	Film Temperature, T_f			
		F.M.T.	P.T.	I.P.T.	G-K
215	520	250	-	240	235
250	520	-	255	245	250

F.M.T. - Flush mounted thermocouple   I.P.T. - Imbedded thermocouples

P.T. - Probe thermocouple   G-K - Gater-Knuth

Velocity of the Surface of the Liquid Film and Thickness of the
Film. The calculated velocity of the surface of the liquid film and
the flow mean thickness of the liquid film were approximately 7 ft/sec
and 0.001 to 0.002 in., respectively. The above numbers can only be
considered as orders of magnitude a short distance downstream of the
liquid injector since the surface of the liquid film was not smooth
and evaporation of the water was reducing the quantity of liquid
present.

3.3 Results of the Boundary Layer Measurements

The parameters which were established experimentally by either
direct or semi-direct mechanical measurements were the velocity and
temperature profiles in the boundary layer, the bulk rate of flow
of fluids in the system and the pressures and temperatures necessary
to specify the operating conditions of the experimental apparatus.
All of the other parameters discussed in this section were derived
or calculated from the direct or semi-direct measurements   Such

derived parameters were subject to experimental error to varying degrees depending on the particular parameter. The extent of the error in the measured quantities is discussed in Appendix D and in Section 4. In order to present correlations of the experimental data it was necessary to determine numerical values for a number of parameters which were sensitive to experimental errors. Such numerical values represent, in general, an average or mean value for which there exists a range of error.

3.3.1 Methods of Evaluation and Correlation
of the Experimental Data

Velocity and Temperature Determinations. The total temperature measured at a certain elevation in the boundary layer above the test plate was taken to be the average value of the thermocouple output signal as recorded on a direct writing oscillograph. The position of the signal was calibrated on the recording paper against standard reference temperatures.

The velocity at a certain elevation in the boundary layer was calculated from the measured differential velocity pressure by means of Bernoulli's equation

$$u = \left[2 \, \frac{\Delta p}{\rho} \right]^{1/2} \tag{D-3}$$

where Δp = differential velocity pressure

ρ = local density of the gas at the elevation of the total pressure tube

The density was determined from the equation of state with compressi-
bility factors. The temperature employed to make the aforementioned
calculation corresponded to that value of temperature read at the
elevation of the total pressure tube from the average curve through
the temperature data points.

The "zero" or starting elevation of the total pressure tube
was determined when electrical continuity was established by
contact between the total pressure tube and an insulated contact
wire mounted flush with the plug surface. The plug surface was
flush with the surface of the test plate. The elevation of the
total pressure tube throughout the remainder of a traverse was
indicated continuously on an oscillograph by the output of the
probe position determination system as described in Appendix B.

The total temperature thermocouple on the boundary layer
probe moved the same increments of traverse as the total pressure
tube, both being mounted on the same shaft The thermocouple was
set approximately 0.010 in lower than the total pressure tube.
As a result, during the first few increments of traverse of the
probe head upward from the plate the thermocouple probe was touching
the surface of the probe plug and in contact w th the liquid film
While in this position the temperature indicated by the thermocouple
was near the value of temperature of the film As soon as the
traverse had progressed sufficiently to move the thermocouple out
of the liquid film, the indicated temperature would increase step-
wise by approximately 100F The stepwise jump in temperature
occurred for a probe motion of a few thousandths of an inch. The

occurrence of the stepwise jump marked the reference position for the thermocouple (see Appendix D).

Thickness Parameters. The experimental data points of velocity and temperature of one measurement set were graphed as a function of the corresponding measured elevation above the test plate. The profile of the boundary layer was determined by visually drawing a curve through the data points, the curve representing the mean profile. The thickness of a boundary layer was determined in one of two ways:

1. For the velocity profiles above the dry test plate or the temperature profiles above the wetted test plate the thickness was the elevation above the test plate at which the average curve reached 99% of the free stream value of either velocity or temperature.

2. For the velocity profiles above the wetted test plate the thickness was the elevation above the test plate at which an extrapolation of the average curve beyond the measured data appeared to reach 99% of the free stream value of velocity.

The latter technique was required to obtain a value for the thickness of the velocity boundary layer above a wetted plate since the probe did not always traverse completely through the boundary layer.[*] The free stream velocity was determined in two ways. In the first method the free stream velocity was calculated from the bulk flow rate measurements and the known area of the test section

---

[*]The failure to complete the traverse was the result of a mechanical difficulty.

corrected for displacement effects of the velocity boundary layer.
The second method was to extrapolate the mean curve beyond the data
at the same rate of circular curvature existing at the terminus of
the data. The value of velocity at which this extrapolated curve
become tangent to the vertical was taken as the free stream
velocity. The two values of free stream velocity determined in
this manner differed by no more than 3 ft/sec in all cases. The
influence of this uncertainty in the value of the free stream
velocity on the parameters derived from the boundary layer pro-
files is noted in the discussion of the results.

The free stream value of total temperature was the value
measured by the probe thermocouple in the free stream above the
temperature boundary layer or the value of the temperature of the gas
leaving the gas generator as measured by the monitoring thermocouples
at the fore end of the lead section. In all cases the two
aforementioned measurements agreed within $\pm$ 5 F.

Correlations yielding a boundary thickness as a function
of length ($\delta = f (Re_x)$) were not strictly applicable from the
beginning of the lead section since the flow in the constant area
lead section was subject to a negative axial pressure gradient
created by the displacement effect of the growing boundary layer
and also influenced by the three dimensional effects introduced
by the rectangular cross section of the flow passage. The profile
of the velocity boundary layer at the entrance to the test section
was likely to be fuller and thinner than would have resulted for
ideal flow over a flat plate. The flow in the test section, however,

was maintained at a constant static pressure. Hence, a growth

correlation for a constant pressure boundary layer based on flow

length would yield a qualitative comparison, at least for the dry

test plate. The correlation employed was derived from Reference

31 for the experimentally determined power law distribution of the

boundary layer measured over the dry test plate. The correlation

was

$$\delta = 0.322 \ x \ Re_x^{-0.187} \tag{2-38}$$

No attempt was made to establish a growth correlation for the

boundary layer over the wetted test plate.

A relation for the ratio of the thickness of the temperature

boundary layer to the thickness of the velocity boundary layer

as a function of x after a stepwise change in wall temperature

was obtained from Reference 35. The relation is for incompressi-

ble flow over a smooth flat plate with a stepwise temperature

discontinuity. The relation is

$$\frac{\Delta}{\delta} = \left[1 - \left(\frac{x_0}{x}\right)^{\frac{4(n+2)}{5(n+1)}} \right]^{\frac{n}{2+n}} \tag{2-39}$$

where

   n = denominator of power law exponent

   x_0 = length of lead section

   x = total distance of flow

The relation was employed in a comparative manner with respect to the measured growth of the boundary layer to indicate the difference between the growth of the temperature boundary layer over a smooth plate and the corresponding growth determined experimentally for the case of the liquid film.

The momentum thickness, δ_2, and the enthalpy deficit thickness, Δ_2, were calculated by the graphical integration of mean curves through the experimental data points graphed as a function of the measured elevation above the test plate. The finite difference equations employed in the graphical integration were derived from the definitions of the momentum thickness, equation 2-15, and the enthalpy-deficit thickness, equation 2-30. In the latter equation the specific heat of the gas in the boundary layer is assumed constant. The finite difference equations were

$$\delta_2 = \sum_1^n \left(\frac{T_e}{T}\right) \left(\frac{u}{u_e}\right) \left(1 - \frac{u}{u_e}\right) \Delta y_n \qquad (2\text{-}40)$$

and

$$\Delta_2 = \sum_1^n \left(\frac{T_e}{T}\right) \left(\frac{u}{u_e}\right) \left(1 - \frac{T - T_f}{T_e - T_f}\right) \Delta y_n \qquad (2\text{-}41)$$

where T_f = temperature of the liquid film.

The average values of the parenthetical functions were the average values of that function within the height increment Δy_n as determined from the mean curves down through the experimental data

points. In adapting equations 2-15 and 2-30 to the above equations, ρ/ρ_e was introduced as T_e/T.

Correlation of Profiles. The shape of the velocity and temperature profiles were correlated by power law distributions. Thus

$$\frac{u}{u_e} = (\frac{y}{\delta})^{\frac{1}{n}} \qquad (2\text{-}23)$$

and

$$\frac{T - T_f}{T_e - T_f} = (\frac{y}{\Delta})^{\frac{1}{m}} \qquad (2\text{-}34)$$

The law of the wall correlation was applied to the dry and wet velocity and the wet temperature data in order to compare the experimental results with the predicted law of the wall. The data was treated by the following equations in the correlation, namely,

$$y^+ = \frac{y\, u_\tau}{\nu_s} \qquad (2\text{-}20a)$$

$$u^+ = \frac{u}{u_\tau} \qquad (2\text{-}20)$$

and $\qquad T^+ = \frac{1 - (T/T_f)}{\beta} \qquad (2\text{-}33)$

where $\qquad \beta = \frac{q_s\, u_\tau}{c_p T_f \tau_s} \qquad (2\text{-}21)$

Friction Coefficient. The friction coefficient over the dry test plate was obtained by two methods from the experimentally measured velocity profiles.

Method 1: The value of the friction velocity, u_τ, was determined by the correlation of the experimental data to the universal velocity profile (UVP) graphed as the velocity defect parameter, $\frac{u-u_e}{u_\tau}$, as a function of the dimensionless distance, y/δ (see Figure 9). Thus

$$(u_\tau)_{exp} = (u-u_e)_{exp}/(\frac{u-u_e}{u_\tau})_{UVP} \qquad (2\text{-}42)$$

where the right hand side of equation 2-42 was evaluated at a sufficient number of points to establish the value of u_τ. The average local friction coefficient was obtained as

$$\bar{c}_f' = 2\,\frac{(\bar{u}_\tau)^2_{Best\ fit}}{\bar{u}_e^2} \qquad (2\text{-}43)$$

Method 2: This method is taken after Clauser (36). The method employs three equations to construct a graph having u/u_e as a function of $u_e y/\nu$ with the friction coefficient as a parameter in a family of curves. The equations are

$$\frac{u}{u_\tau} = 5.6\,\log\,(\frac{u_\tau y}{\nu}) + 4.9 \qquad (2\text{-}44)$$

which is the law of the wall after Clauser, and

$$\frac{u}{u_\tau} \equiv \frac{u}{u_e} \sqrt{\frac{2}{c_f}} \qquad\qquad (2\text{-}44a)$$

and

$$\frac{u_\tau y}{\nu} \equiv \frac{u_e y}{\nu} \sqrt{\frac{c_f}{2}} \qquad\qquad (2\text{-}44b)$$

The latter two equations are working equations employed to construct the graph. The friction coefficient associated with a set of boundary layer measurements is determined by graphing the measured data in the aforementioned manner and noting with which curve of constant friction coefficient the data agrees.

The law of the wall as given by equation 2-44 and the wall region of the universal velocity profile (Figure 9) are different representations of the same universal characteristic of the turbulent boundary layer. As a consequence, the friction coefficients determined by both of the above methods should be in agreement if the experimental data are internally consistent in both real and dimensionless coordinates.

In both of the above methods the friction coefficient determined was the average local friction coefficient for the increment of length from $x - x_o = 3$ in. to $x - x_o = 17$ in.

The value of the friction coefficient for the gas flow over the liquid film was determined relative to the friction coefficient for the flow over the dry test plate. The relative magnitudes of the two coefficients were established by assuming that any change in the wall shear between the two cases would be reflected in a

corresponding change in the momentum thickness determined for the two cases at the same location in the test section. Thus

$$\frac{(\overline{c_f})_{wet}}{(\overline{c_f})_{dry}} = \frac{(\delta_2)_{wet \ at \ x}}{(\delta_2)_{dry \ at \ x}} \qquad (2\text{-}45)$$

In applying this method it was assumed that the characteristics of the flow through the lead section were the same in both cases. The above technique does not take note of the effect of mass transfer from the liquid film on the friction coefficient. The sults will show that the influence of the mass transfer was more than an order of magnitude less than the corresponding change in the momentum thickness, and hence, could be neglected.

A numerical value for the average local friction coefficient for the wetted test plate was obtained from equation 2-45 by introducing the values of the momentum thickness and a value for the friction coefficient for the dry test plate. Once a numerical value of the friction coefficient was obtained, numerical values for the shear stress and friction velocity were determined. The latter two parameters were employed in correlating the experimental data and in calculating other parameters.

Stanton Number. The Stanton number was computed by means of the integral energy equation using a value of the enthalpy-deficit thickness calculated by equation 2-41. The differential form of the integral energy equation applied in the present investigation is given by equation 2-32. Written in finite difference form

equation 2-32 becomes

$$\frac{\Delta(\Delta_2)}{\Delta x} - \frac{\overline{\dot{m}_v''}}{\rho_e u_e} = \frac{q_s}{\rho_e u_e c_p} (T_e - T_f) = \overline{S} \qquad (2-46)$$

where $\overline{S}$ = average value of the Stanton number over the incremental

length Δx.

The mass transfer term in equation 2-46 was neglected in the

determination of the Stanton number since its value was an order

of magnitude less than the Stanton number. The term relating to

the influence of the change in the temperature differential (see

equation 2-32) was approximately 1 percent of the resultant

value of the Stanton number and was neglected.

Heat and Mass Transfer Parameters. The average heat flux to

the liquid film, $\overline{q}_s$, was separated into three terms as

$$\overline{q}_s = \overline{q}_v + \overline{q}_h + \overline{q}_t \qquad (2-47)$$

where

$\overline{q}_v$ = heat going into latent heat of vaporization

$\overline{q}_h$ = heat going into sensible enthalpy increase of the

liquid (averaged over the whole test plate)

$\overline{q}_t$ = heat transferred to the test plate.

The value of $\overline{q}_h$ was determined from the measured temperature in the

test plate at the location injector slot, the equilibrium temperature

of the liquid film and the flow rate of the injected water. The

value $\overline{q}_t$ was determined from the application of the Fourier conduction

equation to the test plate using the measured temperature drop through the test plate. The value of $\overline{q}_v$ was determined employing equation 2-47 and the integral energy equation written in finite difference form including the mass transfer parameter, $\dfrac{\overline{\dot{m}}_v''}{\rho_e u_e}$. The average rate of mass transfer from the surface of the film was calculated from

$$\overline{\dot{m}}_v'' = \frac{\overline{q}_s - \overline{q}_h - \overline{q}_t}{\Delta h_v} \qquad (2\text{-}48)$$

where Δh_v = latent heat of vaporization at temperature T_f.

In calculating the heat transfer parameter, β, (see equation 2-21), the shear stress at the surface of the liquid film was that value corresponding to the average value of the shear stress obtained from the calculatee friction coefficient as discussed in the previous subsection.

3.3.2 Results of the Dry Wall Experiments

Figure 21 presents the velocity profiles in the boundary layer measured at three stations along the dry test plate. The stations of measurement were 3, 9, and 17 in. from the injector slot, and 21, 28, and 35 in. from the start of the lead section. The ordinate is the distance above the test plate in inches while the abcissas are velocity in feet per second. The nominal flow conditions in the test section at which the data were obtained are indicated in the figure. The different data point symbols indicate data obtained during individual traverses of the probe head at any one position along the test plate. The short dash curve traces the growth of the velocity boundary layer along the
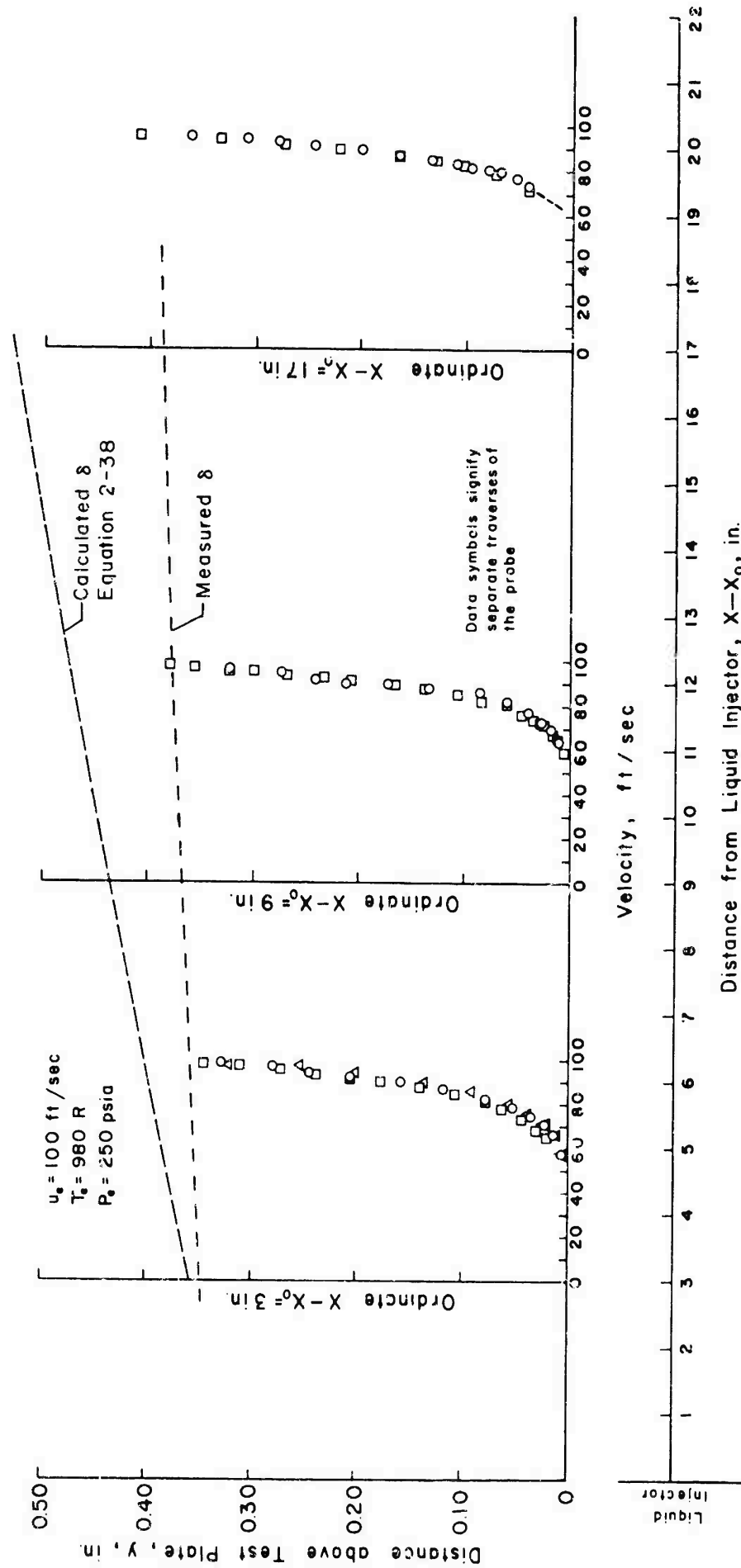
Figure 21. Velocity Profiles Measured in the Boundary Layer on the Dry Test Plate as a Function of the Distance from the Liquid Injector

test plate (the thickness at a station is where the curve crosses the ordinate). The long dash curve based on equation 2-38 presents the reference correlation for the growth of the velocity boundary layer on a flat plate. The velocity profiles display very little growth from the first station of measurement where $\delta = 0.35$ in. to the last station of measurement where $\delta \simeq 0.38$ to 0.40 in. The growth along the test plate determined experimentally is substantially less than the predicted growth based on a flat plate correlation. If the three profiles presented in Figure 22 are superimposed, affine similarity is displayed.

Figure 22 presents the dimensionless velocity parameter, u/u_e, as a function of the dimensionless distance from the wall, y/δ, for the three measurement sets obtained over the dry test plate. The straight line drawn through the data points represents a power law correlation with an exponent of $1/8.3$. The single power law correlates the collection of all data points of the velocity boundary layer measured over the dry test plate.

Table 5 presents the values of the momentum thickness determined at $x - x_0 = 3$, 9, and 17 in by graphical integration of the velocity profiles shown in Figure 21 The estimated error for the values of momentum thickness resulting from uncertainities in the values of the measured velocity data and the thickness of the boundary layer is ± 15 percent
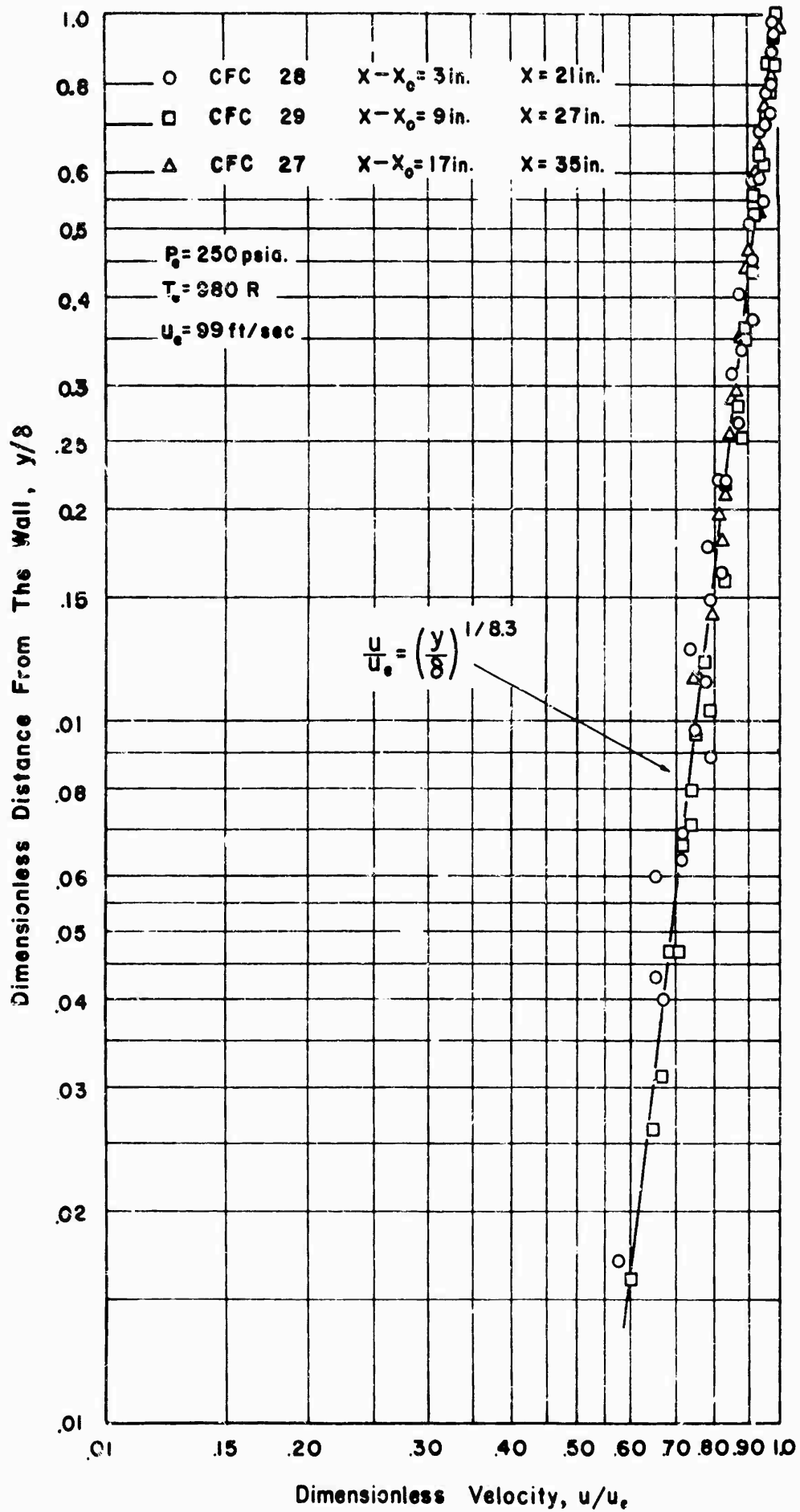
Figure 22. Power Law Correlation for the Velocity Profiles Measured in the Boundary Layer on the Dry Test Plate

Table 5

Values of the Momentum Thickness for the Boundary Layer
Over the Dry Test Plate

Position, $x - x_0$ (in.)	Momentum Thickness, δ_2 (in.)
3	0.027
9	0.029
17	0.031

Figure 23 presents the experimental data points graphed according to the method after Clauser for the determination of the local friction coefficient. The ordinate is the dimensionless velocity ratio, u/u_e, and the abscissa is the Reynolds number based on the elevation above the test plate and the free stream velocity, $\frac{u_e y}{\nu}$. The data correlates to a local friction coefficient of approximately 0.003. Since the data points shown in Figure 23 were obtained at distances between $x - x_0 = 3$ in. and $x - x_0 = 17$ in., the value of the friction coefficient is interpreted as the average local friction coefficient over the aforementioned interval of length.

Table 6 presents the values of the average local friction coefficient determined from the data presented in Figures 22 and 23 for the interval of length from $x - x_0 = 3$ in. to $x - x_0 = 17$ in.
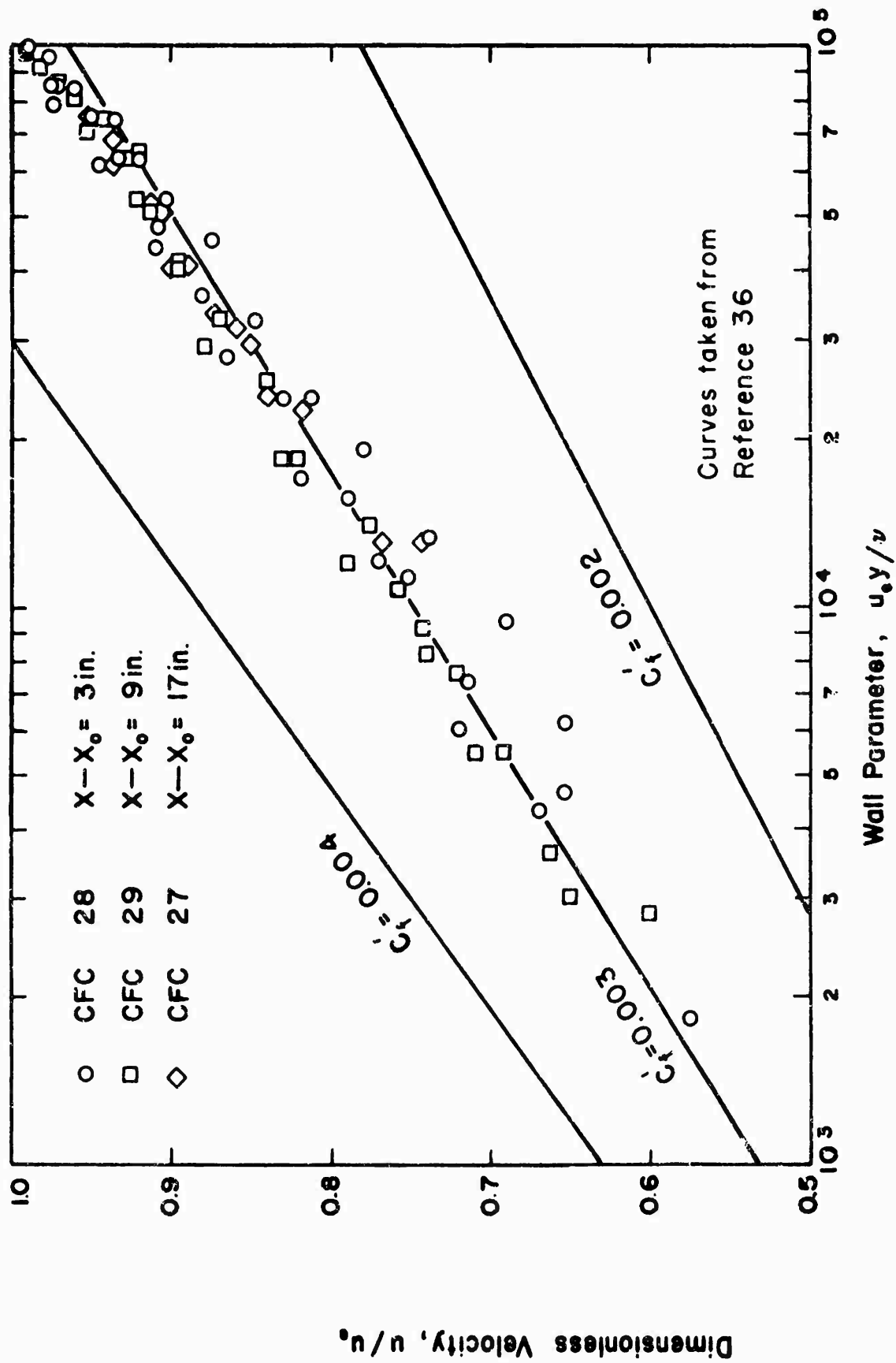
Figure 23. Velocity Data for the Dry Test Plate Correlated by the Method of Clauser.

Table 6

Values of the Shear Parameters for the Dry Test Plate

Method	$\overline{c_f}$	$\overline{\tau}_s$ lb/ft^2	$\overline{u}_\tau$ ft/sec
UVP	0.0019	0.20	3.0
Clauser	0.003	0.32	3.8
Spalding and Chi	0.0025	0.27	3.5

The method employed and corresponding value are noted. A reference value obtained by the method of Spalding and Chi (37) for the local friction coefficient on a flat plate is also presented. The reference value was based on the average value of the momentum thickness presented in Table 5. In the last two columns of Table 6 are presented the numerical values of the derived parameters of average shear stress, $\overline{\tau}_s$, and the average friction velocity, $\overline{u}_\tau$.

Figure 24 presents the dimensionless velocity parameter, u^+, as a function of the dimensionless distance parameter, y^+, for the velocity boundary layer on the dry test plate. The individual data points are not shown for reasons of space; the shaded areas correspond to the pattern of the data points. Three correlation patterns are presented, one each for the three values of the friction coefficient presented in Table 6, and the respective values are noted in the figure.

Measurements of the temperature distribution in the dry test plate showed the surface temperature of the dry plate to be
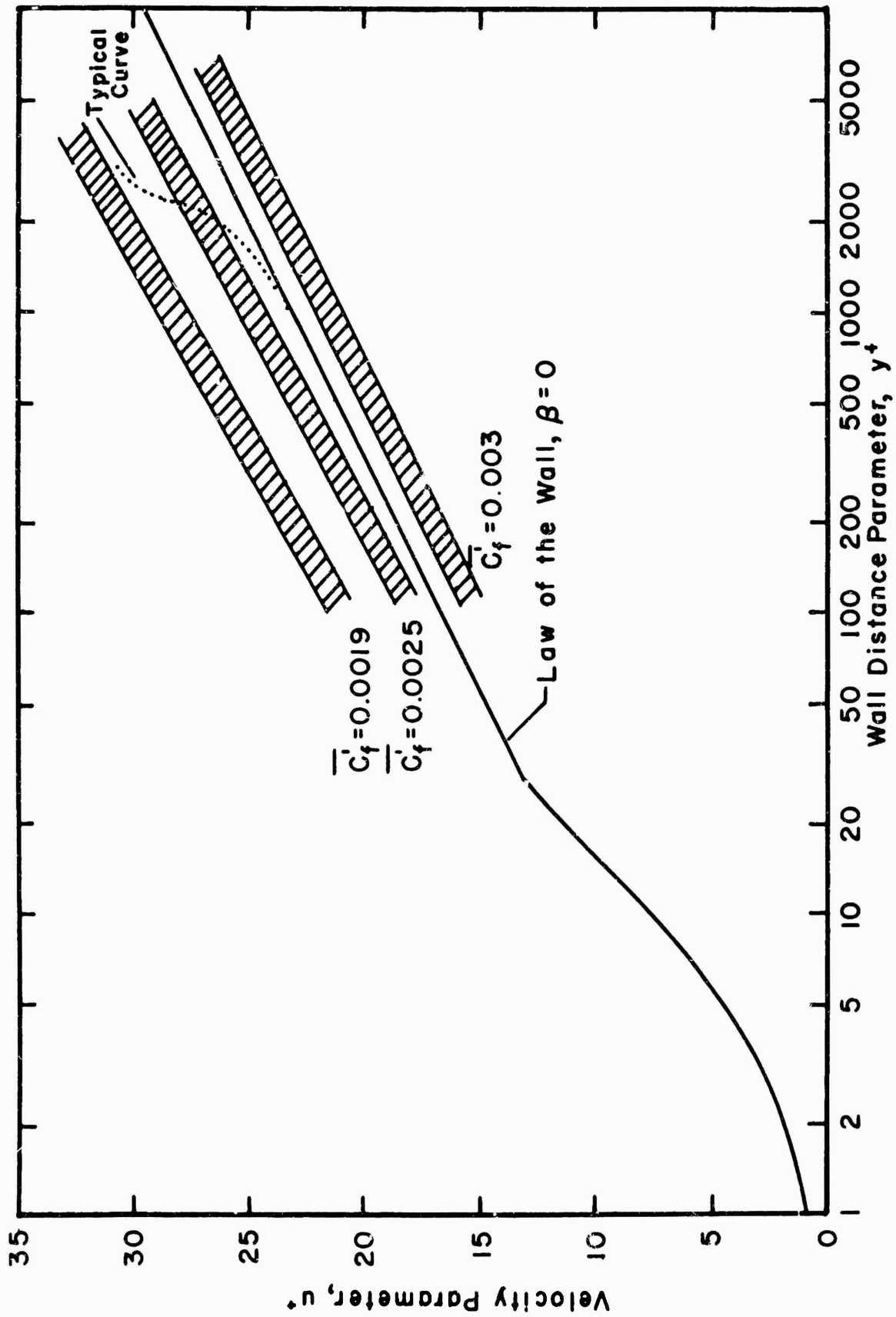
Figure 24. Law of the Wall Correlation for the Boundary Layer on the Dry Test Plate

approximately 485F. Corresponding to that surface temperature the average heat flux to the dry plate was computed to be 0.7 B/ft^2-sec $\pm$ 25% for a free stream temperature of 525F. The value of 0.7 B/ft^2-sec represents within approximately 10% the calculated heat flux to the wetted test plate.

3.3.3 Results of the Wet Wall Experiments

Figure 25 presents the velocity profiles in the boundary layer measured at four stations along the wetted test plate. The stations of measurement were 3, 5, 9, and 17 in. from the injector slot. The ordinate is the distance above the test plate in inches and the abscissas are velocities in feet per second. The velocity profiles display no detectable growth from the first station of measurement to the last station. The boundary layer on the test plate was taken to be 0.4 of inch thick for purposes of data evaluation. It will be recalled from the data presented in Figure 21 for a dry test plate that the velocity boundary layer was 0.35 in. thick at the first station of measurement at $x - x_0 = 3$ in.

It should be noted again that the velocity at the wall is not zero feet per second because of the presence of the liquid film. The velocity of the surface of the liquid film was approximately 7 ft/sec based on the flow mean thickness. The flow mean thickness of the liquid film was approximately 0.001 to 0.002 in.

Figure 26 presents the temperature profiles in the boundary layer measured at four stations along the wetted test plate.
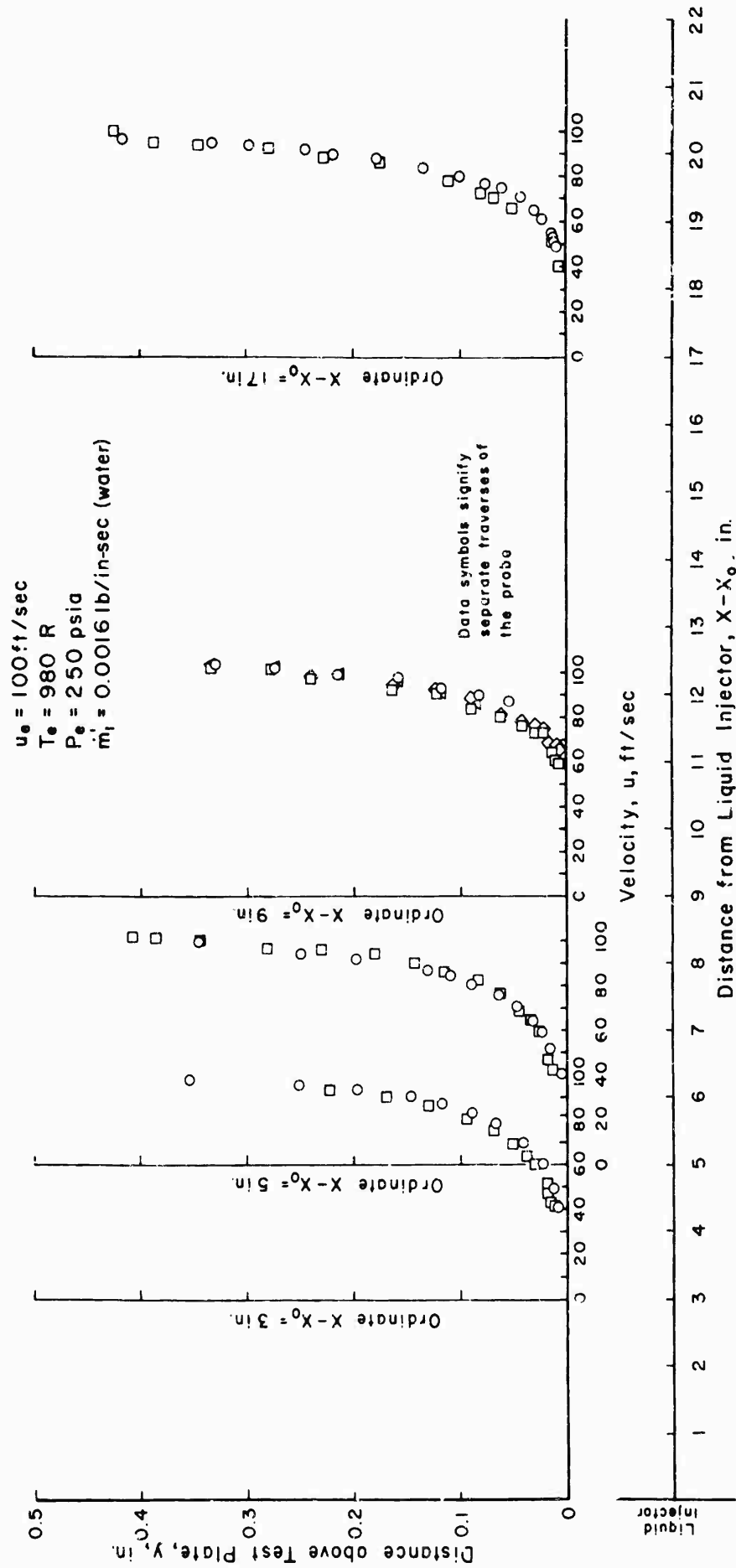
Figure 25. Velocity Profiles Measured in the Boundary Layer on the Wetted
Test Plate as a Function of the Distance from the Liquid Injector
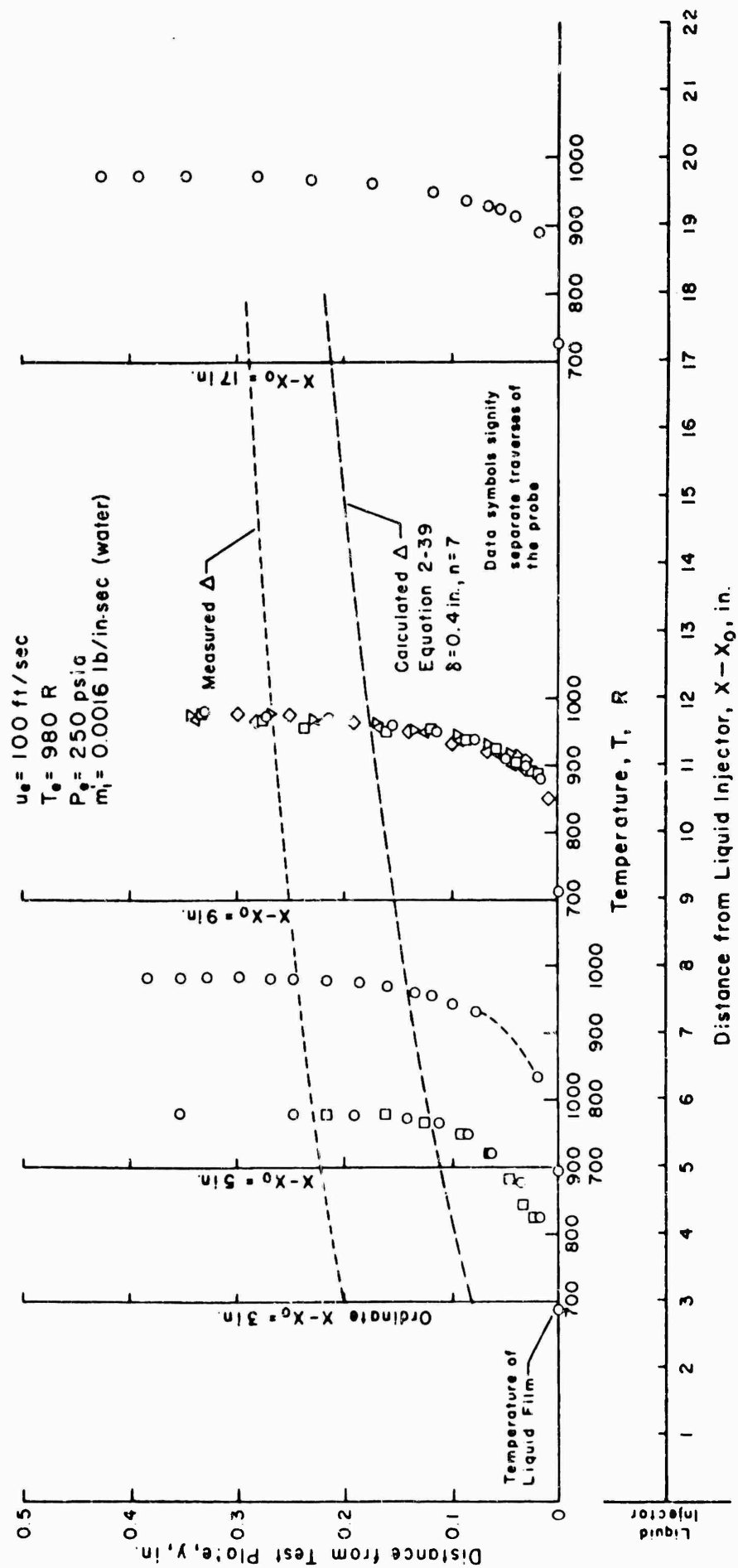
Figure 26. Temperature Profiles Measured in the Boundary Layer on the Wetted Test Plate as a Function of the Distance from the Liquid Injector

The stations of measurement were 3, 5, 9, and 17 in. from the injector slot. The ordinate is the distance above the test plate while the abscissas are temperatures in degrees Rankine Unlike the velocity boundary layer, the temperature boundary layer essentially begins growing at the injector slot. The short dash curve traces the growth of the thickness of the temperature boundary layer along the test section. The long dash curve (based on equation 2-39) presents the growth of the temperature boundary layer over a smooth dry plate possessing the same temperature discontinuity and free stream conditions present in the case of the wetted test plate. The experimentally measured temperature boundary layer was 0.2 inches thick at the first station of measurement. The rate of growth decreases as the flow moves downstream with the thickness reaching a value of 0.29 in at the station 17 in. from the injector slot. If the profiles presented in Figure 26 are superimposed, affine similarity is displayed by the last three profiles but the first profile is distorted toward a more laminar like profile.

Figure 27 presents the dimensionless velocity, u/u_e, and the dimensionless temperature, $\dfrac{T-T_f}{T_e-T_f}$, for the wetted plate as a function of the dimensionles distance from the wall. The ordinate is the ratio of the distance above the plate, y, to either the thickness of the velocity boundary layer, δ, or the thickness of the temperature boundary layer, Δ. The straight line drawn through the data points presents a power law correlation of the
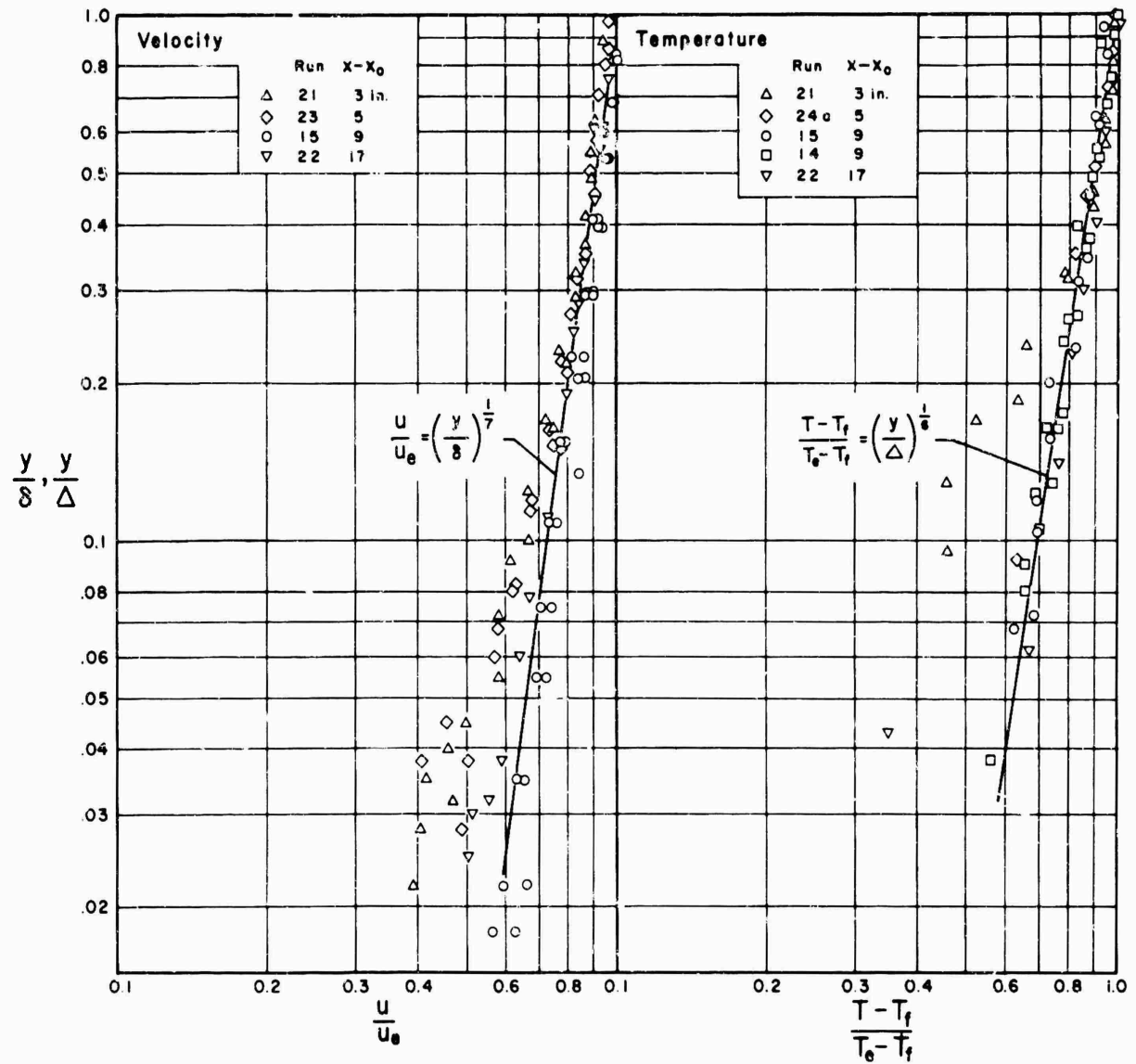
Figure 27. Power Law Correlation for the Velocity and
Temperature Profiles in the Boundary Layer
on the Wetted Test Plate

form $\frac{u}{u_e} = (\frac{y}{\delta})^{1/7}$ for the velocity data. The power law distribution correlates the data at all four stations of measurement for a dimensionless distance above the plate y/δ greater than 0.1. The data for which y/δ is less than 0.1 shows a high degree of deviation from the power law distribution.

The profiles of temperature for the last three stations of measurement at 5, 9, and 17 in. from the injector slot correlate to a power law of the form $\frac{T-T_f}{T_e-T_f} = (\frac{y}{\Delta})^{1/6}$. The data obtained at the first station of measurement does not correlate to a straight line.

Table 7 presents the values of the momentum thickness obtained from the graphical integration of the average profiles of the temperature and velocity at three stations of measurement.

Table 7

Values of Momentum Thickness for the Boundary
Layer over the Wetted Test Plate

Distance Along Test Plate, (in.)		Momentum Thickness, δ_2 (in.)
Total, x	From Injector Slot, $x-x_0$	
21	3	0.038 (u_e = 99 ft/sec)
27	9	0.032 (u_e = 104 ft/sec)
35	17	0.042 (u_e = 99 ft/ sec)
"	"	0.049 (u_e = 102 ft/sec)
"	"	0.045 (Average)

The three values of momentum thickness presented for $x - x_0 = 17$ in.

display the influence of the uncertainty in the value of the free stream velocity on the calculated momentum thickness. The gas generator instrumentation indicated that the velocity in the test section was 102 ft/sec while the probe measurements indicated the free stream velocity to be 99 ft/sec. The difference in the two measured values of velocity result in a 14 percent difference in the computed momentum thickness. The measurement set obtained at $x - x_o = 9$ in. was for a free stream velocity of 104 ft/sec or slightly higher than the value of 100 ft/sec quoted as nominal for the investigation.

A numerical value for the average local friction coefficient for the flow over the liquid film was calculated from equation 2-45. In the calculation the value employed for the average local friction coefficient for the dry test plate was the average of the two experimental values presented in Table 6. The value was $(\overline{c_f'})_{dry} = 0.0024$. The momentum thicknesses employed in the calculation were those values determined at $x - x_o = 17$ in., and appear in Tables 5 and 7. The value of the average local friction coefficient for the wetted test plate calculated in the aforementioned manner was $(\overline{c_f'})_{wet} = 0.0035$ within an estimated error of $\pm$ 30 percent. The derived values of shear stress and friction velocity were 0.38 lb/ft^2 and 3.9 ft/sec, respectively. The error figure noted above is the maximum value which could arise due to the compounding of the uncertainities in the values of the momentum thicknesses employed in the calculation, each with an estimated error of $\pm$ 15 percent.

Figure 28 presents the dimensionless velocity parameter, u^+, as a function of the dimensionless distance parameter, y^+, for the velocity profile measured at $x - x_0 = 17$ in. The value of the friction velocity required to correlate the data to Figure 28 was that value of 3.9 ft/sec corresponding to an average local friction coefficient of 0.0035. The solid curves in Figure 28 are reproduced from Figure 10 and display the influence of the roughness parameter on the law of the wall.

Figure 29 presents the dimensionless temperature parameter, T^+, as a function of the dimensionless distance parameter, y^+, for the temperature profile measured at $x - x_0 = 17$ in. The value of heat transfer parameter, β, required to correlate the data to Figure 29 was that value based on the average shear parameters corresponding to a friction coefficient of 0.0035 and the heat flux values presented in Table 10. The solid curve in Figure 29 is the generalized temperature distribution for air with $\beta = 0$.

Table 8 presents the values of the enthalpy-deficit thicknesses computed by graphical integration of the average curves through the experimental data at three stations of measurement. The three stations of measurement were 3, 9, and 17 in. from the injector slot.
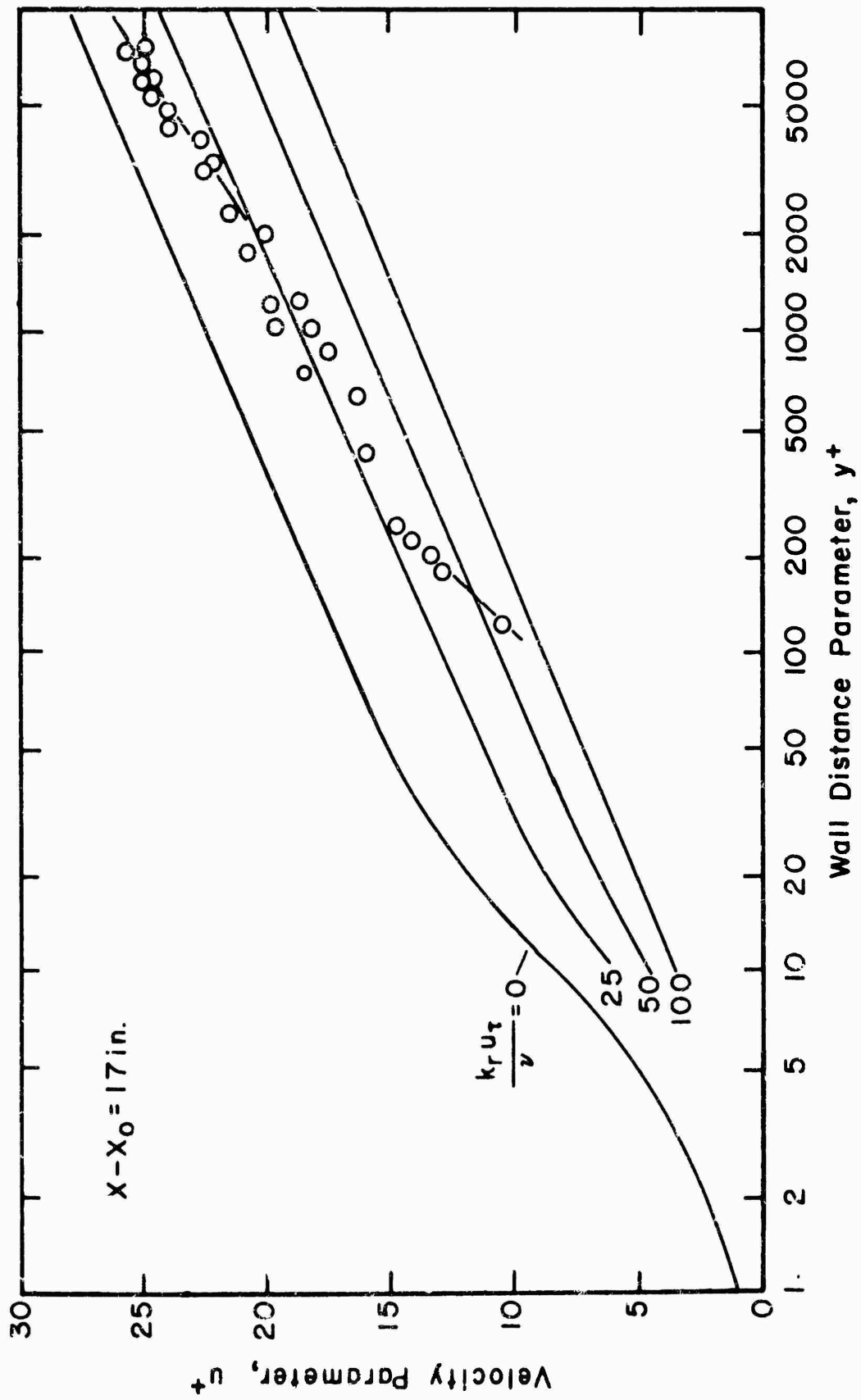
Figure 28. Law of the Wall Correlation of the Velocity Profile in the Boundary Layer on the Wetted Test Plate at $x - x_0 = 17$ in.

128
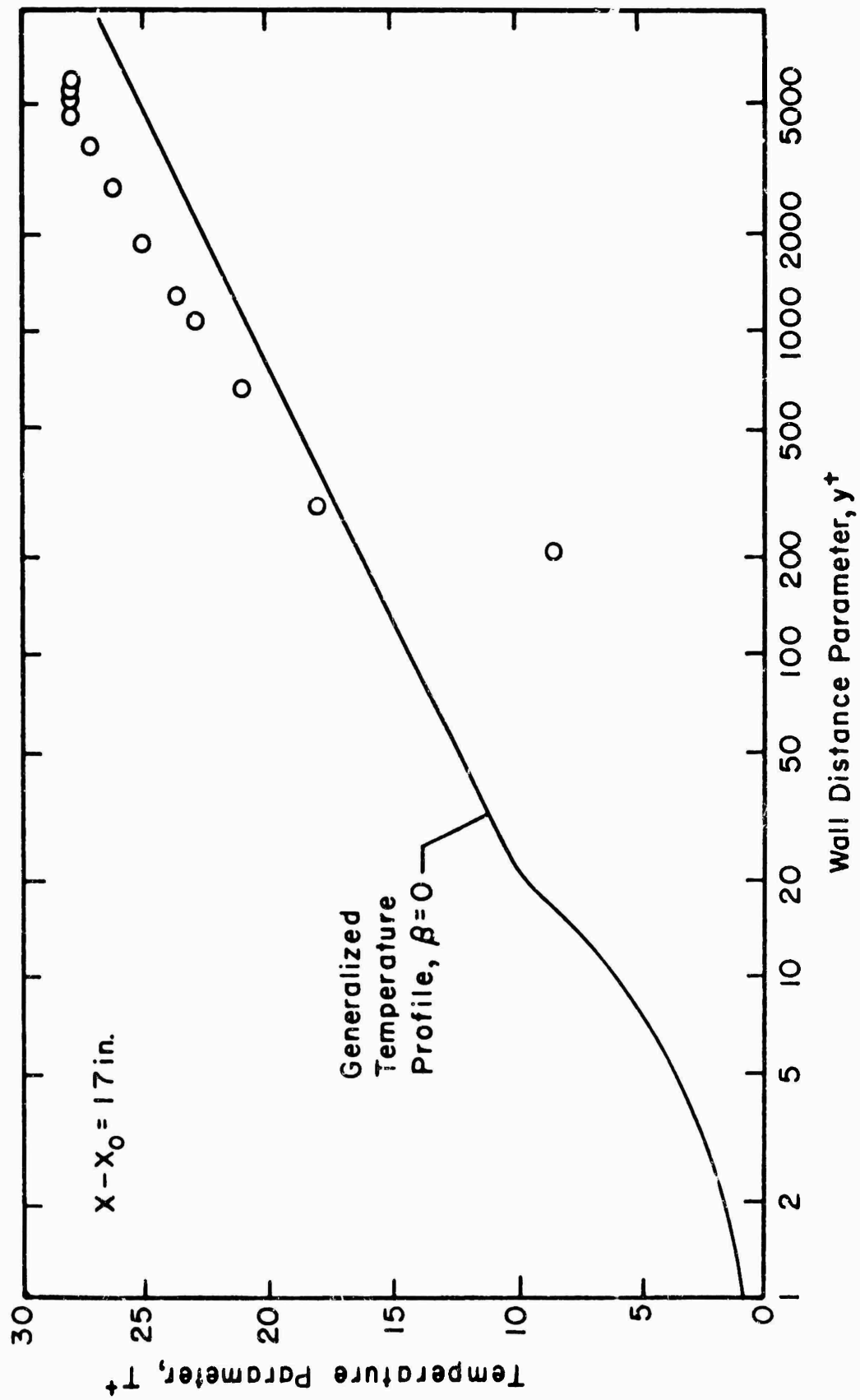
Figure 29. Correlation of the Temperature Profile in the Boundary Layer at
x − x₀ = 17 in. to the Generalized Temperature Distribution

Table 8

Values of the Enthalpy-Deficit Thickness for the Wetted Test Plate

Distance from Injector Slot, $x - x_0$ (in.)	Enthalpy-Deficit Thickness, Δ_2 (in.)
3	0.024 (u_e = 99 ft/sec)
9	0.029 (u_e = 104 ft/sec)
17	0.026 (u_e = 99 ft/sec)
"	0.025 (u_e = 102 ft/sec)

Table 9 presents the overall Stanton numbers calculated by equation 2-46 using the values of enthalpy-deficit thickness presented in Table 8. The calculation assumes no mass transfer. The length interval is from $x - x_0 = 0$ to the value of $x - x_0$ shown in the table.

Table 9

Calculated Values of the Overall Stanton Number for the Wetted Test Plate

Distance from Injector Slot, $x - x_0$ (in.)	Stanton Number, $\overline{S}$
3	0.008
9	0.0034
17	0.0015

No results are presented for the average local Stanton number determined between any two stations of measurement.

3.3.4 Heat and Mass Transfer Parameters for the Wetted Test Plate

Table 10 presents the average values of the heat and mass transfer parameters calculated from the experimental data for the length of test plate from the injector slot to the last station of measurement at $x - x_0 = 17$ in. The shear parameters required to make the calculation correspond to an average local friction coefficient of 0.0035. The equation or method employed to calculate the values given is presented in the last column.

Table 10

Average Values of the Heat and Mass Transfer Parameters
for the Wetted Test Plate from $x - x_0 = 0$ to $x - x_0 = 17$ in.

Parameter	Average Value	Equation or Method
Stanton Number, $\overline{S}$	0.0014	
Heat transfer to film	6.6 $\dfrac{B}{ft^2\text{-sec}}$	Graphical Integration of average data curves and equations 2-45, 2-47 and 2-48
Heat transfer for evaporation of water	5.5 $\dfrac{B}{ft^2\text{-sec}}$	
Heat transfer for sensible enthalpy	0.4 $\dfrac{B}{ft^2\text{-sec}}$	
Heat transfer to test plate	0.7 $\dfrac{B}{ft^2\text{-sec}}$	
Mass transfer from film, $\overline{m}''_v$	0.006 $\dfrac{lb}{ft^2\text{-sec}}$	Equation 2-48
Mass transfer parameter, $\dfrac{\overline{m}''_v}{\rho_e u_e}$	0.00085	
Heat transfer parameter, B	0.012	Equation 2-21

4. DISCUSSION OF RESULTS

4.1 Film Characteristics

It will be recalled that the film characteristics experiments were
of an exploratory nature designed to describe the characteristics of the
liquid film over which the boundary layer measurements were to be con-
ducted. The results as presented in the preceding section and the dis-
cussion of the results in the present section are, in the opinion of the
author, quite special to the subject investigation and should not be con-
strued as being general statements valid for conditions different from
those of the present investigation. Except where specifically noted the
liquid used was water.

4.1.1 Formation, Coverage and Termination
of the Liquid Film on the Test Plate

The results of the cold flow studies using water indicated that
a film formed on the surface of the test plate at the point of injection
and continued downstream as a film flow. The use of Freon 113 as the
injected liquid in cold flow was not evaluated due to the severe inter-
facial instability which occurred with the use of that liquid. Figure 17
which presents the only photograph obtained of a Freon 113 film in hot
flow reveals the same severe instability observed visually in cold flow.
Subsequent to the experiment with Freon 113 in hot flow, only water was
used as the injected liquid.

The cold flow experiments conducted with water did not fully reveal the difficulties which were to be encountered later in the hot flow experiments with respect to coverage of the test plate by the liquid, and in particular, the subsequent termination of the liquid film. The breakdown of the liquid film leading to dry areas on the test plate was observed in the cold flow experiments but at substantially lower flow rates than those employed in the hot flow experiments.

In the hot flow experiments the coverage of the test plate by a liquid film did not result in a uniform termination of the liquid film within the desired 3 inch interval at some length downstream of the liquid injector. The general nature of erratic termination of the liquid film as displayed in Figure 16 was the rule with only an occasional non-reproducible termination in the desired manner. The coverage of the test plate by the liquid was never observed to break down in internal dry spots, i.e., dry spots bounded all around by a liquid film.

The poor coverage of the test plate by liquid at sufficiently low flows to permit some kind of termination was attributed primarily to the following two factors: (1) the presence of the divider fences and the corners of the test section which served as sources for dry areas to originate, and (2) the presence of scale or small roughness elements on the test plate which induced breakdown of the film.

The typical non-uniform termination was attributed not only to prior breakdown of the film upstream but also to non-uniform spanwise flow distribution originating at the injector, coupled with a relatively low rate of evaporation. Even with the partitioned liquid injector and separate control valves, non-uniform spanwise injection was not completely

eliminated. A slightly higher local flow would tend to form a channel during termination, the slightly larger liquid flow requiring a longer length to evaporate. The low rate of evaporation meant that slight non-uniformities of spanwise flow rate were exaggerated in the region of termination.

4.1.2 Stability and Entrainment

The photographs of the liquid films presented in Figure 19 correspond to the operating conditions at which the boundary layer measurements were made. The frequency of the appearance of the larger instability waves is much greater than for the stable film shown in Figure 18. Further, entrained droplets are clearly visible at $x - x_0 = 6$ in., and appear as characteristic short white streaks at $x - x_0 = 15$ in. The entrainment at the latter position appears to be less than at $x - x_0 = 6$ in. The slight entrainment at $x - x_0 = 3$ in. may arise from the presence of an "induction length" required to establish the interfacial instability such that entrainment can occur. Whether the entrained droplets appearing at $x - x_0 = 15$ in. have just been generated or whether they persisted from further upstream is not known.

The liquid film at the nominal conditions of the boundary layer measurements appeared to be in the early stages of instability. Figure 20 reveals that for the same gas flow conditions larger liquid flow rates result in films for which there appears both more instability waves and more entrainment.

4.1.3 Roughness

The surface of the liquid film at the nominal flow conditions at which the boundary layer measurements were conducted appears in Figure 19. The crests of the larger instability waves were estimated to be on the order of 0.010 in above the surface of the test plate by comparison with the photographs in Figure 13. The flow mean thickness of the film was calculated to be 0.001 in. to 0.002 in. The height of the substructure waves, or the pebbled portion of the film, was estimated by the method of comparison of shadows at 0.005 in. or less.

The estimated thicknesses of the viscous sublayer and the buffer layer (see Table 2, Section 2.4.2) of the gaseous boundary layer above the liquid film are less than 0.001 in. and 0.003 in., respectively. The heights of the larger instability waves exceed the thickness of the entire inner region comprised of the two aforementioned layers. Hence, it should be expected that the structure of these two regions of the boundary layer was disrupted by the surface waves, and the boundary layer would be influenced by the roughness of the film. In Section 2 the apparent height of the roughness of the liquid film was estimated to be between 0.003 in. and 0.006 in. or 0.007 in. This estimate and the approximate maximum wave height observed agree in order of magnitude. One point is noted here, the large waves on the surface of film might act as distributed roughness elements as opposed to a uniform roughness. Further, the larger waves are moving in the same direction as the gas flow with a velocity on the order of 7 ft/sec or greater, that velocity represents nearly 10 percent of the free stream velocity.

The principal conclusion to be made from the foregoing is that the

liquid film in the subject investigation did not appear to be a hydrauli-
cally smooth surface with respect to the gas flow and possessed a signi-
ficant velocity in the direction of the gas flow.

4.1.4 Temperature of the Liquid Film

The measured temperature of the liquid film was in agreement with
the theory within the accuracy of the experimental technique (see
Table 4). The equilibrium temperature was reached within 3 to 6 inches
after injection (the initial temperature at the injector slot being
approximately 50F less than the equilibrium temperature). For the re-
mainder of the flow path downstream the temperature of the liquid
remained near the equilibrium value of 250F.

The film temperature at a free stream pressure of 250 psia was 250F
whereas the boiling point was 400F for the same pressure. The vapor
pressure of water at 250F is 30 psia, or 12% of the total pressure of the
gas stream. This would indicate that the mass concentration of vapor at
the surface of the film was low.

4.1.5 Summary

The indicated state of the liquid film over which the boundary layer
measurements were conducted is summarized as follows:

1. The interfacial structure was unstable with the presence of
larger instability waves over all parts of the film.

2. Entrainment of liquid was detected above the film over an area
from 3 to 6 inches beyond the point of injection to the end of the test
plate.

3. The surface of the film was not hydraulically smooth with

respect to the gaseous boundary layer and possessed a significant velocity in the direction of the gas flow.

4. The temperature of the film was more or less uniform over the entire plate, there being only a short induction length after the injector before the equilibrium temperature value of 250F was acquired.

5. The concentration of water vapor above the film was low.

4.2 Boundary Layer Measurements

The present section is divided into three subsections. The first subsection discusses the results of the measurements of the profiles of velocity and temperature in the boundary layer. The second subsection discusses the calculated parameters derived from the measured results The last subsection discusses the influence and possible sources of errors and uncertainties in the experimental results. The observations and statements presented in the first two subsections are made in light of the discussion of error and uncertainty presented in the last subsection.

4.2.1 Measured Profiles of Velocity
and Temperature

Figure 22 shows that the velocity profiles measured in the boundary layer formed over the dry test plate form a well ordered collection of data for all three stations of measurement. The non-dimensional velocity data correlate well to a single power law distribution with an exponent of 1/8.3. The single power law correlation indicates the similarity of the three turbulent boundary layers measured at the three axial locations. The foregoing results are in relative agreement with what would be

anticipated for a turbulent boundary layer on a flat plate.

Figure 27 shows that the velocity profiles measured in the boundary layer formed over the wetted test plate form a fairly well ordered pattern correlating to a 1/7 power law profile for $y/\delta \geq 0.1$. Although the presence of experimental error precludes a positive statement with respect to the difference in the power law distributions of the velocity profiles measured over the wetted and dry test plates, the slightly less full profiles obtained over the wetted test plate are consistent with the presence of roughness effects and higher shear stress at the surface of the liquid film.

The rate of growth of the velocity boundary layer over the dry test plate was much less than that predicted for the growth of a turbulent boundary on a smooth flat plate (see Figure 21). It is possible that this result can be attributed to the uncertainty in the determination of the thickness of the boundary layer or the free stream velocity. A similar result was noted, however, for the boundary layer on the wetted test plate where the thickness appeared to be a constant value of approximately 0.4 in. The geometry of the apparatus could have influenced the growth characteristics of the boundary layer such that flat plate correlations based on length are not applicable. This latter point is discussed in Section 4.3.

The temperature profiles measured over the liquid film at $x - x_0 = $ 5, 9, and 17 in. correlated well to a 1/6 power law distribution. The profile measured at $x - x_0 = 3$ in. was displaced significantly to the left. The last three measurements, in correlating to a single power law, display an affine similarity which is not predicted for temperature profiles after a stepwise change in wall temperature.

The predicted temperature profile for air in incompressible flow
on a smooth flat isothermal plate is close to 1/6th. Indicated in
Figure 27 is the fact that for all stations of measurement the profiles
in the temperature boundary layer were less full than the corresponding
velocity profiles. For a stepwise change in wall temperature the tem-
perature profiles are found to be fuller than the velocity profiles (see
Section 2.4.5). Hence, it is seen that relative positions of the measur-
ed profiles of velocity and temperature yield no indication that a step-
wise change in surface temperature was present upstream. Further, the
thickness of the measured temperature boundary layer was significantly
greater than for the temperature boundary layer predicted on a smooth
plate (see Figure 26).

Comparing the velocity and temperature profiles as they were measur-
ed, the 1/7th and 1/6th profiles, respectively, indicate that the in-
fluence of the stepwise change in surface temperature may have been much
less than some other influence, for example, surface roughness. Further
indication of this is seen in the thicker temperature boundary layer as
compared to the prediction for a smooth plate. The other alternative to
these results is to seek an experimental error which was consistent
enough in itself to yield the apparent consistent power laws to which the
data correlates. The possible errors are discussed in Section 4.2.3.

The known, identifiable differences between the dry test plate and
the wetted test plate which could lead, in part, to the observed results
are (1) smooth or surface roughness, (2) nearly adiabatic or heat trans-
fer, (3) stationary or moving boundary, (4) no mass transfer or mass
transfer, and (5) no entrainment or entrainment. Other effects may have

been present which could not be readily identified. One such effect may have been the result of the forward facing 0.030 in high step of the liquid injector. Such a step is an order of magnitude larger than the thickness of the viscous sublayer and the buffer layer of the boundary layer. In passing over such a step the uniform flow established in the boundary layer for these two regions in the lead section could be totally disrupted. The consequence of this disruption on the subsequent growth of the boundary layer may or may not have been significant.

Other effects which may have been present for the liquid film but not the dry plate are the following. The temperature profile measured at $x - x_0 = 3$ in. is distinctly inconsistent with those measured at the other three positions downstream, being shifted well to the left of the latter (see Figure 27). The same trend is displayed by the velocity measurements at $x - x_0 = 3$ in. and 5 in. Of the possible causes of the leftward shift one might well have been the disruptive effect of entrained droplets on the measured parameters. This will be noted later. Another possible cause, and one which would not be detected by pitot tube or thermocouple measurements, would be the formation of a stationary eddy generated after the injector slot. The generators for such an eddy were possibly the injector lip and the sudden change in surface roughness. Such an eddy would displace the boundary layer upward much as would a solid hump on the test plate. The gas passing upward over the eddy would not be intimately involved in either momentum or heat transfer until the gas again approached the test plate. The displacement effect of such a stationary eddy would account for the apparent rapid growth in both the velocity and temperature boundary layers in just three inches. Further,

the scatter noted in the measured velocity and temperature data obtained immediately above the liquid film may have resulted from such an eddy or similar distrubance. The foregoing is noted but not concluded.

4.2.2 Calculated Parameters

The calculated parameters of both momentum thickness and the enthalpy-deficit thickness for the wetted test plate display an inconsistency as a function of length. From Table 8 it can be seen that the calculated values of the enthalpy-deficit thickness at the three positions along the test plate fluctuate between 0.023 in. and 0.029 in. The fluctuation is such that the calculated enthalpy-deficit thickness was a maximum at the midway point of the test plate and decreases to either side. The foregoing type of variation is unacceptable on physical grounds, namely, the flow over the wetted test plate would have to first have been nearly adiabatic, and more unlikely, the gas would have to have been _heated_ by the liquid film over the last half of the test plate as evidenced by the decrease in the enthalpy-deficit thickness from $x - x_0 =$ 9 in. to $x - x_0 = 17$ in. A similar erratic behavior in the calculated values of momentum thickness is displayed by the results in Table 7. The aforementioned results are likewise unacceptable on physical grounds with respect to momentum exchange between the liquid film and gas flowing above the film.

The foregoing results reflect, in part, the leftward scatter of the measured data noted in the preceding section. The results derived from the measurements obtained at the fore end of the test plate are held to be not representative of what is actually occurring. Since the disruption of the measurements obtained over the wetted test plate tends to

decrease toward the aft end of the test plate, only those parameters cal-
culated from the measurements obtained at $x - x_0 = 17$ in. will be em-
ployed in further discussion. Further, note is taken here that the re-
sults obtained at $x - x_0 = 17$ in. may also be unreliable but they are
nonetheless considerably less reflective of disruptive effects than those
obtained at the fore end of the test plate.

The dispersion of the two values of the average local friction
coefficient determined for the dry test plate ($\overline{c_f} = 0.0019$ by UVP and
$\overline{c_f} = 0.003$ after Clauser) is indicative of either a systematic error in
the determination of the velocity in the boundary layer, or an error in
the determination of the free stream velocity and/or the thickness of the
boundary layer. The two values determined by the two methods should be
in agreement since both methods reflect the same universal character of
a turbulent boundary layer at constant pressure on a flat plate. The
transducer employed to measure the differential velocity pressure in the
boundary layer over the dry test plate may have sustained a shift in its
calibration curve when operating at 250 psi as compared to the pre-run
and post-run calibrations conducted at ambient pressure. A shift of 5
percent of the range of the calibration to larger than the actual differ-
ential pressure would result in a 2 5 percent increase in the indicated
velocity near the free stream value of velocity and a 10 percent increase
in the indicated velocity near the test plate An error of this kind in
the magnitudes just noted would be sufficient to cause the observed de-
viation of the two values of the friction coefficient. The assumption
that such an error exists brings the two values together at a common
value of $\overline{c_f} \simeq 0.0025$. Further, the presence of such an error would

lead to a 10 percent smaller value for the momentum thickness calculated from the measured velocity profiles. The same systematic error would also cause the measured velocity profiles to be fuller than were actually present.

The four measurement sets obtained for the wetted test plate did not employ the same transducer. Hence, no statement can be made regarding the presence of a similar systematic error fo the velocity measurements over the wetted test plate.

The error between the two experimental values for the average local friction coefficient for the dry test plate is approximately ± 25 percent based on the dispersion from the reference value after Spalding and Chi. The latter value was calculated employing the average value of the momentum thickness for the boundary layer on the dry test plate.

The value of the average local friction coefficient determined by equation 2-45 for the wetted test plate, $\overline{c_f'} = 0.0035$, is 40 percnet larger than the average value of the corresponding parameter evaluated for the dry wall, $\overline{c_f'} = 0.0025$. The value of the friction coefficient for the wetted test plate relative to the value of the same parameter for the dry test plate was calculated from the ratio of the corresponding momentum thicknesses at $x - x_0 = 17$ in. Both of the values of momentum thickness were subject to experimental errors of ± 10 to ± 20 percent based on the scatter of the data and transducer hysteresis. Since there is no way of determining how the aforementioned errors combine in the calculation of the friction coefficient, no reliable estimate of the appropriate error for that parameter can be stated In Section 2, it was predicted that on tne basis of the estimated roughness of the liquid

film and the presence of heat transfer, the friction coefficient over the wetted test plate would be 40 to 50 percent greater than for the dry test plate. Hence, even with a large experimental error the predicted increase and observed increase in the friction coefficient for the wetted test plate do reflect a substantial agreement.

The ratio of the mean value of the average local friction coefficient and the average value of the Stanton number determined from the measurement set at $x - x_o = 17$ in. for the wetted test plate is 2.4. The corresponding value the same ratio predicted on the basis of the direct Reynolds analogy is 2 (see equation 2-35). With due consideration of the previously noted experimental error and the unknown influences of surface roughness and surface velocity of the liquid film on the transport mechanisms of momentum and heat in the present investigation, the experimental results indicate the presence of the Reynolds analogy correlation.

The generalized velocity profiles presented in Figures 24 and 28 reflect the relationship between the measured values of velocity in the boundary layers and the values of the parameters calculated from the measured values. For the case of the dry test plate the pattern of all data points correlated to the value of $\overline{c_f} = 0.0019$ fall well above the predicted curve, i.e., the law of the wall. The pattern falls slightly below the predicted value when the value of $\overline{c_f} = 0.003$ is employed. The average value of $\overline{c_f} = 0.0025$ correlates the data in a pattern lying approximately + 2 ordinal units above the predicted curve. The patterns are all straight whereas normally a turbulent boundary layer will correlate to the law of the wall in a manner as indicated by the dotted line

in Figure 24. The failure of the correlated data to follow the normal
pattern may be further evidence of the systematic error noted earlier
since a progressive overestimate of the velocity as the wall is approach-
ed would yield a less curved pattern to the correlated data.

The generalized velocity profile for the boundary layer measured
over the wetted test plate at $x - x_0 = 17$ in. (see Figure 28) lies below
both law of the wall for a smooth flat plate and the correlated data for
the dry test plate. The lower position of the correlated data is expect-
ed and reflects the influence of roughness on the law of the wall. The
amount of the downward shift of the velocity profile for the wetted test
plate with respect to the velocity profile for the dry test plate (as
shown in Figure 24) corresponds to a roughness parameter $\frac{k_r u_r}{\nu}$ of 25 to
50. This range of the roughness parameter corresponds to the transition
region. The aforementioned correspondence is in approximate agreement
with the roughness regime predicted for the liquid film in Section 2.

The pattern of the data presented in Figure 28 agrees more closely
with the profile typical of turbulent boundary layers as discussed with
respect to Figure 24 and noted thereon. The correlated data which were
obtained nearest the wall drop below the general pattern. Such a drop
may indicate either an influence caused by the proximity of the moving
liquid film or an inaccuracy of measurement.

The measured temperature profile at $x - x_0 = 17$ in. correlates to a
curve which lies above and parallel to the generalized temperature pro-
file for air on a smooth flat plate. The agreement in direction of the
experimentally determined curve with that for a smooth plate indicates
that the measured temperature profile was representative of what was to

be expected. No comment can be made, however, regarding the vertical location of the correlated data since the data are correlated in a manner which is in inverse proportion to the heat transfer parameter, β, the value of which was not accurately determined herein.

Table 10 shows that approximately 85 percent of the calculated heat transfer to the liquid film resulted in the evaporation of the water, 5 percent was absorbed as sensible enthalpy of the water, while the remainder was lost to the test plate. The average value of the mass transfer was 0.006 lb/ft^2-sec, or a mass transfer parameter of approximately 0.0001. The value of the mass transfer parameter was an order of magnitude or more, les than either the Stanton number or the indicated increase of the average local friction coefficient for the wetted test plate as compared to that of the dry test plate. As a result the influence of mass transfer on the calculated parameters could be neglected.

4.2.3 Factors Influencing the Experimental Results

The three principal factors believed to influence the experimental results were (1) error in the determination of the velocity and temperature in the boundary layer and in the free stream velocity, (2) variation in the average value of the bulk flow parameters from experiment to experiment, and (3) unknown factors special to the experimental investigation.

Experimental error. The known sources of errors in the determination of the velocity profiles in the velocity boundary layer for which estimates of magnitude can be established are those due to transducer hysteresis and the uncertainty in the value of the free stream velocity. The error in the velocity determination due to transducer hysteresis

was ± 2.5 percent near the free stream value, increasing to ± 10 percent near the test plate. The uncertainty in the value of the free stream velocity was approximately ± 2 to 3 percent. The above two do not include the possibility of systematic error as noted in Section 4.2.2.

The known sources of errors in the determination of the total temperature profiles are those resulting from possible calibration shift of the thermocouple and the error band associated with the noise level of the recorded output of the thermocouple (see Appendix D). The former error was noted to be ± 3 percent during the three month span of time in which data were acquired. The latter error due to signal noise was estimated to be a maximum ± 10 percent of the temperature difference between the free stream and the test plate (26JF) for measurements near the test plate and to be a maximum of less than ± 5 percent of the same temperature difference for y/Δ greater than 0.1. The free stream temperature as indicated by three thermocouples showed agreement to within ± 2 percent of the aforementioned temperature difference.

The velocity and temperature measurements were employed in turn to establish the thickness of the velocity and temperature boundary layers. The error in these two parameters cannot be definitely established

The influence of the aforementioned errors in the velocity and the temperature on the derived parameters of momentum and enthalpy-deficit thickness cannot be definitely established since the manner in which the various errors might have combined is not known. The influence of the transducer hysteresis error on the momentum thickness was approximately ± 10 to ± 15 percent and the influence of the uncertainty in free stream velocity was approximately ± 5 to + 10 percent. The influence attributable

to the random scatter of the data was approximately ± 5 percent. It is highly doubtful that the resultant error was ever as much as the sum of the individual errors.

The influence due to the long term calibration shift of the thermo-couple on the calculated enthalpy-deficit thickness if such a shift occurred during a single experiment would be approximately ± 5 percent. The influence of the error inherent with the signal noise of the temperature measurement was estimated to be ± 10 percent at the most. The influence of the error in the velocity determination on the enthalpy-deficit thickness was approximately ± 5 to ± 10 percent at the most. As in the case of the momentum thickness, it is highly doubtful that the resultant error in the calculated value of the enthalpy-deficit thickness was ever as much as the sum of the individual errors.

Variations in the Bulk Flow Parameters. Table E.1, Appendix E, summarizes the deviation of the bulk flow parameters from the nominal flow conditions for the seven measurement sets. The variations of the operating parameters from run to run lead to difficulties in comparing the ensemble collection of data. The worst single deviation of the experimental series occurred in CFC-15 and CFC-27 where the free stream velocity was 4 ft/sec off from the nominal value. Otherwise the various flow parameters varied by little more than ± 2 percent from run to run. The influence of the combination of the slight deviations, how-ever, cannot be reliably established

Unknown Factors. The three most prominant factors the influence of which cannot be established in the investigation were (1) entrainment of liquid above the film, (2) the presence of the unstable surface of the

liquid film and the step changes in boundary conditions at the point of injection, and (3) the geometry of the experimental apparatus.

The presence of entrained liquid, which was purposefully established in the investigation, could have radically influenced the experimental determination of velocity and temperature in the boundary layer. The measured values of velocity near the liquid film at the fore end of the test plate scatter very badly from the power law distribution. The scatter could have been the result of ingestion of droplets into the total pressure tube leading to erroneous pressure measurements. The temperature indicated by the probe thermocouple could have been systematically incorrect due to the impact of the droplets on the sensing element.

The influence of the surface of the unstable film, as well as the step change in boundary conditions caused by the injection of the liquid, may have lead to unidentified influences on the structure of the boundary layers. Such an influence was noted in Section 4.2.1 with respect to the possible existence of a stationary eddy.

Finally, the geometry of the apparatus, having a rectangular flow channel and a 0.030 in. step at the injector slot, probably did not simulate a true flat plate. The deviation of the flow from that identified with a flat plate is not known and cannot be incorporated in the observed results. The presence of the boundary layer probe could have caused displacement of the flow in the boundary layer, and hence, erroneous measurements. The probe was, however, constructed along lines of good design practice (38), (39). Figure 13 reveals no bow wave or other disturbance of the liquid film at the location of the probe post

5. CONCLUSIONS AND RECOMMENDATIONS

5.1 Conclusions

The conclusions presented below are based on the results of the research reported herein.

1. The liquid film of water was unstable, displaying larger instability waves which lead to liquid entrainment in the gas stream.

2. The measured temperature of the liquid film agreed with the value of temperature predicted by Gater and by Knuth.

3. The surface of the liquid film was not hydraulically smooth with respect to the gaseous boundary layer.

4. The turbulent velocity boundary layer formed over the liquid film correlated to a 1/7th power law after a certain distance downstre? of the liquid injector.

5. The temperature boundary layer formed over the liquid film correlated to a 1/6th power law after a certain distance downstream of the liquid injector.

6. No effect predicted for the stepwise temperature discontinuity occurring at the liquid injector was observed in the measured temperature profiles.

7. The friction coefficient evaluated for the flow over the liquid film was 1.40 times (± 30 percent) greater than the friction coefficient evaluated over the same test plate without liquid injection.

8. The relative magnitudes of the friction coefficient and the Stanton number evaluated over the liquid film are in approximate agreement with the same relative magnitudes predicted by Reynolds analogy.

9. The presence of the liquid film and/or entrainment of the liquid from the film in the gas stream adversely influenced the physical measurements performed in the boundary layer

10. No identifiable effect was noted which would indicate that the physical mechanisms present in the fluid flow of the subject investigation were significantly different from the physical mechanisms already identified elsewhere for gas-liquid film flows.

5.2 Recommendations

The results of the subject investigation did not reveal any substantial difference in either the structure of the boundary layers over the unstable liquid film or the physical mechanisms involved as compared to conditions which would be predicted on the basis of previously acquired information. However, the quantitative aspects of the interaction between the liquid film and gaseous boundary layer were not established with sufficient accuracy to permit a thorough description of the effects present. It is recommended then, that an investigation similar to the one reported herein be performed in the presence of a stable film of liquid. In the investigation the techniques of measurement and experimental procedure should be directed toward a more precise evaluation of the interaction of the liquid film and the boundary layer.

Further, it is recommended that any investigation of unstable liquid films utilize experimental techniques which yield accurate results even in

the presence of entrainment. Such an approach may well preclude boundary layer measurements.

LIST OF REFERENCES

LIST OF REFERENCES

1. Gater, R. S., L'Ecuyer, M , and Warner, C. F., "Liquid Film Cooling. Its Physical Nature and Theoretical Analysis," TM-65-6, Jet Propulsion Center, Purdue University (1965).

2. Kestin, J., and Richardson, P.D., "Heat Transfer Across Turbulent Incompressible Boundary Layers," J. Heat and Mass Transfer, June 1963.

3. Knuth, E. L., "Mechanics of Film Cooling--Part 2," Jet Propulsion, January 1955.

4. Kinny, G. R., Abramson, A.E., and Sloop, J. L., "Internal-Liquid-Film-Cooling Experiments with ir-Stream Temperatures to 2000°F in 2- and 4-inch Diameter Horizo ;al Tubes," NACA Rept. 1087 (1952).

5. Knuth, E. L., "Evaporation from Liquid Wall Films into a Turbulent Gas Stream," 1953 Heat Transfer and Fluid Mechanics Institute (Stanford University Press, Stanford, California, 1953.

6. Knuth, E. L., "The Mechanics of Film Cooling--Part 1," Jet Propulsion, November-December 1954.

7. Charvonia, D. A., "A Study of the Mean Thickness of the Liquid Film and Characteristics of the Interfacial Surface in Annular, Two-Phase Flow in a Vertical Pipe," I-59-1, Jet Propulsion Center, Purdue University (1959).

8. Hanrathy, T. J., and Enger, "Interaction Between a Turbulent Air Stream and a Moving Water Surface," A.I.Ch.E. J., September 1957.

9. Chien, S., and Ibele, W., "Pressure Drop and Liquid Film Thickness of Two-Phase Annular and Annular-Mist Flows," J. Heat Transfer, ASME, February 1964.

10. Gili, L. E., Hewitt, G. F., and Lacey, P. M. C., "Sampling Probe Studies of the Gas Core in Annular Two-Phase Flow--II Studies of the Effect of Phase Flow Rates on Phase and Velocity Distribution," Chem. Eng. Sci., September 1964

11. Hartley, D. E., and Roberts, D. C., "A Correlation of Pressure Drop Data for Two-Phase Annular Flows in Vertical Channels," Queen Mary College, University of London, Nuclear Research Memo. Q. 6, May 1961.

12. Bennett, J. A. R., and Thornton, J. D., "Data on the Vertical Flow of Air-Water Mixtures in the Annular and Dispersed Flow Regions, Part I: Preliminary Study," Trans. Inst. Chem. Eng., September 1961.

13. Collier, J. G., and Hewitt, G. F., "Data on the Vertical Flow of Air-Water Mixtures in the Annular and Dispersed Flow Regions, Part II: Film Thickness and Entrainment Data and Analysis of Pressure Drop Measurements," Trans. Inst. Chem. Eng., September 1961.

14. Schneiter, G. R., "Mass Transfer in Annular, Two-Phase Flow," F-66-2, Jet Propulsion Center, Purdue University (1966).

15. Fulford, G. D., "The Flow of Liquids in Thin Films," Advances in Chemical Engineering, 5, (Academic Press, Inc., New York, 1964).

16. Luikov, A. V., "Heat and Mass Transfer in Evaporation," Inter. Chem. Eng., April 1963.

17. Luikov, A. V., "Heat and Mass Transfer in Capillary - Porous Bodies," Advances in Heat Transfer (Academic Press, Inc., New York, 1964).

18. Kelley, J. B., and L'Ecuyer, M. R., "Transpiration Cooling - Its Theory and Application," TM-66-5, Jet Propulsion Center, Purdue University (1966).

19. Emmons, D. L., "Effects of Selected Gas Stream Flow Parameters and Coolant Physical Properties on Film Cooling of Rocket Motors," TM-62-5, Jet Propulsion Center, Purdue University (1966).

20. Dorrance, W. H., Viscous Hypersonic Flow (McGraw-Hill Book Co., Inc., New York, 1962).

21. Barrow, H., "An Experiment on Flat Plate Turbulent Boundary Layer Flow- The Effect of Local Fluid Addition on Friction and Velocity Distribution," J. Roy. Aero. Soc., February 1958.

22. Olson, R. M., and Eckert, E. R. G., "Experimental Studies of Turbulent Flow in a Porous Circular Tube with Uniform Fluid Injection Through the Tube Wall," ASME Paper No. 65-APM-29 (1965).

23. Danberg, J. E., "Characteristics of the Turbulent Boundary Layer with Heat and Mass Transfer at M=6.7," United States Naval Ordnance Laboratory, NOL TR 64-99 (October 1964).

24. Eckert, E. R. G., and Drake, R. M., _Heat and Mass Transfer_, (McGraw-Hill Book Co., Inc., New York, 1959).

25. Deissler, R. G., and Loeffler, A. L., "Analysis of Turbulent Flow and Heat Transfer on a Flat Plate at High Mach Numbers with Variable Fluid Properties," NACA TN 4262 (1958).

26. Kestin, J., and Richardson, P. D., "Heat Transfer Across Turbulent Incompressible Boundary Layers," J. Heat and Mass Transfer, June, 1963.

27. Clauser, F. H., "The Turbulent Boundary Layer," _Advances in Applied Mechanics_, _4_, (Academic Press, Inc., New York, 1956).

28. Schlichting, H., _Boundary Layer Theory_, (McGraw-Hill Book Co., Inc., New York, 1960).

29. Rotta, J. C., "Turbulent Boundary Layers in Incompressible Flow," _Progress in Aeronautical Sciences_ (Pergamon Press, New York, 1962).

30. Mezey, R. S., "Mass Transfer and Pressure Drop in Annular Two-Phase Flow," TM-65-4, Jet Propulsion Center, Purdue University (1965).

31. Kutateladze, S. S., and Lent'ev, A. I., _Turbulent Boundary Layers in Compressible Gases_, (Academic Press, Inc., New York, 1964).

32. Owen, P. R., and Thomson, W. R., "Heat Transfer Across Rough Surfaces," J. Fluid Mech., March 1963

33. Rubesin, M. W., "The Effect of an Arbitrary Surface Temperature Variation Along a Flat Plate on the Convective Heat Transfer in an Incompressible Turbulent Boundary Layer," NACA TN 2345 (1951).

34. Spalding, D. B., "Heat Transfer to a Turbulent Stream from a Surface with a Stepwise Discontinuity in Wall Temperature," International Congress on Heat Transfer.

35. Reynolds, W. C., Kays, W. M., and Kline, S. J., "Heat Transfer in a Turbulent Incompressible Boundary Layer, II - The Step Wall Temperature Distribution," NASA Memo 12-2-58 (1958).

36. Clauser, F. H., "Turbulent Boundary Layers in Adverse Pressure Gradients," J. Aero. Sci., February 1954.

37. Spalding, D. B., and Chi, S. W., "The Drag of a Compressible Turbulent Boundary Layer on a Smooth Flat Plate with and without Heat Transfer," J. Fluid Mech., January 1964

38. Folsom, R. G., "Review of the Pitot Tube," Trans. ASME, October 1956.

39. Moffat, R. J., "Gas Temperature Measurement," Temperature, Its Measurement and Control in Science and Industry, Part 2, Applied Methods and Instruments (Reinhold Publishing Corp., New York, 1962).

40. Baines, W. D., and Peterson, E. G., "An Investigation of Flow Through Screens," Trans. ASME, July 1951.

41. Tables of Thermal Properties of Gases, Nat. Bur. of Stan. Circular 564, November 1955.

42. Keenan, J. H., and Keyes, F. G. Thermodynamic Properties of Steam, (John Wiley & Sons, Inc., New York, 1936).

APPENDIX A

NOMENCLATURE

Symbol

c_f	friction coefficient
c_f'	local friction coefficient
$\overline{c_f'}$	average local friction coefficient
c_p	specific heat
C_v	mass fraction of vapor, ρ_v/ρ
d	diameter
D	diffusion coefficient
F_1	term expressing the influence of entrained droplets in equation 2-10
h	enthalpy
k	thermal conductivity
k_r	effective height of roughness elements
L	Lewis number, $\rho D c_p/k$
$\dot{m}'$	flow rate per unit spanwise length
$\dot{m}''$	mass flux at wall in y direction
n	denominator of the power law exponent
P	pressure
P	Prandtl number, $c_p \mu/k$
q_s	heat flux
Q	volume flow rate
Q_1	term expressing the influence of entrained droplets in equation 2-11

R	gas constant
Re	Reynolds number, $u(\text{length})/\nu$
S	Stanton number, $q_s/c_p \rho_e u_e \Delta T$
$\bar{S}$	average Stanton number, $\bar{q}_s/c_p \rho_e u_e \Delta T$
S_i	Stanton number for constant wall temperature
T	temperature
T^+	dimensionless temperature parameter, $(1-T/T_s)/\beta$
u	velocity in the x direction (parallel to the test plate)
u^+	dimensionless velocity parameter, u/u_τ
u_τ	friction velocity, $(\tau_s/\rho)^{\frac{1}{2}}$
v	velocity in the y direction
W_v	term expressing the influence of entrained droplets in equation 2-12
W_v'	term expressing the influence of entrained droplets in equation 2-13
W^+	dimensionless liquid flow rate, $\dot{m}_1'/\rho_1 \nu_1$
x	length of flow from the start of the lead section
x_o	length of flow in x direction from the start of the lead section to the liquid injector slot
y	distance from the wall
y^+	dimensionless wall distance parameter, yu_τ/ν
Δy_n	height increment employed in graphical integration
Z	compressibility factor

Greek Symbols

β	heat transfer parameter, $q_s u_\tau/c_p T_s \tau_s$

γ	specific weight
δ	thickness of the velocity boundary layer
δ_2	momentum thickness
δ_B	continuous sublayer thickness of the liquid film
δ_f	flow mean thickness of the liquid film
δ_f^+	dimensionless liquid film thickness
δ_m	modal thickness of the wave disturbances
δ_r	relative film thickness
δ_T	maximum wave amplitude
Δ	thickness of the temperature boundary layer
Δ_2	enthalpy-deficit thickness
ε	eddy viscosity
κ	eddy conductivity
λ	apparent roughness height
μ	dynamic viscosity
ν	kinematic viscosity
ρ	density
τ	shear stress

Subscripts

d	dry
e	free stream
f	liquid film or surface thereof
g	gas
l	liquid
r	state of roughness

s   surface

t   turbulent

v   vapor

x   x direction or local

APPENDIX B

DESCRIPTION OF THE EXPERIMENTAL APPARATUS

APPENDIX B

DESCRIPTION OF THE EXPERIMENTAL APPARATUS

The gas source employed in the subject investigation was an air blowdown wind tunnel in which a portion of the air flow was heated by combustion with a liquid fuel. The principal features of the apparatus were that it had a wide range of operating conditions, i.e., flow rate, gas temperature and pressure, reproducibility of operating conditions from run to run, low drift about the operating point over run times up to one hour, and was safe and reliable enough to work with in the test cell during operation of the apparatus.

Figure B.1 presents a photograph of the basic configuration of the experimental apparatus. The apparatus which could be operated either in cold or hot flow used compressed air as the working fluid and methyl alcohol as a fuel. The principal parts of the apparatus as arranged in the direction of flow were: (1) the control valves, (2) the primary injector, (3) the primary combustor, (4) the secondary or diluent air injector, (5) the secondary mixer, (6) the lead and test sections, and (7) the nozzle. The present appendix discusses briefly the design, construction and operation of the aforementioned parts together with a description of the supporting equipment and instrumentation employed in the investigation.

162
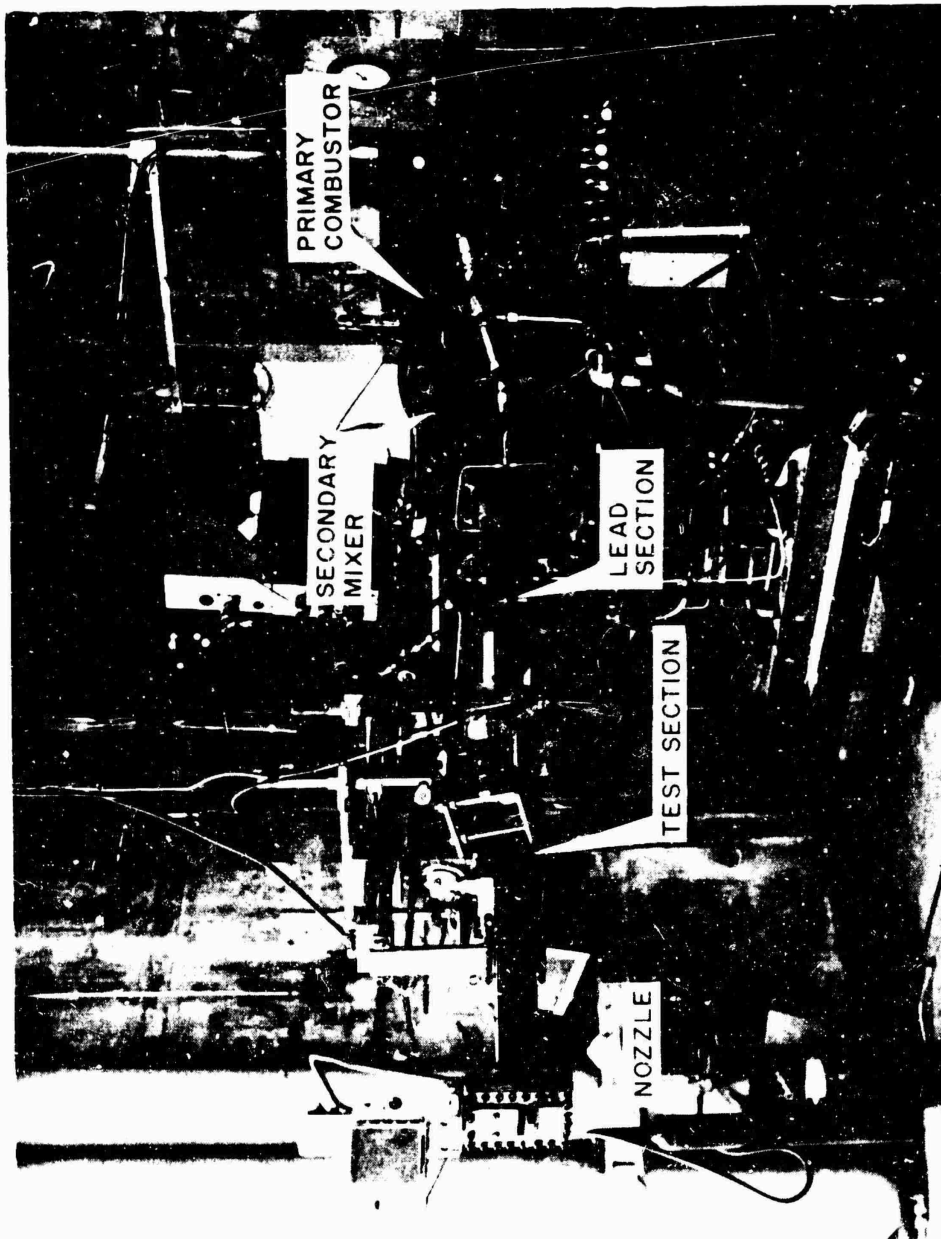
Figure B.1. Photograph of the Basic Configuration of the Experimental Apparatus

B.1 The Gas Generator

Figure B.2 presents a simplified sectional drawing of the gas generator portion of the experimental apparatus. Table B.1 lists the parts of the gas generator and describes the function of each.

Table B.1 Components of the Gas Generator

Part	Function
Primary Injector	To inject the fuel and air to be burned into the primary combustor.
Flameholder	To mix the fuel and air after injection and provide turbulence to hold the flame.
Primary Combustor	To provide a contained volume for combustion.
Secondary Injector	To inject diluent air to reduce temperature of working fluid to th desired value.
Perforated cone and turbulence grids	To thoroughly mix the diluent air with the combustion products from the primary in order to establish a uniform temperature throughout the gas flow.

Table B.2 presents the output characteristics of the gas generator for both the overall range of operation and the nominal run point at which the boundary layer measurements were conducted.
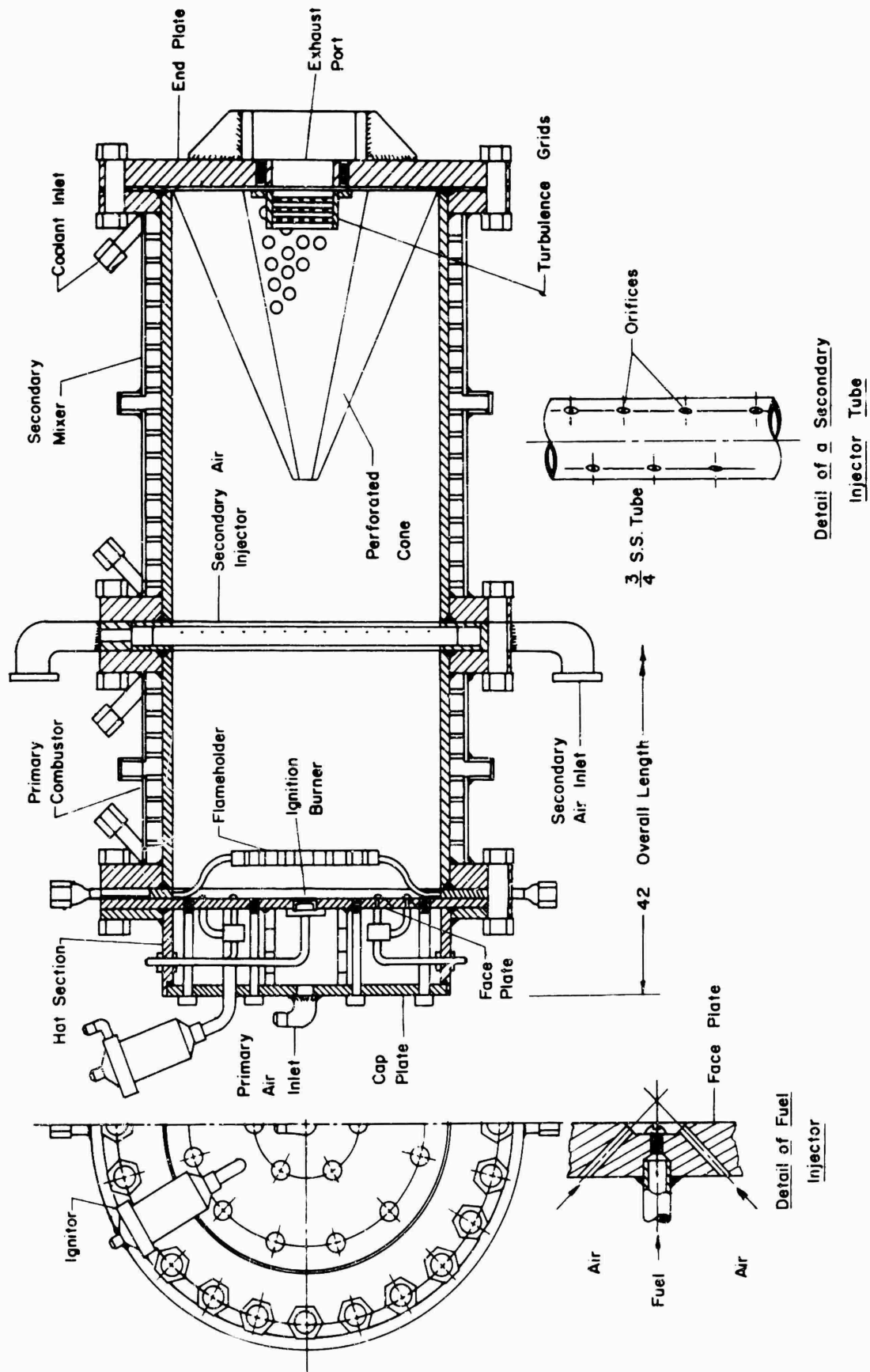
Figure B.2. Sectional Drawing of the Gas Generator

Table B.2 Output Characteristics of the Gas Generator

Parameter	Overall Range	Nominal Point
Total Pressure, psia		
Cold flow	up to 400	
Hot flow	125 - 350	250
Total Temperature, R		
Cold flow	500	
Hot flow	800 - 1000	980
Air Flow Rate, lb/sec		
Cold flow	up to 15	
Hot flow	1.5 - 12.0	2.70
Fuel Flow Rate, lb/sec	0.04 - 0.25	0.07

The air flow entering the gas generator was divided such that approximately 30 percent of the total flow entered the primary combustor to be burned with the fuel while the remaining 70 percent of the air flow was injected into the secondary mixing chamber. Approximately five percent of the fuel was injected from the ignition fuel injector located in the center of the primary injector while the remaining fuel was injected from the main portion of the primary injector. The fuel and the primary air (representing approximately 200 percent excess air) were burned in the primary combustor at a temperature of approximately 2500F with a thermal efficiency of approximately 50 percent. Smooth, stable combustion rather than high thermal efficiency was desired. The low

thermal efficiency was the result of insufficient volume in the primary combustor to permit complete combustion of the fuel.

The primary injector comprised three principal parts as shown in Figure B.2, namely, the face plate, the hat section air manifold and the cap plate. Ninety-five percent of the methyl alcohol fuel was injected through two concentric rings having a total of 30 separate fuel injector buds located on the face plate (see detail in Figure B.2). The face plate was fabricated from a circular piece of stainless steel plate 1/2 in. thick. On each side of the fuel injectors were two 0.100 in. diameter injector orifices for air directed at 45° to the direction of the fuel flow, the combination forming a triplet. The primary air was introduced into the injector manifold by a single 1.0 in. tube fitting. The fuel was manifolded by 1/4 in. O.D. stainless tube to six clusters of heavy wall tubing, each with five tubes, welded into the back of the face plate; these clusters fed fuel to the 30 fuel injectors. The ignition fuel which was required as part of the start sequence was manifolded directly to the center of the face plate and was injected through four small orifices against a copper splash ring. Air for the combustion of the ignition fuel was supplied through a ring of small orifices concentric to the ignition fuel injector orifices.

The flameholder consisted of a central perforated disc of stainless steel supported by eighteen 1/4 in. tubes of the same material which ran radially to an outside ring. Cooling water was introduced through a 1.0 in. tube fitting on the outer ring and flowed into the central disc through nine tubes and out from the central disc by the other nine tubes to leave the flameholder by a 1.0 in. tube fitting located 180° from the

input fitting. The flameholder was of all welded construction In the assembled gas generator the flameholder was sandwiched between the primary injector and the primary combustor

The primary combustor and secondary mixer chambers were of similar design and construction differing only in length. The former was 10 in long and the latter was 20 in. long. The inner wall was a section of 13 in. I.D. circular mild steel pipe having a wall thickness of 1/2 in. Welded at each end of the pipe section were one inch thick mild steel flanges with twenty-four 1 in. nominal bolt holes equispaced on a bolt circle of 20 in. The coolant passages were formed from extruded lead stripping with a 1/4 in. by 3/4 in cross section which was wrapped in a spiral around and soldered to the pipe. The outer jacket of the coolant passages was formed from half sections of 1/8 in. wall, 16 in. I.D. stainless steel tube with an expansion joint located in the middle. The jacket was sealed all around by weldments. Inlet and outlet fittings for the coolant, which was water, were welded over holes in the outer jacket and located at either end of the lead spiral All cooled parts were incorporated in a single pass coolant path.

The secondary air injector was fabricated from seven parallel 3/4 in. O.D. stainless steel tubes set in a 13 in I.D outer ring which served as a distribution manifold Each tube was drilled with a 0 125 in O.D. hole every 3/8 in along its length in such a way that two rows of orifices were formed directed downstream 45° off from the direction of gas flow from the primary combustor (see detail in Figure B 2). This arrangement enhanced turbulent mixing immediately downstream from the injector tubes. The injector tubes were fed from the outer ring which

in turn was fed secondary air through two 2 in. pipe fittings located 180° apart welded on the outermost part of the ring.

Downstream of the secondary air injector was located a stainless steel cone perforated with 1/2 in holes. The cone pointed upstream and was clamped between the end plate and aft flange of the secondary mixer chamber. Turbulence grids were mounted just ahead of the 2 in. x 4 in. exit port located in the center of the end plate. The perforated cone and turbulence grids induced mixing of the secondary and primary gases. The end plate was fabricated from 1 in. thick mild steel plate reinforced by gussets welded on the outside.

The flanged sections of the gas generator were bolted together with twenty-four 1-8 studbolts. The gaskets between the separate sub-assemblies were either 1/32 in thick aluminum or 1/16 in thick composition asbestos. Concentric serrations to aid sealing at the gaskets were machined on the injector face plate, the end plate and the flanges; no serrations were present on the flameholder or secondary air injector.

Operation. Figure B.3 presents a simplified schematic diagram of the flow system for the experimental apparatus. The air used in the experiments was drawn from the high pressure supply tanks which comprise the blowdown air supply for the Jet Propulsion Center. The tanks were charged with a maximum pressure of 2400 psig. The compressed air was delivered to an isolating valve located on the roof of the test cell by pipe line from the supply tanks. The isolating valve on the roof was a 2 in. 1500 ASA Annin pneumatically operated open/closed valve. It was present as a safety feature to isolate the high pressure air from the test cell housing the apparatus in the event of a severe mechanical
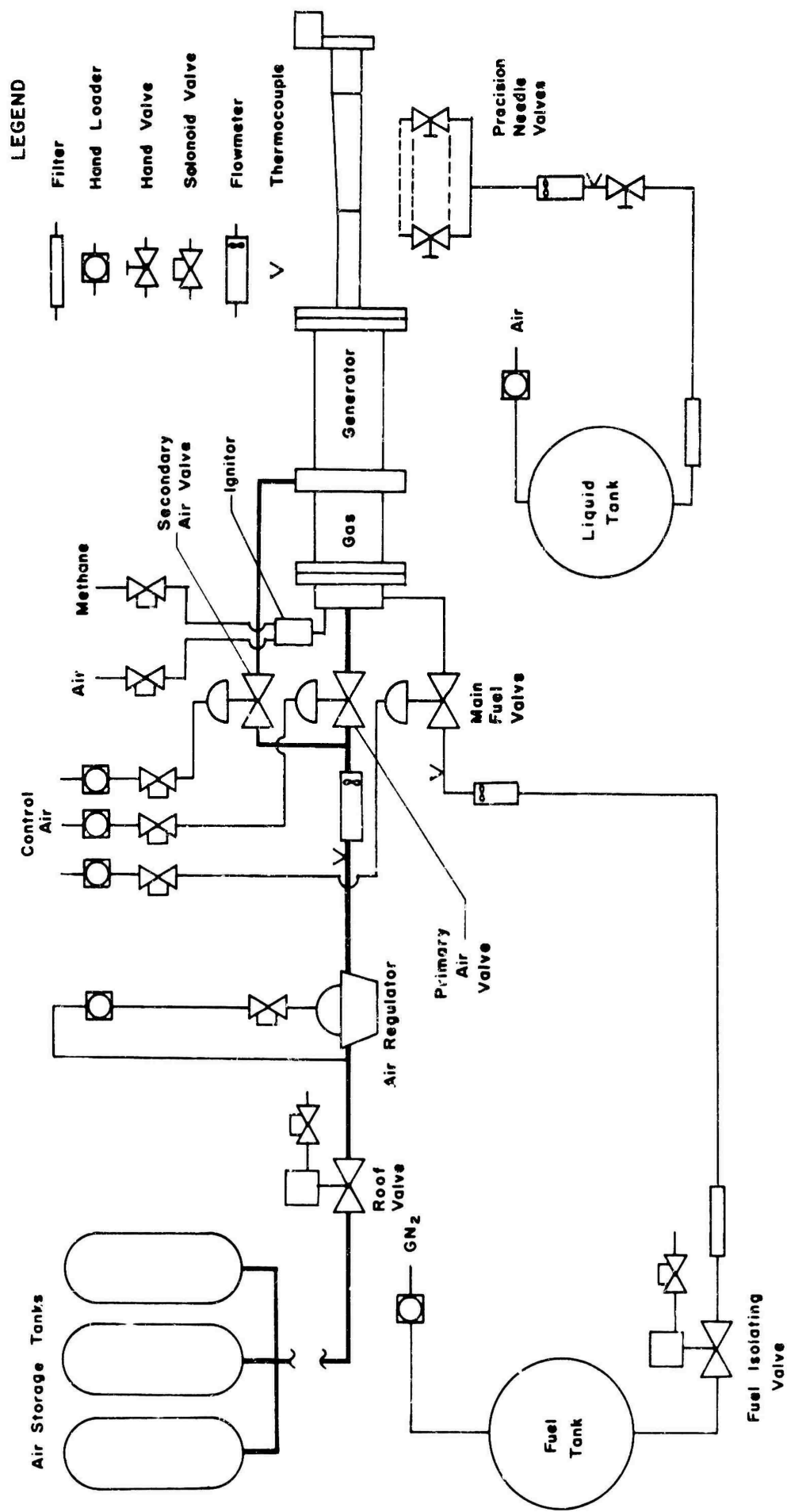
Figure B.3. Schematic Diagram of the Flow System for the Experimental Appartus

malfunction of the gas generator.

The air to be used in the apparatus was reduced from the supply line pressure by a 2 in. Grove Powereactor dome regulator located immediately downstream from the roof isolating valve. The Grove regulator was loaded by means of a small volume Grove pressure regulator. The volume flow rate of air was measured with a 2 inch Brook's turbine flowmeter located after a straight section of pipe downstream of the regulator. The weight flow rate of air was determined from the frequency output of the flowmeter and the static pressure and temperature of the air measured immediately ahead of the flowmeter. The static pressure was measured with a Wiancko static pressure transducer and the temperature was measured with an iron-constantan thermocouple. The three aforementioned parameters were recorded during an experiment on Brown self-balancing stripchart recorders.

The air flow to the gas generator was controlled by two Annin Domotor valves, a 2 in. valve for the secondary air and a 3/4 in. valve for the primary air. Control air for these pneumatic valves as well as for other pneumatic functions in the system was supplied at pressures of 400, 100, 45, and 30 psig from either Grove Powereactor regulators or Nullmatic small volume regulators.

The methyl alcohol fuel was stored in 55 gallon shipping drums and transferred to a 6 cu. ft. run tank located outside the building housing the test cell. The fuel was pressurized with gaseous nitrogen by means of a small volume Grove pressure regulator. The fuel tank was isolated from the building by a pneumatically operated Annin valve located beneath the fuel tank. The flow rate of fuel was measured with a 1/8 in.

Potter turbine flowmeter, the frequency output of which was recorded on a Brown recorder. The fuel flow rate was controlled by means of a modified 3/4 in. Annin Domotor valve which was rebuilt to control with precision the relatively small flow rate of fuel.

Before the gas generator was started in hot flow the air pressure and fuel tank pressure were set to the desired value. Coolant water was supplied to the gas generator by a Worthington turbine pump driven by an electric motor. The three Annin Domotor valves were pre-set using Null-matic control regulators to give the proper start flow rates of primary air, secondary air and fuel.

The ignition source for the gas generator was a small combustor (see Figure B.2) which burned gaseous methane and air ignited by dual spark plugs.

The ignition sequence was controlled by an automatic sequencer. The ignition sequence was as follows:

1. The methane-air ignitor was started.

2. When the ignitor reached the desired temperature, the automatic sequence was initiated.

3. The ignition fuel and primary air valves opened simultaneously and a pilot flame was established in the center of the primary injector off of the ignition fuel injector.

4. Two seconds later, the primary fuel and secondary air valves opened simultaneously.

5. The ignitor combustor was shut down and a second or two later, mainstage ignition was accomplished by the pilot ignition flame.

The whole automatic start sequence required approximately six or seven seconds. Once mainstage ignition was accomplished (usually at reduced flow rates), the operator brought the gas generator up to the

desired run point using the controls for the Annin Domotor valves.

During operation of the gas generator monitoring of the various pressures associated with the system was accomplished either by Bourdon tube pressure gages or Wi cko pressure transducers. The outputs of the latter were displayed to the operator by milliameters and also recorded on Brown stripchart recorders. Flow rates of fuel and air were also displayed to the operator by milliameters and recorded on stri chart recorders. The temperature of the gas leaving the gas generator was measured by two chromel-alumel thermocouples located immediately downstream of the end plate at the entrance to the lead section. The output of one of the thermocouples was displayed to the operator on a direct reading milliameter while the other output was recorded on a stripchart recorder. The total pressure of the gas immediately downstream of the last set of turbulence grids in the lead section was the value employed to set the total pressure of the run point. The total pressure was measured, displayed and recorded in the manner as previously described.

After the desired operating point had been achieved approximately ten minutes were required for the test section to achieve thermal equilibrium. Only then were the experiments begun. During run point operation the gas generator exhibited a random drift about the run point of $\pm$ 10F of total temperature and $\pm$ 0.5 psi of total pressure.

B.2 The Test Section, Lead Section and Nozzle

Figure B.4 presents a sectional drawing of the test section. The test section had a rectangular cross section 4 in. x 1 1/2 in. at the fore end and an overall length of 24 in. between flanges. The test section had three principal parts, namely, the test plate, a three sided
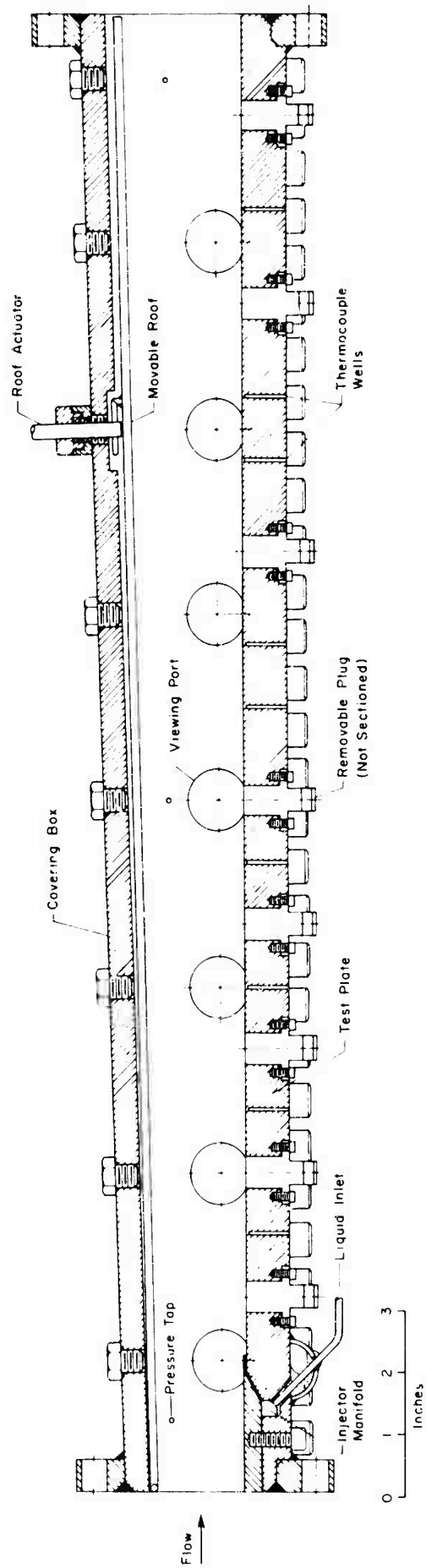
Figure B.4. Sectional Drawing of the Test Section

covering box which formed the side walls and top, and a movable roof hinged at the fore end of the test section and attached to a positioning shaft 15 in. from the fore end and protruding through the top of the covering box. The roof, which could be positioned by an electric motor, permitted the cross sectional area to be varied so as to achieve a zero axial static pressure gradient during an experiment

The covering box was fabricated from 1/2 in. thick stainless steel plate cut to the desired shape and welded. In each of the side walls were located seven 1/2 in. thick, 1 in. O.D. circular Pyrex glass windows located on 3 in. centers on both sides of the test section. The windows were used for both visual and photographic observation of the test plate. Each window was sealed with a Viton B O-ring compressed into a circular seal groove by the window flange. The durability of the glass windows was enhanced by fire polishing the edges before installation. (Most of the windows would eventually begin to crack and flake off on the inside but only after a dozen or so starts of the gas generator and total running times of 20,000 to 30,000 secs. at the nominal run point.)

The covering box was attached to the test plate by 3/8-24 high strength bolts on 3/4 inch centers threaded into a longitudinal flange on either side of the covering box and shouldered on the test plate. The longitudinal seals (one on either side) between the covering box and the test plate consisted of one length of 1/16 in. diameter and one length of 1/8 in. diameter Viton A O-ring cord on each side. The end seals of the test section were rectangular tongue and groove joints employing 1/16 in. thick Teflon gaskets in the grooves.

Figure B.5 presents photographs of the top and bottom of the test plate. The test plate was fabricated from 3/4 in. thick 304 stainless steel. The top, or wetted surface of the test plate, was polished in successive stages with grit, ending with red rouge. This polishing made the surface hydraulically smooth to both the liquid and gas flows encountered in the experiments.

Located at the fore end of the test plate was the liquid injector. The final configuration of the injector (see Figure B.4) used in the investigation was a 1/4 in. thick plate 4 in. wide which tapered to an overhung lip 3/8 in. long and 0.020 in. thick. The injector plate sat in a recess machined in the test plate and was drawn down against the test plate by 5 1/4 - 20 screws inserted from beneath the test plate. The seal between the injector plate and the test plate was accomplished with 1/16 in. cross section Viton A O-ring cord and technical "G" cement. The lip of the injector pressed down on a strip of 100 mesh, 0.010 in. thick brass gauze. The liquid entered from beneath the test plate through 7 1/8 in. O.D. tubes, each tube leading to a separate manifold cavity below the injector plate. The flow of liquid in each of the seven tubes was controlled by a separate precision needle valve. The combination of the needle valves, separate manifold cavities and wire gauze gave the best control of the distribution of liquid spanwise across the test plate. The central 50 percent of the wetted surface of the test plate could be isolated from the outer portion of the test plate by two longitudinal fences 0.030 in. high. This construction was employed to isolate the liquid film in the central region of the test plate from the liquid film nearest the walls of the test section. The latter portion of the film would be influenced by corner effects.
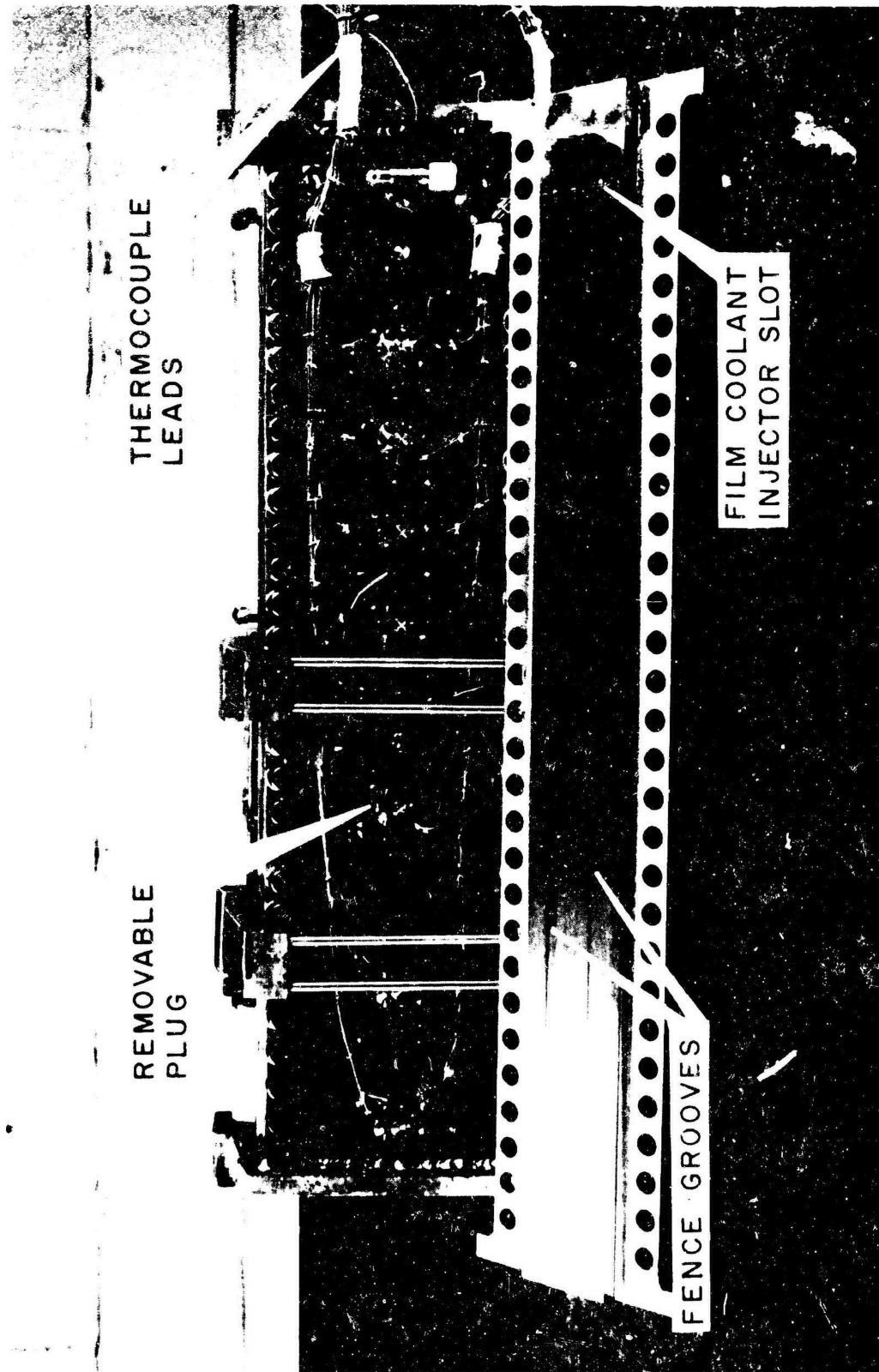
176

Figure B.5. Photographs of the Top and the Bottom of the Test Plate

The test plate was instrumented with 38 iron-constantan thermocouples inserted and sealed in holes drilled from the underside to within 0.030 in. of the wetted surface. The thermocouples were distributed longitudinally along the central 1 in. of the test plate. Spot welded to the underside of the test plate were 16 chromel-alumel thermocouples distributed in a manner similar to that of the iron-constantan thermocouples, i.e., along the central 1 in. of the test plate.

Located along the centerline of the test plate at various distances from the liquid injector were eight 1/2 in. diameter plugs running through the test plate and polished flush with the wetted surface (these are not visible in Figure B.5). These plugs were selectively removed to provide access to the surface of the test plate for the boundary layer probe. One plug was constructed with a flush mounted thermocouple to measure the temperature of the liquid film directly.

The liquid to be injected onto the test plate was transferred from storage containers to a 3 cu. ft. run tank located in the test cell. The run tank was pressurized with air by means of a Grove Powereactor pressure regulator loaded by a small volume Grove pressure regulator. The liquid was tubed first to needle valves located in the control room. These valves were employed as a course adjustment of the flow rate of the liquid.. The liquid line returned to the test cell. The flow rate of liquid was measured with a Brooks Elf flowmeter located upstream of the seven precision needle valves mentioned earlier. The frequency output of the flowmeter was displayed to the operator by a milliameter and recorded on a stripchart recorder.

Ahead of the test section was the lead section. The lead section had a rectangular cross section 4 in. x 1 1/2 in. and was 18 in. long. The walls and flanges were 1/2 in. thick stainless steel. The internal surface of the lead section had a smooth machine finish. Located 1/2 in. in from the upstream end of the lead section was a 1 in. thick pack of 1/16 in. diameter, 3 mesh wire screens. The screen pack served to introduce a flat velocity and temperature profile in the lead section and at the same time quiet the random flow fluctuations resulting from the combustion in the primary. The average value of the x-component of the turbulance in the test section was estimated to be approximately $u'/u_e = 0.015$ (based on Reference 40)

Downstream of the test section was a nozzle. The throat region of the nozzle was preceded by a 12 in. long straight rectangular channel so that the converging of the flow at the throat would not begin in the test section. This convergence effect was observed in an earlier version of the nozzle which was 10 in. shorter.

B.3 The Boundary Layer Probe

Figure B.6 presents two photographs of the boundary layer probe employed in the subject investigation. Figure B 7 presents a sectional drawing of the probe.

The principal parts of the probe were: (1) the head on which were mounted the sensing elements, (2) the movable shaft on which the head was mounted and which served to move the head during a traverse, (3) the plug which was inserted into the test plate, (4) the body in which were located the shaft seals, and (5) the bottom support in which the movable shaft terminated and from which the output lines were withdrawn. The

STATIC PRESSURE TUBE

THERMOCOUPLE

THERMOCOUPLE

TOTAL PRESSURE TUBE

MOVABLE SHAFT

1/2 INCH

PROBE HEAD

REMOVABLE PLUG

BODY ASSEMBLY

ELECTRICAL OUTPUT LINES
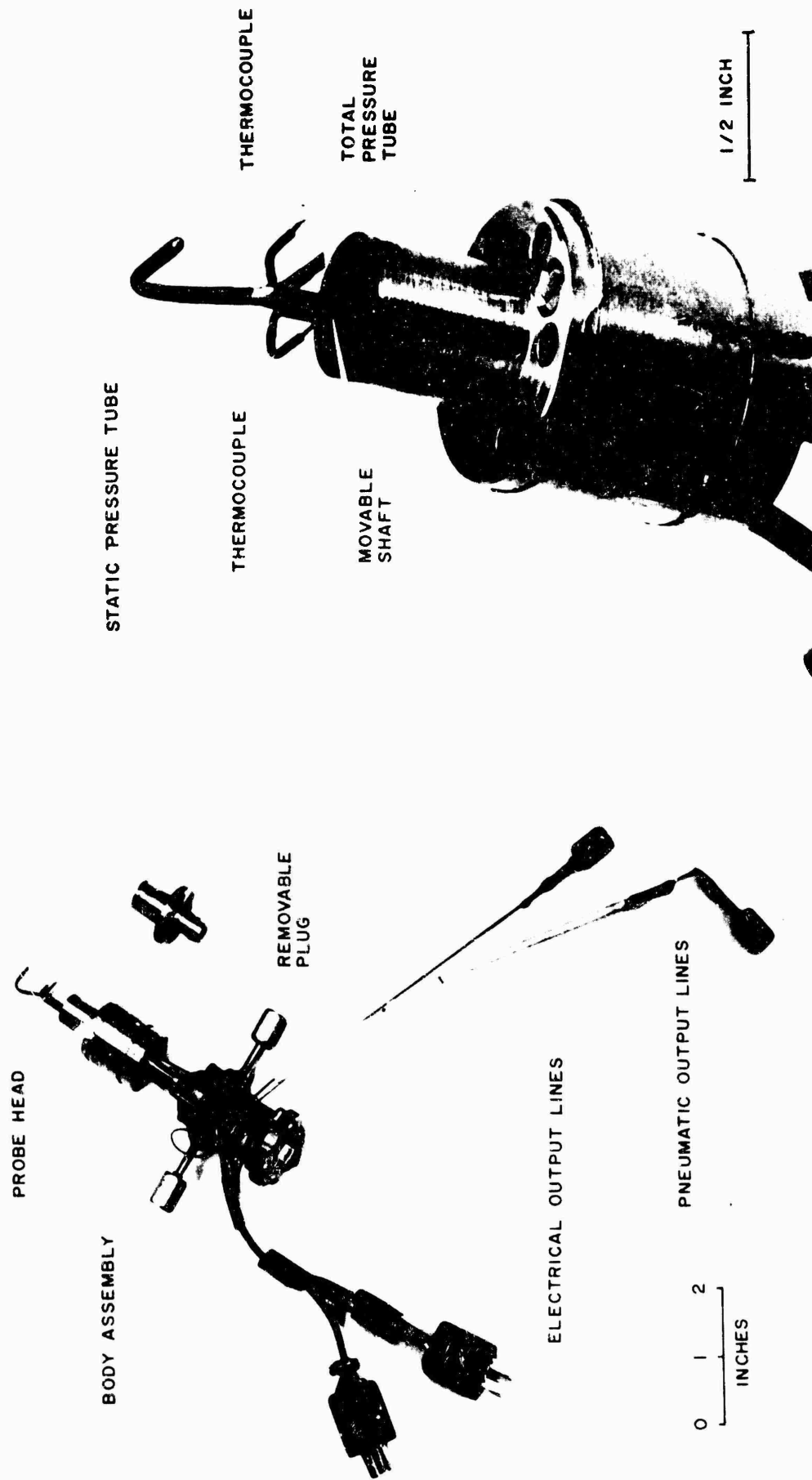
PNEUMATIC OUTPUT LINES

0 1 2
INCHES

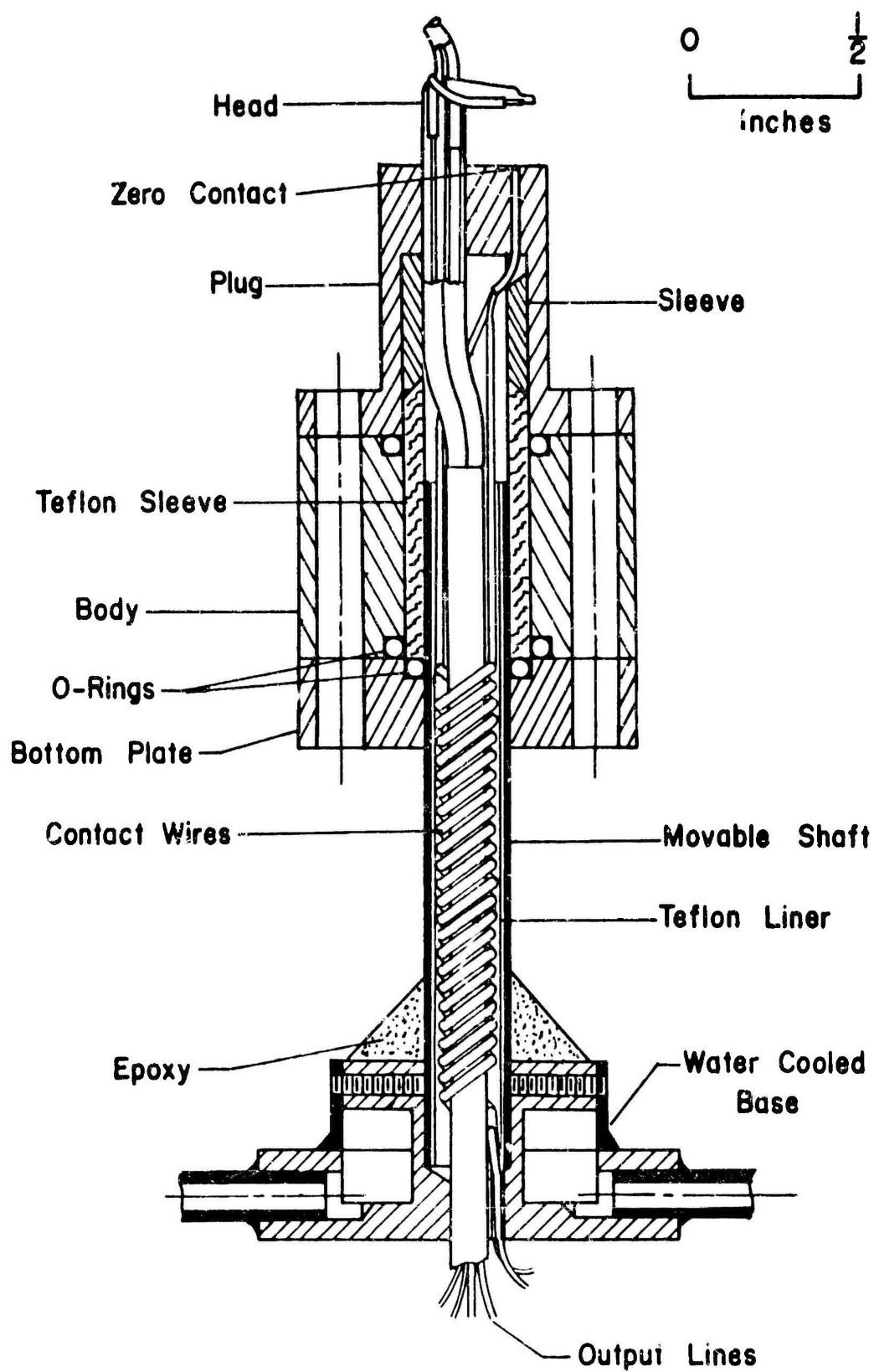Figure B.6.   Photographs of the Boundary Layer Probe

Figure B.7. Sectional Drawing of the Boundary Layer Probe

bearing screw located at the bottom of the support was the point where the up and down transversing motion was applied to move the head.

The head of the probe carried four sensing elements, namely, a total pressure tube, a modified Prandtl tube for sensing static pressure*, and two thermocouple probes** located on either side of the total pressure tube. The output lines for the pressure probes and the thermocouple wires were carried inside the movable shaft to the bottom support (see Figure B.7). The cross section of the shaft protruding through the plug was oval in shape with a length of 1/8 in. and a width of 1/16 in. The total pressure tube which was directed upstream was 0.30 in. long. The tube started at the base of the head as a circular tube 0.043 in. O.D. and changed to a flattened oval 0.050 in. across and 0.003 in. high. The metal wall on the lower edge of the oval port was honed to a thickness of less than 0.001 in. while the upper edge of the oval was honed to approximately 0.002 in. The total pressure tube was inclined downward toward the surface of the plug but the flattened portion of the tube and the oval port faced directly upstream.

The portion of the Prandtl tube which was directed parallel to the plug surface (and to the gas stream) was a 0.4 in. long, 0.043 in. O.D. tube, with a closed hemispherical tip. Behind the tip were cross drilled

---

* The Prandtl tube was subsequently mounted on a separate plug and inserted immediately behind the probe.

** During operation of the probe, one of the thermocouples failed leaving only one with which the temperature measurements were made.

six No. 80 holes, three holes at 90 to the other three holes, giving a total of 12 holes.for sensing the static pressure outside the boundary layer.

The thermocouples were made from commercial twin lead 0.003 in. O.E. chromel-alumel thermocouple wire enclosed in a 0.015 in. O.D. stainless steel sheath and insulated with magnesium oxide. The sheathed wire was supported by 0.030 in. O.D. stainless tubes silver soldered to the top of the movable shaft. The junctions of the thermocouples were formed by silver soldering together two 0.030 in. long bare thermocouple wires protruding from the sheath. The silver solder extended to and was bonded to the sheath to prevent moisture from entering the magnesium oxide insulation. The effective diameter of the junction was taken to be 0.015 in. for purposes of determining the elevation of a thermocouple head above the surface of the plug. The sheathed thermoccuple wires were carried inside the movable shaft to the bottom support from which the wires were carried to a plug type connector.

Located beneath the tip of the total pressure tube and protruding 0.001 in. above the plug surface were two insulated contact wires (see Figure B.7). The two wires ran inside the probe body but outside the movable shaft, and exited at the bottom support. When the probe head was lowered such that the bottom of the total pressure tube touched either wire, electrical continuity would be established to an external indicating circuit. The contact between the total pressure tube and the wire was employed to determine the "zero" or reference position of the total pressure tube during an experiment.

The boundary layer probe was inserted in a plug hole in the test plate and held by six machine screws. The surface of the plug or the probe was brought up flush (visually) to the surface of the test plate either by observing the probe through a viewing port or by employing a gun barrel borscope inserted through the nozzle. The seal between the probe plug and the test plate was accomplished with a "Viton" A O-ring or thin Teflon gaskets.

Located beneath the test section was the mechanism, herein termed the probe mechanism, which contained the equipment for driving the probe shaft up and down, and which also housed the pressure transducers employed to monitor the pressures measured at the probe head. The mechanism would be located immediately below the particular position of the probe during an experiment. It was supported by two 1 in. O.D. circular steel bars which ran parallel to the test section and were firmly mounted in saddle clamps which fastened to the lead section and nozzle ducts. During an experiment the probe mechanism was supported by the longitudinal bars which were in turn solidly clamped to the flow channel. Some relative motion between the probe mechanism and the test section resulted because of the effects of thermal expansion but this motion ceased once the apparatus had reached equilibrium temperature.

Figure B.8 presents a simplified schematic diagram of the drive mechanism employed both to move the probe shaft and to determine the position of the probe head above the test plate. The bearing screw located in the bottom support of the probe rested on a table, termed the cam table, which was guided in vertical motion by a base plate and driven in vertical motion by a linear cam. The linear cam was mounted on
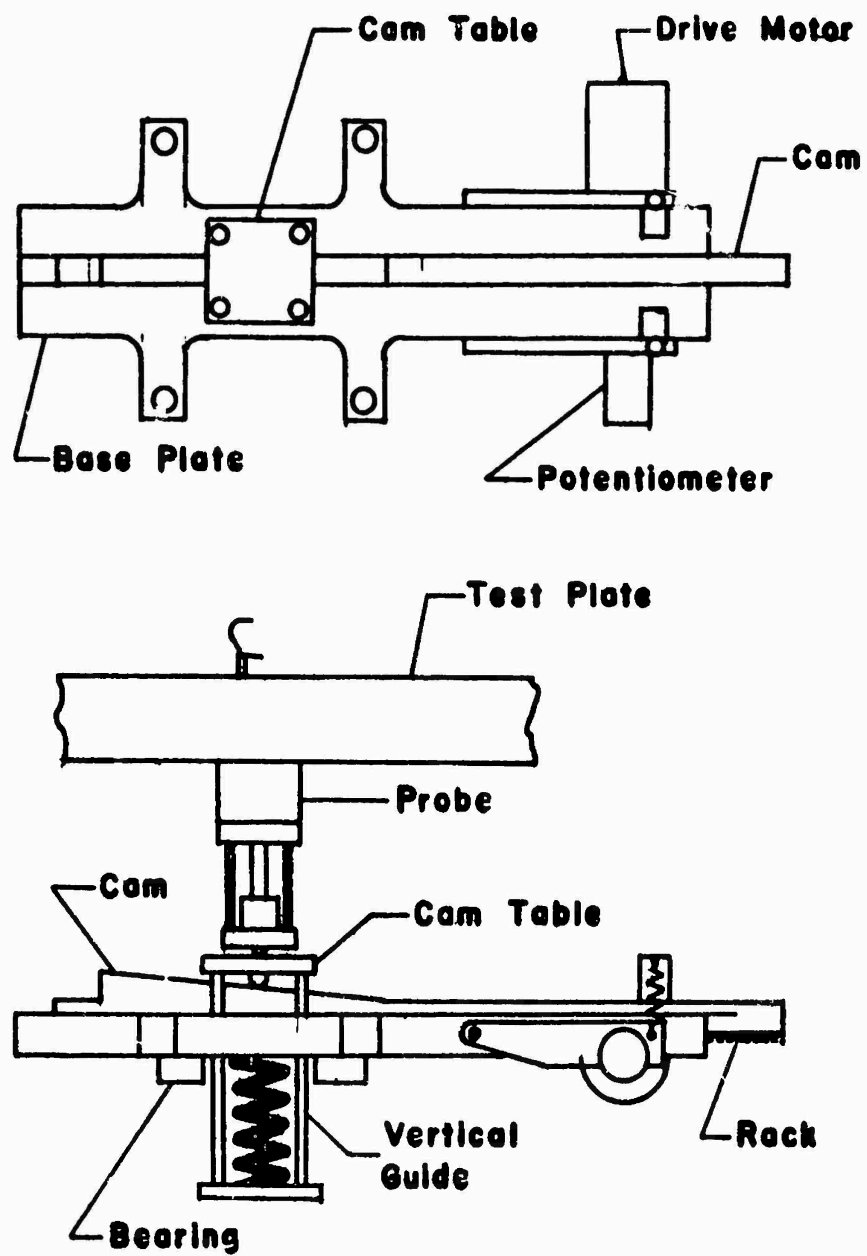
Figure B.8.   Schematic Diagram of the Cam Drive Mechanism

antifriction bearings and guided by a horizontal slot machined in the 3/4 in. thick steel base plate. Cemented to the lower surface of the cam were two rack gears. A motor driven pinion gear engaged one rack for drive power while the second rack engaged a pinion gear mounted on a 10 turn precision Heliopot potentiometer. The cam was held firmly against the bearings by both a spring and also by the pressure load (approximately 12 lbs) transmitted through the probe shaft during an experiment. Both the drive motor and potentiometer were spring loaded against the rack gears to remove any backlash in the gearing system. The resulting arrangement whereby the probe shaft, cam table, cam and potentiometer were in series with no backlash, together with the overall rigid mounting of the equipment, permitted the detection of motion of the probe shaft (and hence, the probe head) by a circular displacement of the potentiometer shaft.

The potentiometer circuit was equipped with a constant voltage source comprised of two 12 volt wet cells maintained at virtually constant temperature. The output of the potentiometer was displayed and recorded on a direct writing CEC oscillograph. The output of the potentiometer and the vertical motion of the probe shaft were related by direct calibration of the assembled system. The calibration was carried out by direct measurement with a micrometer of the distance between the cam table and the bottom of the test section. These measurements were then related to the corresponding outputs of the potentiometer circuit. The output characteristics of the potentiometer circuit were such that the display of displacement on the oscillograph would be most expanded when the probe head was nearest the test plate,

and subsequently decrease as the probe head moved further away from the test plate. When the probe head was near the test plate, a 0.001 in. motion of the probe head was displayed as approximately 0.050 in. displacement on the oscillograph. Similarly, when the probe head was 0.45 in. above the test plate, a 0.001 in. motion of the probe head was displayed as an approximately 0.005 in. displacement on the oscillograph.

A single calibration of the potentiometer output in terms of vertical motion of the cam table served as a master calibration for all experiments in which a particular cam was employed. The relative motion of the apparatus caused by thermal expansion effects was compensated for by obtaining two micrometer measurements during an experiment of the distance between the cam table and the bottom of the test section. The difference between the two micrometer measurements (obtained at the minimum and maximum throw of the cam) were incorporated with the corresponding displacement increment on the oscillograph in a correction factor. The correction factor was then applied to the master calibration curve to obtain the real vertical coordinate corresponding to the position of the probe shaft. The foregoing technique was applicable since the mechanical system of the probe, the cam and motion of the potentiometer shaft were linear, and hence, unaffected by changes in cam orientati n caused by thermal expansion effects. It was not possible to compensate for the increase in the length of the probe shaft caused by thermal expansion of the probe shaft as the probe shaft was driven vertically into the hot gas stream. A liberal estimate of this expansion, however, amounts to only approximately 0.002 in. for a vertical traverse of 0.5 in. of the probe shaft.

The stagnation pressure sensed by the total pressure probe and the static pressure sensed by the Prandtl tube were input to a differential pressure transducer, the output of which was the differential velocity pressure. Both Wiancko pressure transducers (0-10 and 0-50 psid) and Statham strain gage transducers (0-20 and 0-25 psid) were employed during the course of the investigation. The outputs of the differential pressure transducer and the Wiancko static pressure transducer were recorded separately on stripchart recorders. The output of the thermocouples on the probe head were recorded on a direct writing oscillograph.

B.4 Photographic System

Figure B.9 presents a photograph of the arrangement of the photographic system relative to the test section. The camera employed to take the photographs was a 35 mm korex F camera equipped with a close copy lens with an extension tube to permit focusing at distances of a few inches. The light source for the photographs was a 3 microsecond, 3 joule strobe unit designed and built by the Allison Division of General Motors Corporation. The camera and strobe unit were mounted on a remotely controlled mechanism which permitted transversing along the test section in the x-direction.

Figure B.10 presents a schematic diagram of the cross section view of the camera, strobe unit and test section. The camera and the strobe unit were inclined at an angle of 10° to the test plate, and each viewed through the dimetrically opposed Pyrex windows. The strobe unit was located such that the light source, a mercury vapor lamp, was approximately 4 in. from the surface centerline of the test section. The camera was focused at 4 in. Not shown in Figure B.10 are 1 in. O.D.
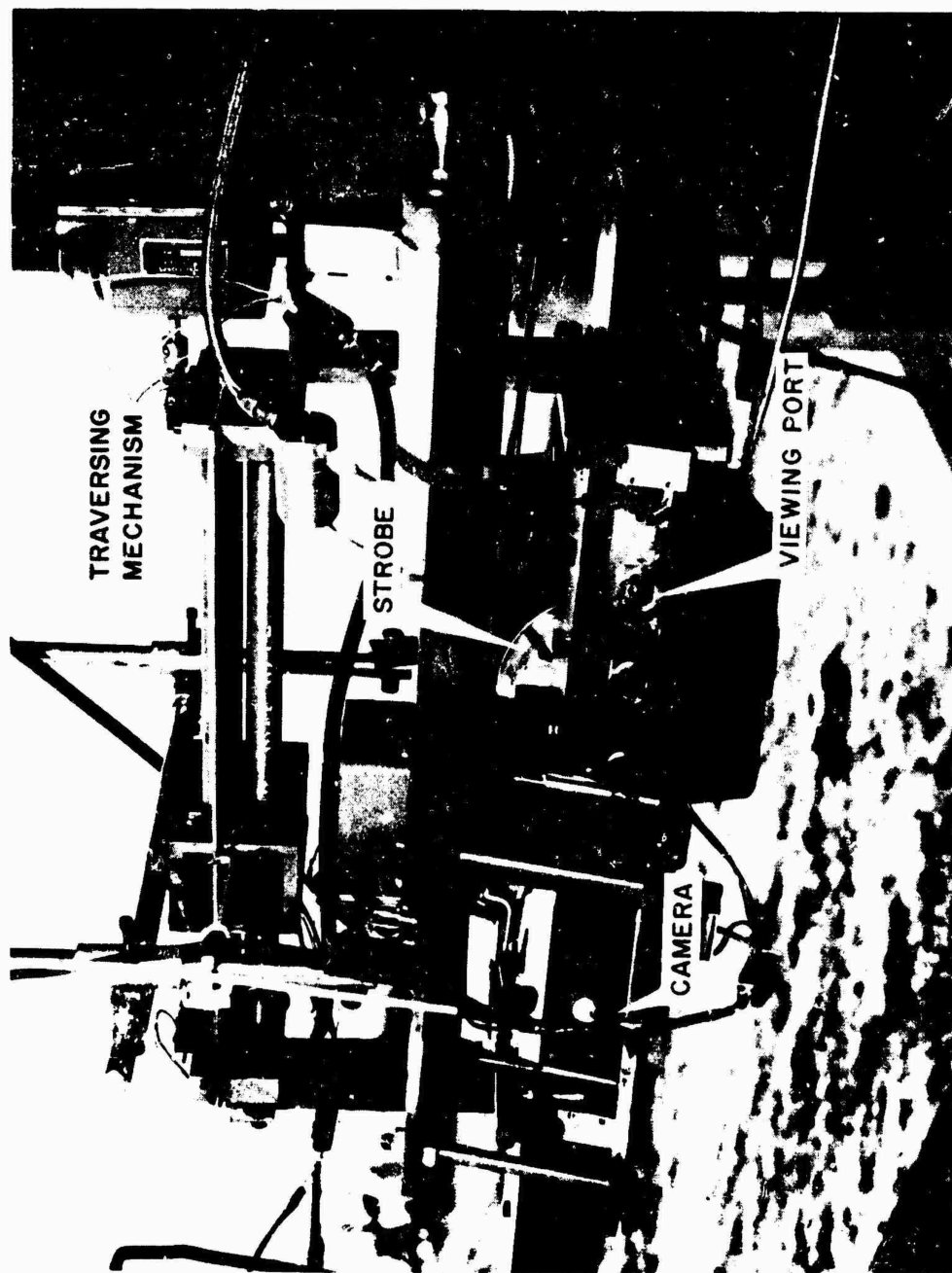
Figure B.9. Arrangement of the Photographic System
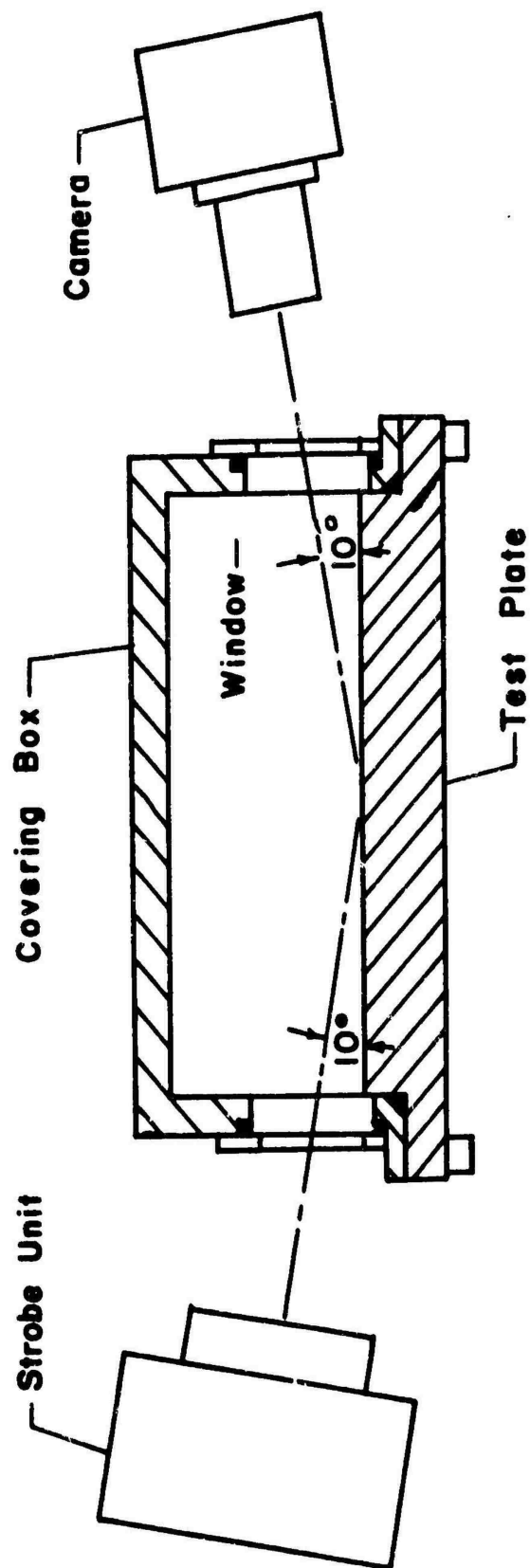
Figure B.10. Schematic Diagram of the Photographic System

tubes, also mounted at 10° to the test section, which served as shades against external light but did not exclude either the incident light from the strobe unit or the light reflected from the test plate to the camera.

The strobe unit and the camera were synchronized by means of an electrical continuity hook-up between the control equipment for the strobe unit and the flash synchronization contacts on the camera. The photographs were taken at 1/15 of a second shutter speed (which is not of consequence since the duration of the strobe flash was the effective shutter speed) at a lens setting of f/22 or f/32 using Kodak Tri-x film. The film was developed with Microdol X developer which resulted in an effective film speed of ASA 600. The prints of the pictures were produced by standard techniques using Kodak F-2 paper.

APPENDIX C

EXPERIMENTAL PROCEDURE

APPENDIX C

EXPERIMENTAL PROCEDURE

C.1 Pre-Run Preparation

The pre-run preparation of the experimental apparatus encompassed three major items, namely, (1) the preparation of the gas generator and instrumentation systems, (2) the calibration of the instruments, and (3) the establishment of the start-up configuration for the entire apparatus prior to the start of an experimental run.

The air storage tanks having a total volume of 2500 cu. ft. were charged with air to a pressure between 1500 and 2400 psi which was sufficient for operation of the gas generator for a period from 2000 to 4000 seconds. The fuel and liquid tanks were filled with methenol and distilled water, respectively. The quantities of liquid in the tanks would permit experimental run durations up to 4500 seconds. Several hours prior to an experiment the instrumentation and electronic systems were turned on to allow for warm-up and stabilization. The camera, if employed, was loaded with film and mounted on the traversing mechanism. The strobe unit was checked to ensure proper functioning and was patched into the synchronization system of the camera. The combined system was then checked again to ensure correct functioning.

The pressure transducers monitoring the operation of the gas generator were calibrated in stepwise increments of 50 or 100 psi employing a precision Bourden tube pressure gage as a standard. The precision gage

was periodically calibrated employing an Ashcroft dead weight tester. The calibration of the turbine flow meters monitoring the air, fuel and liquid flow rates was accomplished by means of a 100 cps reference signal available at the Potter flowmeter electronic tachometers. The tachometers supplied a d.c. analog output proportional to the rotative speed of the flowmeter elements. The temperature of the air, fuel and liquids was recorded on a Brown recorder. The reference junctions where required were maintained at 32 F by ice baths. All of the aforementioned pre-run calibrations were recorded on the same stripchart recorders which recorded the parameters during an experiment.

The differential pressure transducer employed to sense the differential velocity pressure at the probe head was calibrated in step increments of 10 in. of water using a water filled manometer and a small volume Nullmatic pressure regulator. The total calibration range was 70 inches of water. The calibration was recorded on a stripchart recorder. It was determined that due to the low range of the differential pressure transducer, the transducer had to be isolated from one of the input pressures during the ignition transient of the gas generator to prevent overranging and subsequent damage of the transducer. The total pressure input was blocked out by a needle value and the static pressure was input to both sides of the transducer by means of a by-pass value. The by-pass configuration was secured prior to the initiation of the ignition sequence.

The output of the total temperature thermocouple on the probe head was recorded on a direct writing CEC oscillograph. The circuit for the thermocouple was pre-calibrated.

The position determination system for the probe head was a pre-calibrated system (see appendix B). The output of the position potentiometer on the probe mechanism was recorded on a CEC oscillograph. The determination of the reference position cf the probe head was performed during the experiment. The establishment of the start-up configuration for the entire apparatus was performed just prior to ignition. The strip-chart recorders, which were all set to run at 4 inches per minute, were synchronized. The propellant air and fuel and liquid tank pressures were set to the desired valve. The propellant air and fuel were then bled up to the main valves (see Figure B.3). The flow rates desired at ignition were established by opening one valve at a time and setting the desired flow rate of either fuel, primary air or secondary air. Five seconds prior to ignition all of the stripchart recorders were started and ran for the duration of the experiment.

The start-up of the gas generator was accomplished with the automatic start sequencer.

C.2 In-Run Procedure

After mainstage ignition was secured the operator brought the gas generator up to the nominal operating point. A period of time from five to eight minutes was required for the apparatus to reach thermal equilibrium after the operating point had been reached. During the warm-up period the flow rate of liquid to be injected onto the test plate was set and stablized. The film of liquid on the test plate was visually inspected to insure proper coverage. The film of liquid completely covered the central 50 percent of the test plate. The valve blocking

the total pressure input to the differential pressure transducer was opened and the by-pass valve was closed. All the connections on the lines leading to the differential pressure transducer from the probe were leak checked with a soap solution. The smallest detectable leak in these lines was found to introduce an observable shift in the output signal and hence, an error in the measured velocity head.

The movable roof in the test section was adjusted such that a zero axial static pressure gradient was maintained. The pressure gradient in the test section was indicated by a differential pressure transducer monitoring the difference in the static pressures between the fore end and the aft end of the test section.

Photographs to be taken during the experiment were taken remotely employing a system whereby the operator could work the strobe unit, actuate the camera shutter and traverse the camera along the test section from the control room adjacent to the test cell.

Before a measurement set was initiated with the boundary layer probe the tip of the total pressure tube was lowered to make contact with the insulated wire mounted flush to the probe plug, i.e., the "zero" reference position. Contact was indicated by a milliameter in a continuity circuit. When contact was indicated, the position of the probe head was established from knowledge of the dimensions of the probe elements. The distance between the cam table, which moved the probe head up or down, and the bottom of the test plate was measured with a micrometer. The traverse of the probe was accomplished either remotely by an automatic system located in the control room or by the operator using the control module located on the probe mechanism. A complete traverse consisted of

from 12 to 20 discrete steps, with the probe dwelling at each step for a period of 20 to 30 seconds during which time the differential velocity pressure and total temperature were recorded. The output of the probe position potentiometer was recorded continuously and synchronization of the data during the traverse was based on this continuous output. At the upward terminal end of the traverse a second measurement of the distance between the cam table and the bottom of the test plate was secured. During the evaluation of the data the position of the probe head at any point during the traverse could be determined from the cam calibration, the micrometer measurements and the output of the position potentiometer at the "zero" or reference contact between the total pressure tube and the contact wires in probe plug. Two or three complete transverses were made during a single experiment with the probe at one axial location along the test plate.

Before and after each traverse of the probe the outputs of the 38 thermocouples imbedded in the test plate were recorded on a CEC oscillograph. The temperature distribution on the bottom of the test plate as indicated by 16 spot welded thermocouples and the other system temperatures being monitored were continuously recorded on stripchart recorders. The outputs of the individual thermocouples in the system were put through three banks of stepping switches ahead of the recorders or oscillograph.

C.3 Post-Run Procedure

Upon the completion of an experiment the gas generator was shut down. An afterbleed of propellant air was allowed to flow through the gas generator and test section to reduce the temperature of the equipment.

The liquid continued to flow onto the test plate during the cool-down period.

The differential pressure transducer indicating the velocity head was re-calibrated in the same manner as before the experiment. The calibrations of the other pressure transducers in the system did not usually display a shift during the experiment so only the range of the calibration was re-checked following an experiment.

The probe was removed after the experiment to be relocated in another axial position in the test plate. While the probe was out of the apparatus, the head, body and output lines of the probe were subjected to a leak check using 400 psi air. If any leaks were detected on the external solder joints, those leaks were repaired before the probe was employed again.

APPENDIX D

MEASUREMENTS AND DATA REDUCTION

D.1 Physical Properties

The physical properties of air were taken from National Bureau of Standards Circular No. 564 (41). The physical properties of water were taken from Keenan, J. H. and F. G. Keyes, "Thermodynamic Properties of Steam" (42).

The specific weight of air was calculated from the equation of state corrected for compressibility as

$$\gamma = \frac{P}{ZRT} \tag{D-1}$$

The value of the compressibility factor, Z, was obtained from Reference 41.

D.2 General Data Reduction

The pressure transducers employed to measure the static and total pressures in the gas generator system and the test section were calibrated against a precision pressure gage prior to each experiment. The calibration was in the form of discrete pressure steps both ascending and descending; the maximum value of the largest calibration step was in excess of the value recorded during an experiment. The calibration and the corresponding run data were both recorded on the same Brown strip-chart recorder. The numerical value of the particular pressure parameter recorded during an experiment was determined by linear interpolation of the recorded transducer output against the calibration. The

estimated error resulting from the transducer hysteresis and data trans-
cription was estimated at $\pm$ 2 percent at the nominal run value of the
pressure.

All of the temperatures monitored during an experiment with the
exception of the probe total temperature and those temperatures obtained
from the thermocouples imbedded in the test plate were recorded either
on direct reading Brown recorders or on pre-calibrated Brown recorders.
The values of temperature recorded during an experiment were corre-
spondingly read off directly from the recorder chart or determined with
aid of a calibration curve. The output readings from the thermocouples
imbedded in the test plate were recorded on an oscillograph. The os-
cillograph galvonometers were calibrated in 2.0 millivolt increments by
means of a Leeds and Northrup potentiometer. The temperatures measured
by the thermocouples imbedded in the test plate during an experiment were
determined by linear interpolation against the calibration and a conver-
sion table for thermocouples.

The estimated error in the temperatures read from the Brown re-
corders was from $\pm$ 1 to $\pm$ 2 percent at the nominal run value of the tem-
perature. The estimated error of the plate temperatures read from the
oscillograph was $\pm$ 3 percent of the nominal run value of the temperature.

The volume flow rates of air, fuel and water (the liquid injected
onto the test plate) were measured with turbine flowmeters. The flow-
meters which measured the flow rates of fuel and water were calibrated
with the respective liquid in terms of frequency output as a function of
weight flow rate. In this manner a calibration constant was established
for a particular flowmeter through which the weight flow rate and

frequency output were related. The flowmeter employed to meter the flow rate of air to the gas generator was calibrated by the company supplying the instrument as volume rate of flow versus frequency at a static pressure of 600 psig. The flowmeter was subsequently calibrated again at the Jet Propulsion Center, Purdue University, against ASME standard orifices at flow pressures of 400, 600, and 800 psig. The latter calibration and the calibration supplied with the meter agreed within ± 5 percent at the nominal run value. The weight flow rate of air measured during a run was evaluated as

$$\mathring{W} = Q\gamma \tag{D-2}$$

where Q = indicated volume flow rate at the frequency output of the
       flowmeter

   γ = specific weight of the air determined from the measured
       static pressure and temperature of the air immediately
       upstream of the flowmeter, and employing equation D-1.

The output circuit of the flowmeters was calibrated prior to each experiment against known frequencies available in the flowmeter instrumentation. The estimated error in the measurements of the two liquid flow rates was ± 4 percent or less of the nominal run value. The estimated error in the measurement of the air flow rate was taken as the deviation of the two aforementioned calibrations, that is, ± 5 percent.

D.3 Boundary Layer Data

Temperature. The total temperature at a particular elevation above the test plate was measured by a bare chromel-alumel thermocouple

mounted on the probe head. The output of the thermocouple was recorded
on an oscillograph. The thermocouple was calibrated at regular intervals
at two points, ambient temperature near 70F and at the boiling point of
water at ambient conditions, 212F. The calibration points were recorded
on the oscillograph and a scale factor was derived for temperature as a
function of trace position. The scale factor varied by no more than
$\pm$ 3 percent for all the calibrations performed during the three month
period in which the experiments were conducted.

Figure D.1 presents typical output signals of the total temperature
thermocouple as the signal appeared on the oscillograph chart. Figure
D.1a shows a trace obtained at an elevation of 0.040 in. at a location
9 in. downstream of the injector slot. The noise level of the signal
represents approximately $\pm$ 10F to $\pm$ 20F. Figure D.1b shows a trace ob-
tained at an elevation of 0.400 in. at a location 17 in. downstream
from the injector slot. The noise level of the signal is approximately
$\pm$ 10F. The noise level of the thermocouple signal increased as the
thermocouple approached the liquid film. Figure D.1c shows the output
signal for the thermocouple just above the liquid film. The very high
noise level displayed when the thermocouple was immediately next to the
liquid film was the result of the larger surface waves and entrained
liquid coming in contact with the thermocouple.

The total temperature thermocouple moved the same increments
of traverse as the total pressure tube except within 0.010 in. of
the plate (see Appendix B for method of traversing and positioning).
The thermocouple was set 0.010 in. lower than the total pressure
tube. As a result, during the first few increments of the traverse,
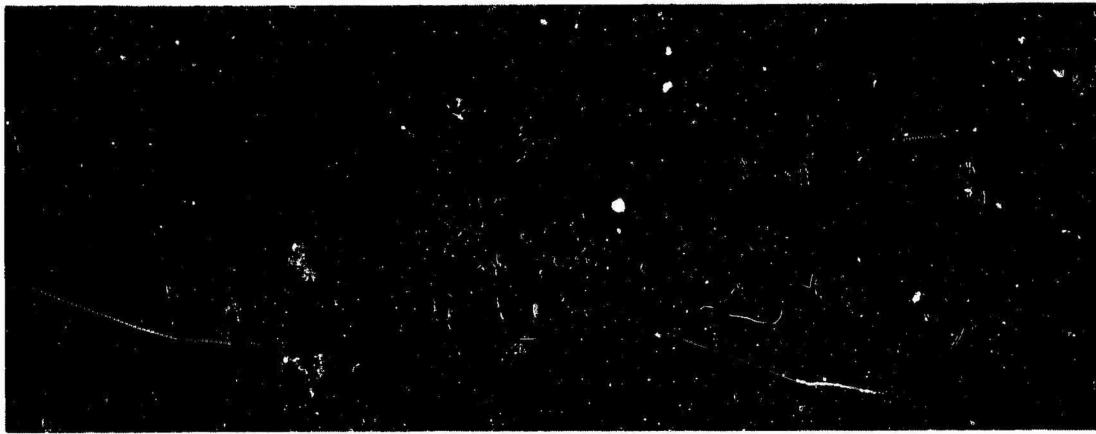
(a) $y = 0.040$ in., $x - x_0 = 9$ in.

(b) $y = 0.400$ in., $x - x_0 = 17$ in.

Position Trace
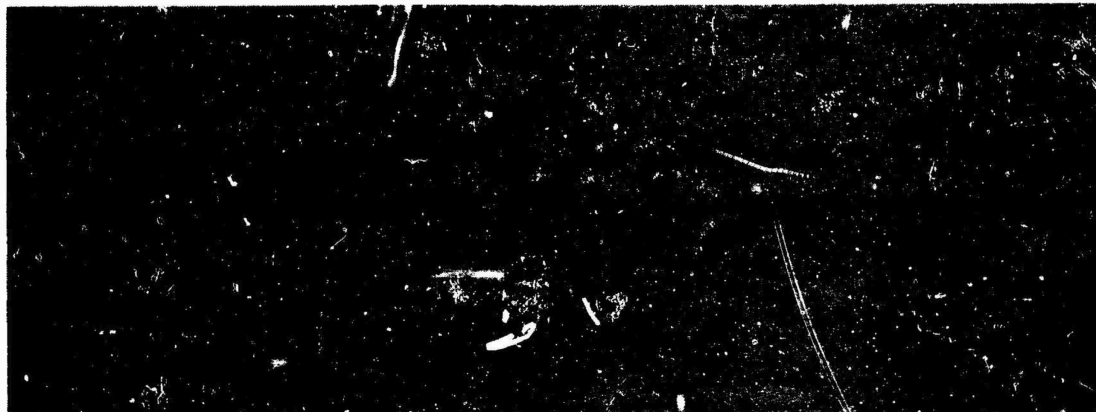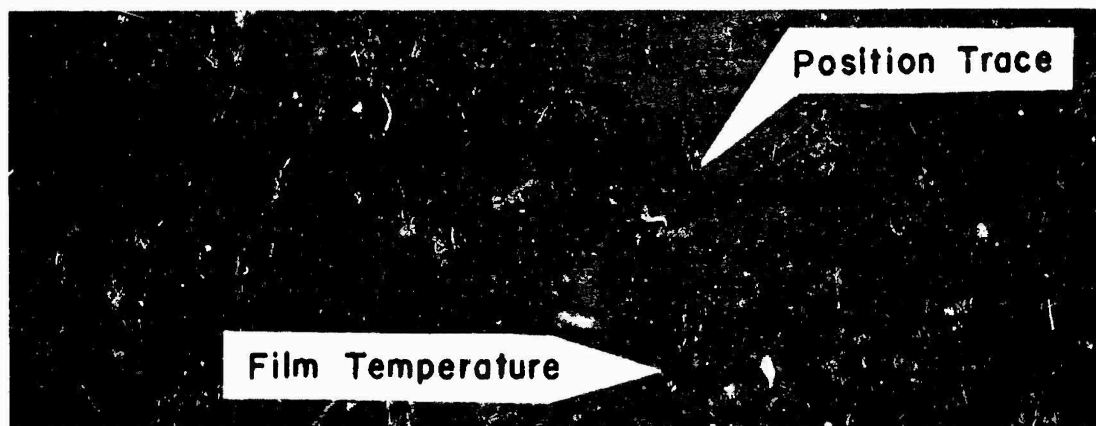
Film Temperature

(c) Stepwise increase of temperature as
     thermocouple leaves liquid film

Figure D.1.   Typical Output Signals from Total Temperature
              Thermocouple

each a few thousandths of an inch, the thermocouple remained in contact with the surface of the probe plug and the liquid film. While in this position the temperature indicated by the thermocouple was within 5F of the temperature of the film. As soon as the traverse had progressed sufficiently to move the thermocouple out of the liquid film, the indicated temperature would increase stepwise by approximately 100F or more. Figure D.1c presents a sample trace showing the stepwise increase in the temperature. The stepwise increase occurred in a traverse increment of less than 0.005 in. The occurrence of the stepwise increase in temperature marked the reference or starting position of the temperature traverse. Since the thermocouple was 0.015 in. in diameter and there existed uncertainty of 0.005 in. in the position of the probe where it left the continuous film, the reading corresponding to the stepwise increase in temperature was taken to be at an elevation of C.010 in., or one half the sum of the diameter of the thermocouple and the uncertainty in position. Since the thermocouple immediately after leaving the continuous film was still influenced by the larger instability waves, the first one or two temperature readings were excluded from the data. In general the elevation of the first usable reading was between 0.015 in. to 0.020 in. above the liquid film.

The estimated error in the determination of the position of the thermocouple head was ± 0.005 in. The maximum estimated error in the determination of a temperature due solely to the long term calibration shift was ± 10F, if such a shift occurred within one experiment. The flow conditions and the design of the thermocouple were such that the errors introduced by conduction, convection and radiation were calculated to be

negligible (39).

In order to check the reproducibility of the aforementioned techniques of temperature measurement, two separate experiments were conducted on different days in which the temperature profiles were determined at the same location under the same operating conditions. The results are shown in Figure 26, Section 3, for the position at $x - x_0 = 9$ in. The curve shown is composed of four traverses, two each from the separate experiments. The different profiles established in the two experiments agree to within $\pm$ 10F.

The experimental data points of temperature obtained at a particular location along the test plate were graphed as a function of the measured elevation above the test plate. The profile of the temperature boundary layer was determined by visually drawing a curve through the mean of the data points.

<u>Velocity</u>. The velocity at a particular elevation in the boundary layer was calculated from the measured parameters by Bernoulli's equation as

$$u = (2\,\frac{\Delta p}{\rho})^{1/2} \tag{D-3}$$

where Δp = differential velocity pressure at a particular elevation

ρ = local density of the gas at the elevation of the total pressure tube.

The local density, ρ, was calculated by equation D.1 assuming air to be the gas. The temperature employed in equation D.1 was read from the mean curve through the temperature data points measured at the same axial location for the particular elevation. The pressure employed in equation D.1 was that of the test section.

The "zero" or reference position for the velocity profile was that elevation at which the total pressure tube made contact with an insulated wire mounted flush with the surface of the probe plug (which was in turn flush with the test plate). The conta.t between the tube and the wire established electrical continuity which was indicated by millimeters to the experimenter. When electrical continuity was indicated, the center of the orifice of the total pressure tube was 0.006 in. above the surface of the plug, and hence, the surface of the plate. Thereafter, the elevation of the total pressure tube was known through the probe position determination system.

The error in the determination of the velocity due to hysteresis of the differential pressure transducer was $\pm$ 2.5 percent near the free stream value of velocity, increasing to $\pm$ 10 percent near the test plate. The error in the determination of the position of the total pressure tube was estimated at $\pm$ 0.002 in. near the test plate, increasing to $\pm$ 0.005 in. at the upward terminus of the traverse. The error resultant from the transcription of the pressure and temperature data required to calculate the velocity from equation D-3 cannot be reliably estimated but it would appear to be less than the error resulting from transducer hysteresis.

APPENDIX E

TABULATED DATA

Table E.1 presents the values of the operating parameters in the test section for the experiments reported herein. Two values of the free stream velocity are listed, one value based on the probe measurements, u_{ep}, and the other value based on the bulk flow rate measurements, u_{eb}. For the column headed "Measurements", $\underline{T}$ signifies temperature traverses and $\underline{u}$ signifies velocity traverses. The last four columns present the deviation of the experimental flow conditions from the nominal flow conditions (see Table 1, Section 1).

Table E.2 presents the data for the traverses made at the location 17 in. downstream of the injector slot for the wetted test plate.

Table E.1

Operating Conditions for the Experiments

Run	Location x-x$_0$(in.)	Measurements	Free Stream Velocity(ft/sec) u$_{ep}$	u$_{eb}$	Temperature T$_e$(R)	Pressure P$_e$(psia)	Liquid Flow Rate ṁ$_l$(lb/sec)	Deviation T$_e$ (R)	P$_e$ (psi)	u$_{ep}$ (ft/sec)	Ṁ$_l$ (lb/sec)
CFC-21	3	T,u	99	103	980	246	0.0065	0	-4	-1	0
23	5	u	101	103	975	249	0.0065	-5	-1	+1	0
24	5	T	-	100	985	248	0.0065	+5	-2	-	0
14	9	T	-	-	975	248	0.0063	-5	-2	-	-0.0002
15	9	u	104	103	980	248	0.0068	0	-2	+4	+0.0003
22	17	T,u	99	99/102	975	247	0.0065	-5	-3	-1	0
28	3	u	99	103	975	250	0	-5	0	-1	-
29	9	u	99	-	990	249	0	+10	-1	-1	-
27	17	u	96	-	980	247	0	0	-3	-4	-

Table E.2

Traverse Data at $x-x_0$ = 17 in. for the Wetted Test Plate

Set 1		Set 2		Set 1	
Elevation	Velocity	Elevation	Velocity	Elevation	Temperature
(in.)	(ft/sec)	(in.)	(ft/sec)	(in.)	(R)
0.008	39.5	0.010	49.2	0.013	805
0.014	52.8	0.012	50.5	0.018	889
0.037	63.4	0.013	53.6	0.041	914
0.049	65.9	0.015	55.8	0.053	927
0.062	69.1	0.024	62.1	0.066	930
0.083	71.3	0.031	65.4	0.087	938
0.113	77.3	0.044	70.8	0.117	951
0.170	85.2	0.061	75.0	0.174	964
0.226	89.1	0.076	76.8	0.230	970
0.276	92.6	0.101	80.4	0.280	977
0.344	95.0	0.135	84.3	0.348	977
0.386	96.0	0.178	87.5	0.390	977
0.423	98.4	0.220	90.3	0.427	977
		0.224	91.6		
		0.298	94.0		
		0.335	95.4		
		0.417	96.8		

DOCUMENT CONTROL DATA - R&D		
(Security classification of title, body of abstract and indexing annotation must be entered when the overall report is classified)		

1 ORIGINATING ACTIVITY (Corporate author)	2a. REPORT SECURITY CLASSIFICATION
Jet Propulsion Center	Unclassified
School of Mechanical Engineering	2b GROUP
Purdue University, Lafayette, Indiana	N/A

3 REPORT TITLE

AN EXPERIMENTAL INVESTIGATION OF THE VELOCITY AND TEMPERATURE PROFILES IN THE BOUNDARY LAYER ABOVE AN UNSTABLE EVAPORATING FILM OF LIQUID UNDER THE INFLUENCE OF A MOVING STREAM OF HOT GAS

4. DESCRIPTIVE NOTES (Type of report and inclusive dates)

N/A

5 AUTHOR(S) (Last name, first name, initial)

Crabtree, Jr., Donald L.

6. REPORT DATE	7a TOTAL NO. OF PAGES	7b. NO. OF REFS
September, 1966	208	42

8a. CONTRACT OR GRANT NO.	9a. ORIGINATOR'S REPORT NUMBER(S)
Nonr 1100(21)	
b. PROJECT NO.	TM-66-9
c	9b. OTHER REPORT NO(S) (Any other numbers that may be assigned this report)
d	JPC-429

10 AVAILABILITY/LIMITATION NOTICES

No Restrictions

11. SUPPLEMENTARY NOTES	12. SPONSORING MILITARY ACTIVITY
N/A	U. S. Navy (Office of Naval Research-Power Branch)

13 ABSTRACT

This thesis presents the results of measurements of the velocity and temperature profiles in the boundary layer above an unstable evaporating film of water. Entrained liquid as droplets was present in the boundary layer. The measurements were made at one liquid flow rate at the following gas flow conditions:

Total temperature — 980R
Total pressure — 250 psia
Gas velocity — 100 ft/sec
Axial static pressure gradient — less than 0.02 psi/ft

Photographs taken at 3μ sec were obtained of the interfacial structure of the liquid film. The temperature of the film was also measured. The experiments were conducted in a tunnel with a rectangular cross section 1 1/2 in. x 4 in. long, onto one side of which was injected the liquid as a film. Measurements in the boundary layer were carried out for both wet and dry walls.

The profiles of velocity and temperature in the boundary layer on the wetted wall correlated to power law distributions of 1/7 and 1/6, respectively; the velocity boundary layer on the dry wall correlated to a 1/8.3 power law distribution.

The friction coefficient for the wetted wall was determined to be 40 percent greater than for the dry wall. The ratio of the friction coefficient to the Stanton number for the wetted wall was 2.4 which is in approximate agreement with that value predicted by Reynolds analogy.

DD FORM 1 JAN 64 **1473**

14.		LINK A		LINK B		LINK C	
KEY WORDS		ROLE	WT	ROLE	WT	ROLE	WT
Boundary layer Profiles, velocity and temperature Liquid film Heat transfer Friction coefficient							

INSTRUCTIONS

1. ORIGINATING ACTIVITY: Enter the name and address of the contractor, subcontractor, grantee, Department of Defense activity or other organization (corporate author) issuing the report.

2a. REPORT SECURITY CLASSIFICATION: Enter the overall security classification of the report. Indicate whether "Restricted Data" is included. Marking is to be in accordance with appropriate security regulations.

2b. GROUP: Automatic downgrading is specified in DoD Directive 5200.10 and Armed Forces Industrial Manual. Enter the group number. Also, when applicable, show that optional markings have been used for Group 3 and Group 4 as authorized.

3. REPORT TITLE: Enter the complete report title in all capital letters. Titles in all cases should be unclassified. If a meaningful title cannot be selected without classification, show title classification in all capitals in parenthesis immediately following the title.

4. DESCRIPTIVE NOTES: If appropriate, enter the type of report, e.g., interim, progress, summary, annual, or final. Give the inclusive dates when a specific reporting period is covered.

5. AUTHOR(S): Enter the name(s) of author(s) as shown on or in the report. Enter last name, first name, middle initial. If military, show rank and branch of service. The name of the principal author is an absolute minimum requirement.

6. REPORT DATE: Enter the date of the report as day, month, year; or month, year. If more than one date appears on the report, use date of publication.

7a. TOTAL NUMBER OF PAGES: The total page count should follow normal pagination procedures, i.e., enter the number of pages containing information.

7b. NUMBER OF REFERENCES: Enter the total number of references cited in the report.

8a. CONTRACT OR GRANT NUMBER: If appropriate, enter the applicable number of the contract or grant under which the report was written.

8b, 8c, & 8d. PROJECT NUMBER: Enter the appropriate military department identification, such as project number, subproject number, system numbers, task number, etc.

9a. ORIGINATOR'S REPORT NUMBER(S): Enter the official report number by which the document will be identified and controlled by the originating activity. This number must be unique to this report.

9b. OTHER REPORT NUMBER(S): If the report has been assigned any other report numbers (either by the originator or by the sponsor), also enter this number(s).

10. AVAILABILITY/LIMITATION NOTICES: Enter any limitations on further dissemination of the report, other than those imposed by security classification, using standard statements such as:

(1) "Qualified requesters may obtain copies of this report from DDC."

(2) "Foreign announcement and dissemination of this report by DDC is not authorized."

(3) "U. S. Government agencies may obtain copies of this report directly from DDC. Other qualified DDC users shall request through

_____."

(4) "U. S. military agencies may obtain copies of this report directly from DDC. Other qualified users shall request through

_____."

(5) "All distribution of this report is controlled. Qualified DDC users shall request through

_____."

If the report has been furnished to the Office of Technical Services, Department of Commerce, for sale to the public, indicate this fact and enter the price, if known.

11. SUPPLEMENTARY NOTES: Use for additional explanatory notes.

12. SPONSORING MILITARY ACTIVITY: Enter the name of the departmental project office or laboratory sponsoring (paying for) the research and development. Include address.

13. ABSTRACT: Enter an abstract giving a brief and factual summary of the document indicative of the report, even though it may also appear elsewhere in the body of the technical report. If additional space is required, a continuation sheet shall be attached.

It is highly desirable that the abstract of classified reports be unclassified. Each paragraph of the abstract shall end with an indication of the military security classification of the information in the paragraph, represented as (TS), (S), (C), or (U).

There is no limitation on the length of the abstract. However, the suggested length is from 150 to 225 words.

14. KEY WORDS: Key words are technically meaningful terms or short phrases that characterize a report and may be used as index entries for cataloging the report. Key words must be selected so that no security classification is required. Identifiers, such as equipment model designation, trade name, military project code name, geographic location, may be used as key words but will be followed by an indication of technical context. The assignment of links, roles, and weights is optional.

DD FORM 1 JAN 64 1473 (BACK)